COMPREHENSIVE STUDY OF THE ENERGY CONSUMPTION OF MEMBRANES AND DISTILLATION

A Dissertation

Submitted to the Faculty

of

Purdue University

by

Jose Adrian Chavez Velasco

In Partial Fulfillment of the

Requirements for the Degree

of

Doctor of Philosophy

December 2020

Purdue University

West Lafayette, Indiana

THE PURDUE UNIVERSITY GRADUATE SCHOOL
STATEMENT OF DISSERTATION APPROVAL

Dr. Rakesh Agrawal, Chair

Davidson School of Chemical Engineering

Dr. Mohit Tawarmalani

Krannert School of Management

Dr. Gintaras Reklaitis

Davidson School of Chemical Engineering

Dr. Linda Wang

Davidson School of Chemical Engineering

Approved by:

Dr. John A. Morgan

Head of the School Graduate Program

ACKNOWLEDGMENTS

I would like to acknowledge my advisor Professor Rakesh Agrawal who provided me the main guidance for this work and shared his knowledge, experience and wisdom with me. I also would like to thank Professor Mohit Tawarmalani for all the help provided to me during the consultations on optimization that I had with him, as well as for several other useful discussions that we had.

I also want to thank Professor Gintaras V. Reklaitis, and Professor Linda Wang for giving me valuable feedback as members of my Ph.D. advisory committee.

To my sincere friends, whom I have the fortune to possess and with whom I had useful discussions regarding our research topics, particularly to Radhakrishna Tumbalam Gooty, Tony Joseph Mathew, Varsha, Zewei Chen, Zheyu Jiang, Taufik Ridha, Yiru Li, and Edwin Rodriguez. Special thanks to Radhakrishna Tumbalam Gooty who worked closely with me in developing the membrane cascade optimization model presented in Chapter 1. Also, special thanks to Radhakrishna Tumbalab Gooty and Tony Joseph Mathew for reading Chapter 2 and providing valuable suggestions.

Thanks to my parents and my sister, who have always given me their sincere affection and have been willing to provide me with all the support in their hands. To my wife and children, for their motivation, support, and love.

Thanks also to the Fulbright-Garcia Robles program, and the Mexican National Council for Science and Technology (CONACYT) for providing me with financial support.

TABLE OF CONTENTS

Page

LIST OF TABLES

LIST OF FIGURES

Figure Page

ABSTRACT

Chavez Velasco, Jose Adrian, Ph.D. , Purdue University, December 2020. Comprehensive Study of the Energy Consumption of Membranes and Distillation. Major Professors: Rakesh Agrawal.

Molecular separations are essential in the production of many chemicals and purified products. Of all the available separation technologies, distillation, which is a thermally driven process, has been and continues to be one of the most utilized separation methods in chemical and petrochemical plants. Although distillation and other commercial technologies fulfilled most of the current separation needs, the energy-intensive nature of many molecular separations and the growing concern of reducing CO_2 emissions has led to intense research to seek for more energy-efficient separation processes.

Among the emerging separation technologies alternative to distillation, there is special attention on non-thermally driven methods, such as membranes. The growing interest in non-thermal methods, and particularly in the use of membranes, has been influenced significantly from the widespread perception that they have a potential to be markedly less energy-intensive than thermal methods such as distillation. Even though many publications claim that membranes are more energy-efficient than distillation, except for water desalination, the relative energy intensity between these processes in the separation of chemical mixtures has not been deeply studied in the literature. One of the objectives of this work focuses on introducing a framework for comparative analysis of the energy intensity of membranes and distillation.

A complication generally encountered when comparing the energy consumption of membranes against an alternative process is that often the purity and recovery that can be achieved through a single membrane stage is limited. While using a multi-stage membrane process is a plausible solution to achieve both high purity and recovery, even for a simple binary separation, finding the most suitable multistage membrane process is a difficult task. This is because, for a given separation, there exists multiple cascades that fulfill the separation requirements but consume different amounts of energy. Moreover, the energy requirement of each cascade depends on the operating conditions. The first part of this work is dedicated to the development of a Mixed Integer Non-linear Program (MINLP) which allows for a given gaseous or liquid binary separation, finding the most energy-efficient membrane cascade. The permeator model, which is derived from a combination of the cross-flow model and the solution diffusion theory, and is originally expressed as a differential-algebraic equation (DAE) system, was integrated analytically before being incorporated in the optimization framework. This is in contrast to the common practice in the literature, where the DAE system is solved using various discretization techniques. Since many of the constraints have a non-convex nature, local solvers could get trapped in higher energy suboptimal solutions. While an option to overcome this limitation is to use a global solver such as BARON, it fails to solve the MINLP to the desired optimality in a reasonable amount of time for most of the cases. For this reason, we derive additional cuts to the problem by exploiting the mathematical properties of the governing equations and from physical insights. Through numerical examples, we demonstrate that the additional cuts aid BARON in expediting the convergence of branch-and-bound and solve the MINLP within 5%-optimality in all the cases tested in this work.

The proposed optimization model allows identifying membrane cascades with enhanced energy efficiency that could be potentially used for existing or new separations. In addition, it allows to compare the optimum energy consumption of a multistage membrane process against alternative separations methods and aid in the decision of

whether or not to use a membrane system. Nevertheless, it should be noted that when a membrane process or any other non-thermal separation process is compared with a thermal process such as distillation, an additional complication often arises because these processes usually use different types of energies. Non-thermal processes, such as membranes, consume electrical energy as work, whereas thermal processes, such as distillations, usually consume heat, which is available in a wide range of temperatures. Furthermore, the amount of fuel consumed by a separation process strongly depends on how its supplied energy is produced, and how it is energy integrated with the rest of the plant. Unfortunately, common approaches employed to compare the energy required by thermal and non-thermal methods often lead to incorrect conclusions and have driven to the flawed perception that thermal methods are inherently more energy-intensive than non-thermal counterparts. In the second part of this work, we develop a consistent framework that enables a proper comparison of the energy consumption between processes that are driven by thermal and non-thermal energy (electrical energy). Using this framework, we refute the general perception that thermal separation processes are necessarily the most energy-intensive and conclusively show that in several industrially important separations, distillation processes consume remarkably lower fuel than non-thermal membrane alternatives, which have often been touted as more energy efficient.

In order to gain more understanding of the conditions where membranes or distillation are more energy-efficient, we carried out a comprehensive analysis of the energy consumed by these two processes under different operating conditions. The introduced energy comparison analysis was applied to two important separation examples; the separation of p-xylene/o-xylene, and propylene/propane. Our results showed that distillation is more energy favored than membranes when the target purity and recovery of the most volatile (resp. most permeable) component in the distillate (resp. permeate) are high, and particularly when the feed is not too concentrated in the most volatile (resp. most permeable) component. On the other hand, when both

the recovery and purity of the most volatile (resp. most permeable) component are required at moderate levels, and particularly when the feed is highly enriched in the most volatile (resp. most permeable) component, membranes show potential to save energy as compared to distillation.

1. OPTIMIZATION OF MEMBRANE CASCADES FOR THE SEPARATION OF GASEOUS AND LIQUID MIXTURES

1.1 Introduction

Membrane technology has gained considerable interest in recent years. Distinctive features often associated to membranes such as modular scale-up flexibility, operational simplicity and relatively low capital cost, make them attractive for the separation of diverse types of mixtures. Some of the applications that have attained commercial success at large scale include water desalination, lube oil dewaxing, removal of CO_2 from natural gas, nitrogen production from air, and so forth. Besides these examples, it has been suggested that the spectrum of separations through membranes can be potentially extended to other mixtures [1, 2]. The remarkable progress achieved in the development of advance materials with enhanced properties, such as higher area-to-volume ratio, and higher resistance, has contributed notably to expanding the use of membranes. Nevertheless, a limitation still present in the majority of membranes is that they have at most moderate permeabilities and selectivity. This poses a challenge for separations that simultaneously require moderate to high purity and recovery of the component of interest; as a single membrane stage is typically not sufficient to meet the specifications. In this scenario, a multistage membrane process is needed to achieve the required purity and recovery. However, even for a binary separation, finding the most suitable multistage membrane process is a difficult task.

It is well known that for a given separation, it is likely to find several membrane cascades that meet the separation requirements, but they differ in terms of the overall energy input and cost [3–5]. The difficulty of designing a membrane cascade initially

arises because the space of possible configurations is not known apriori. Furthermore, the number of possible configurations can be large, which implies considerable effort and time for a process engineer to simulate all the candidates and find the best one. This task becomes even more intricate as each of the configurations could have multiple sets of operating conditions that fulfill the desired separation, but once again, they yield to different energy or cost requirements. The growing concern of reducing CO_2 emissions, which is responsible for global warming, makes critical the operation of more energy efficient separation processes. This is reinforced from the fact that for many chemical processes, separation stages can account for a large fraction of the overall energy input [6]. Since the energy supplied to industrial separation processes comes mainly from the combustion of fossil fuels, operating more energy efficient separation processes could significantly contribute to reducing the carbon footprint. These reasons motivate us in this work to develop a general optimization framework that allows to find optimum membrane cascades along with their corresponding operating conditions that minimize the energy consumption. More specifically, we developed a Mixed Integer Non-linear Programm (MINLP) that is applicable for both liquid and gaseous binary separations through dense membranes.

1.2 Literature review

Designing a multistage membrane separation implies two major decisions; choosing a suitable cascade configuration and selecting the operating conditions. A common strategy employed for this purpose involves in a first step; the selection of one or few potential membrane schemes based on heuristics and engineering criteria. Then, each of those configurations is subject to either sensitivity analysis or optimization with the aim of finding the right operating conditions that minimize a certain objective such as the total cost or the energy consumption. Finally, the configuration that exhibits the best performance is selected. This traditional approach has been followed in several works [5, 7–14]. For instance, Bhide & Stern [8] optimized through a grid search the

total cost of some membrane configurations applied to the separation of CO_2/CH_4. The studied configurations have up to three stages, and account for the recycle of one permeate or retentate stream, or both. Among the evaluated configurations, a three-stage cascade having both a permeate and a retentate recycle was found to be the most economical. Xu & Agrawal [11, 12] developed novel configurations with one or two compressors that exhibited minimal mixing losses. The benefits of the proposed configurations were illustrated for the separation of H_2/CO, and O_2/N_2. In these configurations, the area of one of the membranes was optimized with the goal of minimizing mixing losses. They showed that the new configurations require lower compression work and membrane area than conventional configurations that yield to substantial mixing losses. Nevertheless, it was noted that under some separation conditions, the improvement achieved through the configurations with almost no mixing losses was marginal, although the compared counterparts had large mixing losses. This implies that minimizing mixing losses alone does not guarantee that the overall thermodynamic efficiency is high. A subsequent paper by Xu & Agrawal [15] provides a comprehensive framework that allows detecting the sources of inefficiencies in a cascade and how to mitigate them to enhance the overall thermodynamic efficiency.

Qi & Henson [5] optimized seven configurations with up to three stages for separating CO_2/CH_4. Sensitivities over feed conditions, membrane properties and economic parameters were performed. They found that within some separation regions, either a two-stage or a three-stage cascade with recycle streams lead to the lowest cost. Ahmad et al. [14] carried out sensitivity analysis, using an embedded-user membrane model within HYSYS, to analyze the performance of seven membrane configurations for separating CO_2/CH_4. More specifically, they studied the effect of varying feed conditions and membrane selectivity on the total cost, membrane area, compressor power and methane recovery for each of the simulated configurations to provide guidance on which configuration is the best under a given set of separation conditions.

One of the main disadvantages of analyzing only a few configurations is that one can miss schemes that could be much better, which would result in the design of a sub-optimal separation process. Therefore, to find the most suitable membrane cascade for a given separation, firstly, it is needed to identify, if not all, at least the majority of possible configurations. Agrawal & Xu addressed this problem and provided an easy-to-use method for synthesizing various membrane cascades with n-compressors [4,16]. In summary, this method consists of creating a parent cascade that has the maximum admissible number of stages with only n-compressors. Then, several substructures with lower number of stages are derived from the parental structure by systematically eliminating some of the stages. Whether using this enumeration method or any other similar method, to finally find the configuration that provides the major benefit, it is needed to optimize each of the synthesized configurations.

Pathere & Agrawal followed this approach to design optimum cascades for separating N_2 from the mixture N_2/O_2 [17]. In their work, several configurations with various numbers of stages were derived from a parental cascade known as the Countercurrent Recycle Cascade (CCRC, [18, 19]). Then, for each of the enumerated configurations, two different nonlinear programs (NLP) were formulated and solved. These NLPs, which were solved towards the same objective of minimizing the energy consumption, differ in that one of them restricts the configurations to operate with no mixing losses whereas the other relaxes this constraint. The authors also solved the cascade optimization problem using a third alternative formulation, which in addition to constraining the problem to having no mixing losses, imposes the restriction of having equal set of values for the stage, head and tail separation factors across all the membranes. The results show that when allowing only a few stages, the best configuration operates with mixing losses and with different separation factors across all the stages. Nevertheless, when comparing all the synthesized configurations, ranging from a low to a large number of stages, the configuration that consumes the least energy, which turned out not to have the maximum number of stages explored, but instead, has an

intermediate number of five stages, has almost no mixing losses and nearly constant separation factors across all the membranes. Interestingly, all of the three proposed optimization formulations drive to this optimum cascade and to similar operating conditions, although strictly speaking, the solution obtained from the formulation that allows mixing losses and variable separation factors yields to a slightly lower objective function.

An alternative path to the two-steps procedure of explicit enumeration followed by optimization is to postulate an optimization framework that implicitly enumerates all attractive configurations. This approach requires the formulation, through mathematical constraints, of a superstructure that embeds all the configurations. Then, this superstructure is optimized to find in one step the cascade structure that brings the maximum benefit as well as the optimum operating conditions. As compared to the explicit enumeration, the implicit enumeration approach could be more convenient when the space of possible configurations is large, in which case, optimizing separately each of the enumerated configurations could be computationally more intensive.

Several optimization models which follow the implicit enumeration approach have been reported in the literature [20–26]. For example, Aliaga et al. [20] formulated two MINLP models with the aim of finding the most economical cascade to separate the mixture CO_2/CH_4. Each of these models, which are based on two different master cascades obtained from the method proposed by Agrawal & Xu [16], were solved separately using the SBB algorithm within GAMS [27]. One distinctive feature of this work compared to others is that the optimized superstructures contained a large number of stages (14 stages). This permits to indirectly explore a plethora of substructures with a lower number of stages. Furthermore, the formulated model accounts for different design details such as temperature changes due to permeation across the membranes and to compression. Nevertheless, the accuracy of the obtained solution is questionable since the employed permeator model has some flaws. First,

it assumes that the stage separation factor for all the stages, which was fixed at 24.8, is independent of pressure ratio or stage cut (fraction of the feed that permeates). This implies that for a given inlet concentration, the composition of the permeate is unique, regardless of the trans-membrane pressure ratio or stage cut. However, unless both the downstream pressure and stage cut tend to zero, which is not the case in the separation examples tested in such paper, this assumption is incorrect as permeate composition depends on stage cut and pressure ratio. Furthermore, the component fluxes were assumed to be dependent on the bulk permeate and retentate compositions, but in reality, fluxes depend on the local compositions at the vicinity of the membrane layer, which vary along the membrane length. Thus, this assumption only holds true when the stage cut is very small so that local and bulk compositions are nearly the same. Nevertheless, this situation is not encountered in the tested examples, and most likely would never be encountered in any industrial separation.

Qi & Henson formulated an MINLP to find optimal configurations with minimum cost for the separation of CO_2/CH_4 [21]. Later, in another paper, the authors extended the formulation to multicomponent mixtures [22]. The proposed model was applied to designing cascades for the removal of acid gases from natural gas. Each membrane in the cascade was modeled by assuming a cross-flow pattern that includes the effect of pressure drop due to the bulk flow at the permeate side. The complete permeator model, which was originally given as a system of algebraic differential equations, was converted into a system of algebraic equations through a discretization strategy that combines Gauss-quadrature and fourth order Runge-Kutta-Gill methods. The postulated superstructure includes many possible streams connections that indirectly capture many possible configurations. To be more precise, all permeate and retentate streams have the possibility to be recycled to any stage or to be bypassed and mixed directly with one of the product streams. The optimization problem was solved using the local solver DICOPT ++ [28].

Uppaluri et al. [23] introduced a new superstructure for multicomponent gaseous mixtures that is even more detailed than the superstructure developed by Qi & Henson [22]. In this formulation, the streams not only have different possibilities to be recycled entirely, but they also have the option to be partially distributed to multiple stages. All membranes that compose the cascade were discretized in a series of interconnected compartments which perform small separation tasks. Each compartment was assumed to be perfectly mixed, but the flow pattern between the bulk permeate and retentate streams was allowed to be cross-flow, co-current or counter-current, being modeled these last two patterns as if the membranes were symmetric. Unlike the membrane model of Qi & Henson [22], pressure drop due to bulk flow was not accounted. We note that although the provided formulation considers both retentate and permeate pressures as variables, they were kept constant in the tested examples. Despite the high complexity associated with the high degree of refinement of the superstructure, the optimization problem was successfully solved to minimize the total cost of the proposed cascade network with three stages by using a simulated annealing algorithm. In this algorithm, the structure of the cascade and the flows distribution is changed iteratively by applying stochastic perturbations. In a subsequent paper, Uppalauri et al. [29] proposed a heuristic strategy to decompose the optimization problem in a way that facilitates its solution when both the retentate and permeate pressures are optimized.

Scholz et al. [24] formulated a MINLP with a cost objective function that was applied to design cascades for upgrading biogas. The formulation was given for a general multicomponent gas mixture, but the tested examples correspond only to a binary mixture. The optimization problem was solved using the global optimum solver BARON [30]. However, the authors did not report whether global optimality was guaranteed or not. The proposed superstructure is comparable to that developed by Qi & Henson [22]. Nevertheless, while some features were incorporated in the new network, such as the use of vacuums, other features were disabled, such as

the possibility of recycling retentate streams, or mixing any permeate stream with the final product. Pressures at both permeate and retentate sides were allowed to be optimized. The employed permeator model, which was based on the idealization of counter-current flow pattern for symmetric membranes, was approximated by discretizing each membrane in one hundred elements. Interestingly, the proposed membrane model, which was derived for symmetric membranes operating in counter-current flow pattern, predicts well the separation of CO_2 and H_2S from sour gas mixtures as compared with permeation experiments also carried out under counter-current flow pattern, but using an asymmetrical membrane.

As we observe, a remarkable progress has been achieved in the development of superstructures aimed at finding optimal cascades, some of which are even very sophisticated. However, a challenge still unresolved in most of these works is that the obtained solution from the corresponding optimization problem does not guarantee global optimality. Indeed, with the exception of the work of Bhide & Stern [8], Pathere & Agrawal [17], and possibly Sholz et al. [24] (which does not reveal if global optimality was proved), none of the works cited before guarantee global optimality. In the optimization approach employed by Bhide & Stern [8] the global optimum solution was found by directly exploring the entire feasible region. More specifically, up to three degrees of freedom were discretized and the objective function was evaluated at those points. Pathere & Agrawal [17] followed a similar approach to optimize cascades using a formulation that considers no-mixing losses and equal sets of stage, head and tail separation factors across all membrane stages. Under these constraints, the problem has only one degree of freedom, which was taken as the stage separation factor. This degree of freedom was finely discretized, and the cascade model was solved at each point. To be clearer, for a given value of stage separation factor, a feasible cascade exists with fixed objective function, number of stages, pressure ratios (which can vary stage to stage), flows, and compositions. Although the introduced simplifications help to solve the problem to global optimality, in some cases,

the obtained solution through this formulation can be unattractive from a practical standpoint if it requires more stages or higher pressure ratios than what is practically attainable or economically viable. While an option to resolve this dilemma is to select a suboptimal cascade which requires lower pressure ratios or number of stages, there is no guarantee that such a configuration exists as frequently, the imposed restrictions of no-mixing losses and equal separation factors make unfeasible to operate a cascade with less stages or more restricted pressure ratios. Besides the previous observations, we note that although the optimization approach through a grid search followed by the aforementioned works is computationally inefficient, it was still possible to solve the corresponding problems because the degrees of freedom were restricted to be at most three. Nevertheless, such an optimization technique is clearly impractical for more degrees of freedom as the number of simulations needed to explore the entire feasible region explode combinatorially.

More recently, researchers have proposed alternative formulations for the membrane cascade optimization problem that are more amenable for global optimization using commercial deterministic global optimum solvers. Unfortunately, some of the applied simplifications in these models that seem to facilitate global optimality convergence could significantly compromise the accuracy of the obtained solution in several cases, or if being relaxed, could complicate attaining the global optimum. Adi et al. [31] formulated the first MINLP model applicable to Organic Solven Nanofiltration (OSN) using a superstructure essentially based on that built by Qi & Henson [22], but with some additional stream connections. The model, which was solved to global optimality using the solver BARON [30], was applied to designing a lab process to separate heptane at the maximum possible purity from a mixture of heptane/hexadecane using at most of three stages and a total membrane area of 140 cm^2. To represent the separation that occurs at each membrane, the authors employed a model that assumes perfect mixing at both permeate and retentate sides. This model greatly simplifies the formulated problem as compared to the use of a more rigorous model

like the crossflow model, which is given as a differential algebraic equation system. Nevertheless, while this assumption is reasonable at conditions of small stage cut, such as those typically encountered at lab scale, it is highly unrealistic for most practical stage cut values found at a industrial scale, which are either moderate or high. This is because at non-negligible stage cuts, the local compositions at both permeate and retentate sides are non-uniform, but instead, they vary considerably along the membrane length. Therefore, the postulated optimization model should be used with caution as it could derive in solutions that are far from reality. In this work, we circumvent this limitation by using the cross-flow model which, as compared to the perfect mixing model, is theoretically better supported, and thus, is expected to provide a better accuracy.

The problem of finding optimum cascades for applications of OSN was also addressed by Kunde & Kienle [32] who developed an alternative MINLP model with the objective of minimizing the "separation effort", which is a surrogate of the overall energy consumed by a cascade. The formulation was generalized for multicomponent liquid mixtures, but the model was tested only for the binary separation of decane/hexacosane using a three-stage cascade. The cross-flow model was employed for each of the membranes that comprise the cascade. To incorporate the algebraic differential equations (DEA) that compose this model into the optimization framework, the authors used a discretization approach which assumes linear flux profiles at each of the discretization elements. For the tested separation of decane/hexacosane, only one discretization element was employed for each membrane in the cascade. The resulting MINLP was solved to global optimality for different values of selectivity and feed composition using the global optimum solver BARON [33]. The pressure difference across each membrane was not optimized. An important observation that should be noted is that the feed compositions that were evaluated are atypical to those found in most separations in chemical and petrochemical plants. This is because the considered feed streams were already enriched in the most permeable component (>

99% mol decane). Under this situation, the degree of purification relative to the feed is very small, which makes reasonable to use only one discretization element for the membrane model and to assume linear flux profiles along the entire membrane length. Nevertheless, for other separation conditions, the number of discretization elements needed to maintain a reasonable accuracy in the solution might me much higher. To illustrate this, consider a liquid feed of 50%/50% of p-xylene/o-xylene at 30°C that is passed through a membrane that operates with a trans-membrane pressure difference of 50 bar and a stage cut of 0.99. In this case, more than 10 discretization elements would be needed to predict the permeate composition with less than 10% of error as compared to the analytical solution of the cross-flow model. The disadvantage of employing many discretization elements is that the number of associated variables and non-linear constraints with non-convex nature increases, which in the worse case, could prevent BARON to reach global optimality convergence within a reasonable amount of time.

In this study we propose a novel formulation for the membrane cascade optimization problem with the objective of minimizing the energy consumption. The problem was formulated as a Mixed Integer Non-linear Program (MINLP) based on a superstructure that embeds several meaningful connections. We note that to the best of our knowledge, this is the first unified optimization model that is applicable for both liquid and gaseous binary separations. In our formulation, we employed the cross-flow membrane model in combination with the solution-diffusion theory to represent the separation that occurs at each membrane in the superstructure. These models have exhibited good accuracy in the prediction of the separation of diverse liquid and gaseous mixtures through dense membranes [34–38]. To get rid off of the errors that could arise from the discretization of the DAE that compose the cross-flow model, and which could compromise the obtained solution, we integrate analytically the differential model and incorporate the resulting solution in our optimization framework. Although this approach reduces the number of non-convex constraints as compared to

a fine discretization of the differential model, the solution of the complete optimization problem is still challenging due to the non-convexities of the objective function, mass balance constraints, and the permeator model itself. To expedite global optimality convergence with deterministic global optimum solvers we derive several additional linear and non-linear cuts that help to improve the constructed relaxation. The resulting formulation was successfully solved to global optimality, within a 5% of duality gap, for several separation examples. All tested cases were solved using the global optimum solver BARON v18.5.8 [33] within the software GAMS v25.1.

The rest of this chapter is outlined as follows: in section three, we discuss the single stage membrane model that we employed in the proposed optimization framework. Then, in section four, we present the proposed superstructure and the optimization formulation. Furthermore, in this section, we tested the performance of the proposed formulation using several separation cases taken from the literature. In section five, we illustrate the application of our optimization model with some study cases that are discussed in detail. Finally, in section six, we present some concluding remarks.

1.3 Single stage membrane model

In this section, we describe a unified shortcut model for the permeation process employing dense membranes. The model is applicable for both gaseous and liquid mixtures. In addition, we validate the model with experimental data for the separation of O_2/N_2 and CO_2/CH_4 mixtures. In the rest of the article, we denote the most and the least permeable components as A and B, respectively. Further, we denote the separation of a binary mixture AB as A/B. We use the solution-diffusion theory [39] to model the local flux of each component through the membrane, and the *crossflow model*, proposed by Weller and Steiner [40, 41], to model the overall permeation process.

For both gaseous and liquid mixtures, the solution-diffusion theory is the widely-accepted mechanism of mass transfer through dense polymeric membranes [39]. According to this theory, the constituent components of the mixture are separated due to their differences in solubility and diffusivity within the membrane. Depending on the type of the mixture, the local flux of each component through the membrane can be obtained using the equations below [39].

$$\text{For liquids,} \quad \begin{cases} n_A = PM_A \left[x - y \exp\left(-\dfrac{V_A(P^{\text{ret}} - P^{\text{per}})}{RT} \right) \right] \\ n_B = PM_B \left[(1-x) - (1-y) \exp\left(-\dfrac{V_B(P^{\text{ret}} - P^{\text{per}})}{RT} \right) \right] \end{cases}, \tag{1.1a}$$

$$\text{For gases,} \quad \begin{cases} n_A = PM_A \left[P^{\text{ret}} x - P^{\text{per}} y \right] \\ n_B = PM_B \left[P^{\text{ret}} (1-x) - P^{\text{per}} (1-y) \right] \end{cases}, \tag{1.1b}$$

where n_A, PM_A and V_A (*resp.* n_B, PM_B and V_B) correspond to the local flux, permeance and molar volume of A (*resp.* B). x and P^{ret} (*resp.* y and P^{per}) denote the local mole fraction of A and the total pressure on the retentate (*resp.* permeate) side. Lastly, R and T denote the universal gas constant and the absolute temperature of the mixture. Note that the term inside the square brackets in both (1.1a) and (1.1b) corresponds to the driving force. To develop a unified model, we define the following variables:

$$u = \begin{cases} \ln r, & \text{for a gaseous mixture} \\ \Delta P^{trans}, & \text{for a liquid mixture} \end{cases}, \tag{1.2a}$$

$$\beta = \begin{cases} 1, & \text{for a gaseous mixture} \\ 0, & \text{for a liquid mixture} \end{cases}, \tag{1.2b}$$

$$C_A = \begin{cases} 1, & \text{for a gaseous mixture} \\ V_A/RT, & \text{for a liquid mixture} \end{cases}, \tag{1.2c}$$

$$C_B = \begin{cases} 1, & \text{for a gaseous mixture} \\ V_B/RT, & \text{for a liquid mixture} \end{cases}, \tag{1.2d}$$

where $r = P^{\text{ret}}/P^{\text{per}}$ is the pressure ratio, and $\Delta P^{trans} = P^{\text{ret}} - P^{\text{per}}$ is the trans-membrane pressure difference. We now express (1.1a) and (1.1b) in terms of u, β, C_A and C_B as

$$n_A = PM_A(P^{\text{ret}})^{\beta}\left[x - y\,\mathrm{e}^{(-C_A\,u)}\right], \tag{1.3a}$$

$$n_B = PM_B(P^{\text{ret}})^{\beta}\left[(1-x) - (1-y)\,\mathrm{e}^{(-C_B\,u)}\right]. \tag{1.3b}$$

Figure 1.1 shows a schematic of the permeation process employing a cross-flow pattern. Here, it is assumed that the permeate travels perpendicularly to the membrane. In addition, we make the following assumptions:

1. The pressure drop along the membrane module due to the bulk flow of both permeate and retentate streams is negligible.

2. Concentration polarization does not occur near the surface of the membrane.

3. There is no mass transfer resistance in the bulk permeate and retentate streams.

4. The separation takes place isothermally.

5. Membrane selectivity is independent of the operating pressure and the composition of the mixture.

As a result, the composition in the vicinity of the dense membrane varies only in the feed flow direction on both permeate and retentate sides. We remark that for small values of pressure drop on both retentate and permeate sides, the degree of separation obtained through an asymmetric dense membrane employing cross-flow pattern is close to that obtained for co-current (see Figure 1.2(a)) or counter-current flow patterns (see Figure 1.2(b)) [36]. This is because, the porous layer prevents axial mixing of the local permeate just out of the dense layer. Consequently, the

flux profiles and the net separation remains the same regardless of the flow pattern. Therefore, our model is also applicable for asymmetrical dense membranes operating in co-current or counter-current flow pattern, provided the pressure drop on both permeate and retentate sides is small.

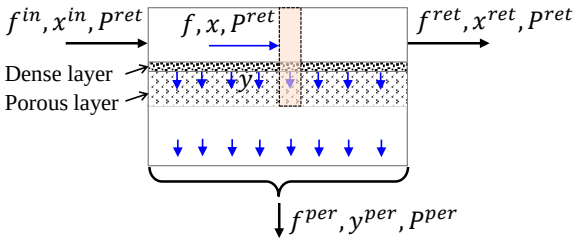

Fig. 1.1. Conceptual representation of crossflow pattern

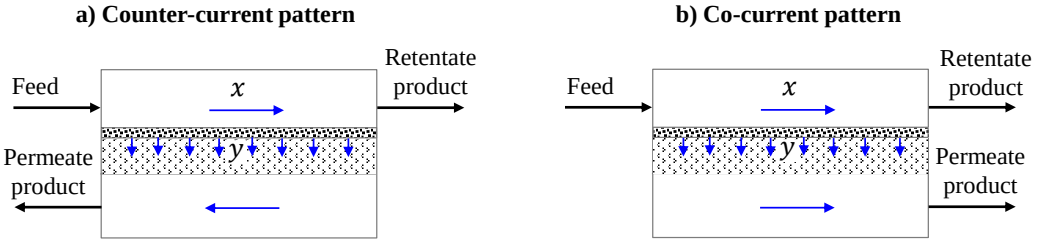

Fig. 1.2. Permeation across an asymmetrical membrane under counter-current and co-current flow patterns. The local composition out of the dense layer (y) as well as the local retentate composition (x) are independent on the flow pattern.

Let the flowrate, pressure and composition of the mixture entering the membrane module be f^{in}, P^{ret}, and x^{in}, respectively. Consider a differential control volume as shown in Figure 1.1 (orange box). Mass balance of component A across the control volume is given by $d(fx) = y\,df$, where x (*resp.* y) corresponds to the local mole fraction of component A on retentate (*resp.* permeate) side, and f corresponds to the

local flowrate of the bulk retentate. The mass balance equation can be rearranged as follows:

$$\frac{dx}{df} = \frac{y-x}{f}, \quad x(f^{\text{in}}) = x^{\text{in}}, \quad f \in [f^{\text{in}}, f^{\text{ret}}], \tag{1.4}$$

where $x(f^{\text{in}}) = x^{\text{in}}$ is the initial condition, and f^{ret} denotes the net flowrate of the retentate leaving the membrane module. Since there is no axial mixing in the porous layer, the local mole fraction of each component on the permeate side is simply the ratio of the local flux of the component to the total local flux *i.e.*, $y = n_A/(n_A + n_B)$ and $(1-y) = n_B/(n_A+n_B)$. Since both the equations are linearly dependent, we use only the former. We substitute n_A and n_B from (1.3) and rearrange to obtain

$$y - x = k + k(S-1)y - \frac{k\,S}{S-(S-1)y}, \tag{1.5}$$

where $S = PM_A/PM_B$ is the selectivity of component A w.r.t component B and

$$k = \frac{(S-1) - \left(S\,\mathrm{e}^{(-C_A\,u)} - \mathrm{e}^{(-C_B\,u)}\right)}{(S-1)^2}. \tag{1.6}$$

We express equation (1.4) as a differential equation in y using (1.5) and solve the resulting equation analytically to obtain

$$S \ln \frac{y^{\text{out}}}{y^{\text{in}}} - \ln \frac{1-y^{\text{out}}}{1-y^{\text{in}}} - k(S-1)^2 \ln \frac{y^{\text{out}} - x^{\text{ret}}}{y^{\text{in}} - x^{\text{in}}} = k(S-1)^2 \ln(1-\theta), \tag{1.7}$$

where $y^{\text{in}} = y(f^{\text{in}})$, $y^{\text{out}} = y(f^{\text{ret}})$, $x^{\text{ret}} = x(f^{\text{ret}})$, and stage cut $\theta = (f^{\text{in}} - f^{\text{ret}})/f^{\text{in}}$. Mole fractions y^{in} and y^{out} are related to x^{in} and x^{ret} via (1.5) *i.e.*,

$$y^{\text{in}} - x^{\text{in}} = k + k(S-1)y^{\text{in}} - \frac{k\,S}{S-(S-1)y^{\text{in}}}, \tag{1.8}$$

$$y^{\text{ret}} - x^{\text{ret}} = k + k(S-1)y^{\text{ret}} - \frac{k\,S}{S-(S-1)y^{\text{ret}}}. \tag{1.9}$$

Therefore, given f^{in}, x^{in}, r (or *resp.* ΔP^{trans}), and stage cut θ, the mole fraction of component A in the retentate, x^{ret}, is determined from (1.7)–(1.9). Then, the mole

fraction of component A in the permeate, y^{per}, is obtained from the overall component mass balance $f^{\text{in}}x^{\text{in}} = f^{\text{ret}}x^{\text{ret}} + f^{\text{per}}y^{\text{per}}$, where $f^{\text{per}} = f^{\text{in}}\theta = f^{\text{in}} - f^{\text{ret}}$.

We now show the validity of the model by comparing the predicted permeate and retentate mole fractions as a function of stage cut against the experimental data for O_2/N_2 and CO_2/CH_4 separations in Figures 1.3 and 1.4, respectively. In the Figures, we also show the predictions from the *perfect mixing model* [40], which is obtained by making the additional simplifying assumption that the mixture on the retentate side is perfectly mixed. Clearly, there is a very good agreement between the cross-flow model ((1.7) –(1.9)) and the experimental data for both the mixtures. On the other hand, the perfect mixing model always underestimates the composition of the retentate and the permeate streams leaving the membrane module. Therefore, the optimization results obtained using (1.7)–(1.9) as the permeator model are more reliable than those obtained using the perfect mixing model.

To the best of our knowledge, experimental data for the composition of the permeate and retentate streams as a function of stage cut is not avaliable for liquid mixtures in the literature. Nevertheless, for some liquid mixtures, a very good agreement was observed [37, 38] between the local flux determined using (1.3) and the experimental value. Although this is not sufficient to validate (1.7)–(1.9) for liquid mixtures, we believe that the predictions of the retentate and permeate compositions are reliable based on the agreement for fluxes.

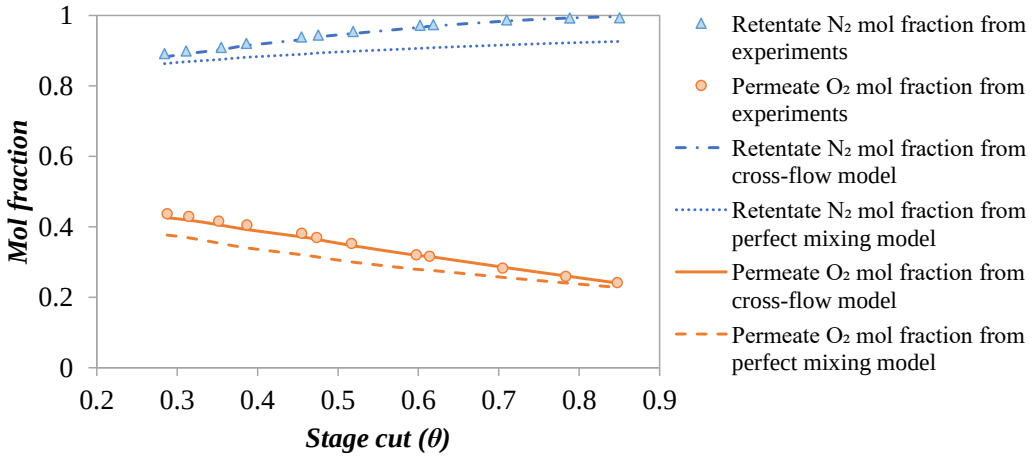

Fig. 1.3. Comparison between experimental data for the separation of O_2/N_2 [34] and the predictions obtained from crossflow model and the perfect mixing model. Here, $P^{\text{ret}}/P^{\text{per}} = 7.83$ bar$/0.93$ bar $= 8.4$, $x^{\text{in}}_{O_2} = 0.205$, membrane permselectivity, $S = 5.3$ (calculated based on the average values of component permeances reported in [34]).

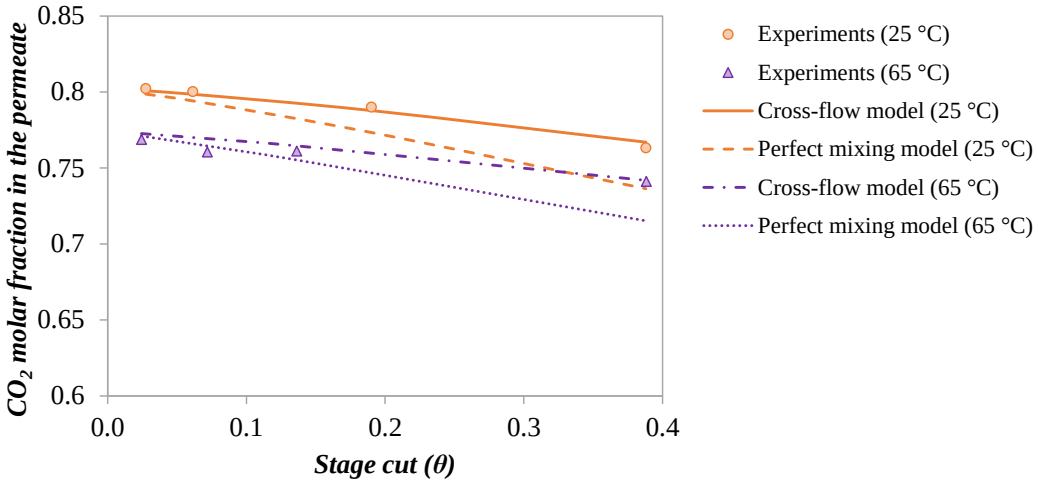

Fig. 1.4. Comparison between experimental data for the separation of CO_2/CH_4 [35] and the predictions obtained from the cross-flow model and the perfect mixing model. Here, $P^{\text{ret}}/P^{\text{per}} = 4.05$ bar$/1.01$ bar $= 4$, $x^{\text{in}}_{CO_2} = 0.60$, the membrane permselectivity at 25 °C is: 3.58, and the membrane permselectivity at 65 °C is: 2.9 [35].

1.4 Problem Formulation

The required input to the problem consists of (1) molar flowrate and composition of the feed and product streams, (2) efficiencies of compressors and turbines/pumps and turbochargers, (3) membrane perm-selectivity, (4) the range of admissible operating pressure ratio/trans-membrane pressure difference, (5) temperature of the mixture, and (6) molar volume of constituent components for liquid mixtures (see Table 1.1). Given a binary mixture along with all the required inputs, the problem is then to identify the membrane cascade requiring at most N stages that consumes the least energy for the separation.

1.4.1 Membrane cascade superstructure

Figure 1.5 (*resp.* Figure 1.6) shows a superstructure consisting of various membrane cascades that utilize at most four membrane stages (*i.e.*, $N = 4$) for the separation of a gaseous (*resp.* liquid) mixture. We use superstructures similar to the one in Figure 1.5 (*resp.* Figure 1.6) for all gaseous (*resp.* liquid) separations considered in this work. We refer the product stream withdrawn from $\mathcal{P}$ (*resp.* from stage N) as the *permeate* (*resp. retentate*) *product stream*.

Throughout the article, we assume that the given gaseous mixture is available at a high pressure and both permeate and retentate product streams are desired at the same pressure as the feed mixture. However, if the gaseous mixture is not available at a high pressure, then an additional compressor is included in the superstructure to compress the feed. Similarly, if the product streams are not needed to be withdrawn at a high pressure, the compressor for the permeate product is eliminated and then a turbine is included in the superstructure to lower the pressure of the retentate product stream and recover energy from it.

Table 1.1.

List of parameters

Symbol	**Definition**
N	Maximum number of stages in the cascade
F, F^{per}, F^{ret}	Molar flowrate of the given feed mixture, permeate product, and retentate product streams, respectively
X^F, Y^{per}, X^{ret}	Mole fraction of component A in the feed mixture, permeate product, and retentate product streams, respectively
E^{comp}	Isothermal compressor efficiency
E^{pump}	Pump efficiency
E^{TC}	Turbocharger efficiency
V_A, V_B	Liquid molar volume of components A and B, respectively (Needed only for liquid mixtures)
T	Absolute temperature of the feed mixture
S	Membrane permselectivity (PM_A/PM_B)
$[r^{\text{lo}}, r^{\text{up}}]$	Admissible range of trans-membrane pressure ratio for a gaseous mixture
$[(\Delta P^{trans})^{\text{lo}}, (\Delta P^{trans})^{\text{up}}]$	Admissible range of trans-membrane pressure difference for a liquid mixture

On the other hand, we assume that the given liquid mixture is always available at a low pressure. We increase the pressure of the feed mixture to an intermediate value using a pump (see Figure 1.6). The feed mixture is then sent to a turbocharger where it is further pressurized to the desired pressure, by transferring the energy released due to the expansion of the retentate product stream (see Figure 1.6).

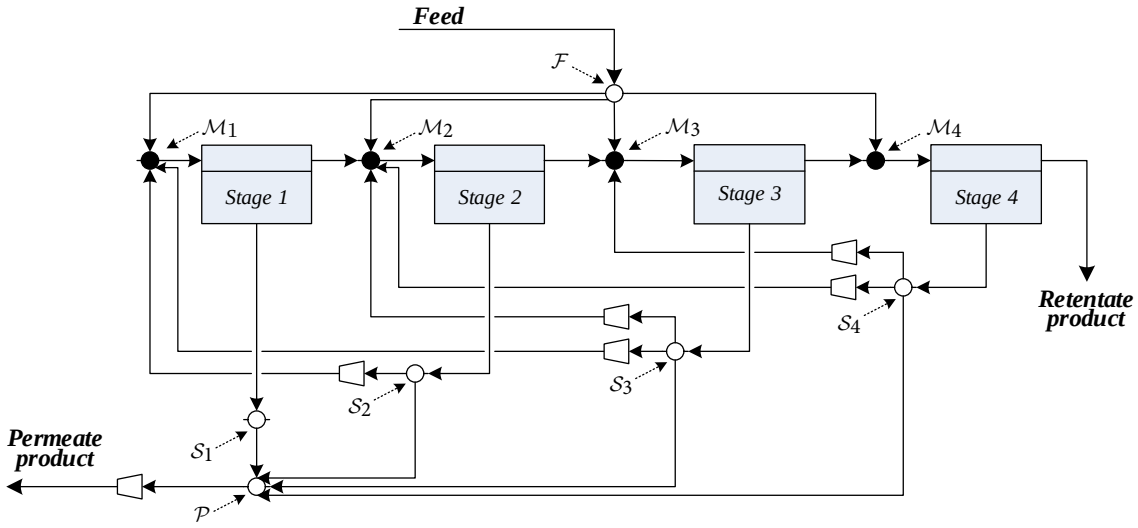

Fig. 1.5. Selected cascade superstructure for the tested separations in gaseous phase

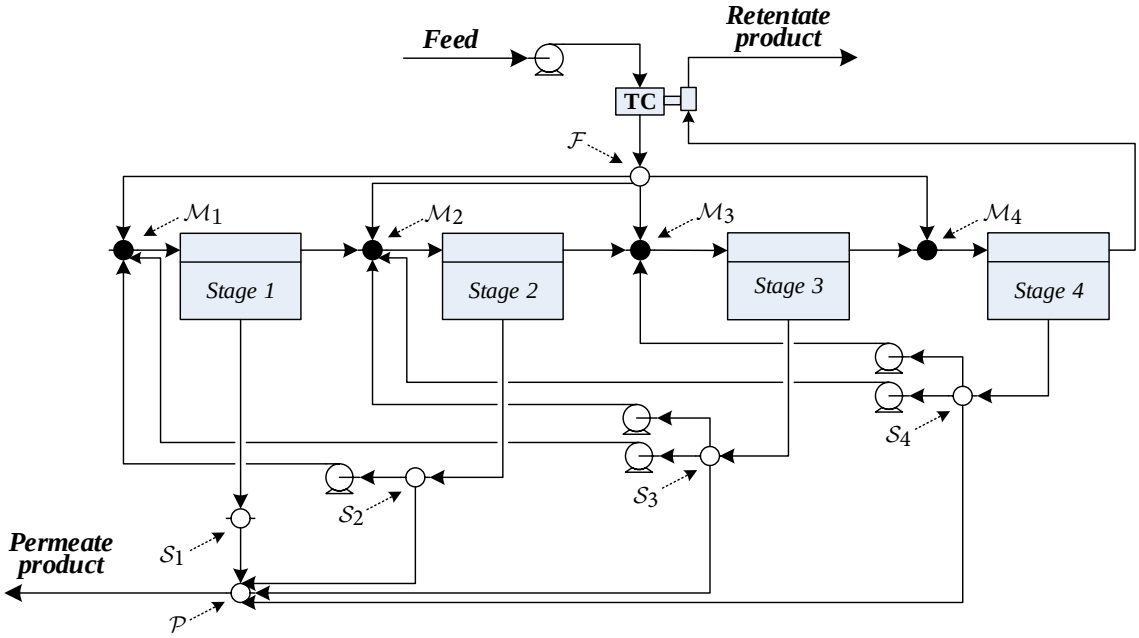

Fig. 1.6. Selected cascade superstructure for the tested separations in liquid phase

The splitter $\mathcal{F}$ (see Figures 1.5-1.6) splits the feed mixture into N streams which are sent to mixers $\mathcal{M}_1$ through $\mathcal{M}_N$. Each mixer $\mathcal{M}_j$ supplies the feed to membrane stage j after mixing the retentate stream from membrane stage $j-1$ and the streams from splitters $\mathcal{F}$, $\mathcal{S}_{j+1}$ and $\mathcal{S}_{j+2}$. The retentate from stage j is sent to mixer $\mathcal{M}_{j+1}$, while the permeate is sent to splitter $\mathcal{S}_j$. Except for $\mathcal{S}_1$ and $\mathcal{S}_2$, each $\mathcal{S}_j$ splits the corresponding permeate stream into three streams which are sent to $\mathcal{M}_{j-1}$, $\mathcal{M}_{j-2}$, and $\mathcal{P}$. $\mathcal{S}_2$ produces only two streams which are sent to $\mathcal{M}_1$ and $\mathcal{P}$. Whereas, $\mathcal{S}_1$ produces only one ouptut stream which is sent to $\mathcal{P}$. All the flows collected at mixer $\mathcal{P}$ forms the final permeate product. Lastly, we impose the following additional restrictions to seek solutions that are more attractive for practical implementation. We require that the feed mixture is sent entirely to one mixer *i.e.*, only one of the arcs originating from splitter $\mathcal{F}$ contains nonzero material flow. Further, we restrict that the permeate stream from each membrane stage is either recycled completely to one of the mixers, or it is withdrawn to be part of the permeate product. In other words, at most one of the arcs originating from splitter $\mathcal{S}_j$ contains nonzero material flow.

In this work, we restrict our attention to those separations where the permeate product stream recovers moderate or high amount ($\geq 80\%$) of the most permeable component at moderate or high purity ($\geq 70\%$). We refer to such separations as *moderate/high purity-moderate/high recovery separations*.

We caution the reader that our superstructure does not contain an exhaustive list of membrane cascades. For instance, the cascade shown in Figure 1.7 is not included in our superstructure. We conjecture that such cascades are not energetically attractive for moderate/high purity-moderate/high recovery separations, so we do not consider them in this work. When needed, inclusion of such cascades in the superstructure is straightforward.

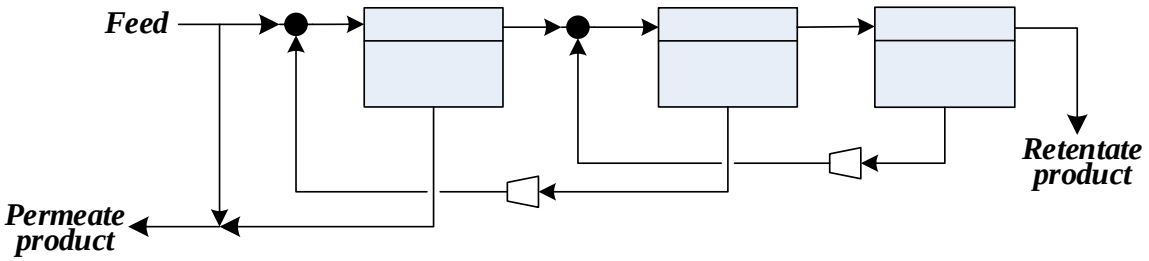

Fig. 1.7. Instance of a membrane cascade that is not included in our superstructure

1.4.2 Objective function

Figure 1.8 shows a representative unit of the superstructure. The definition of variables in Figure 1.8 can be found in Table 1.2. Let N denote the maximum number of membrane stages allowed in a cascade.

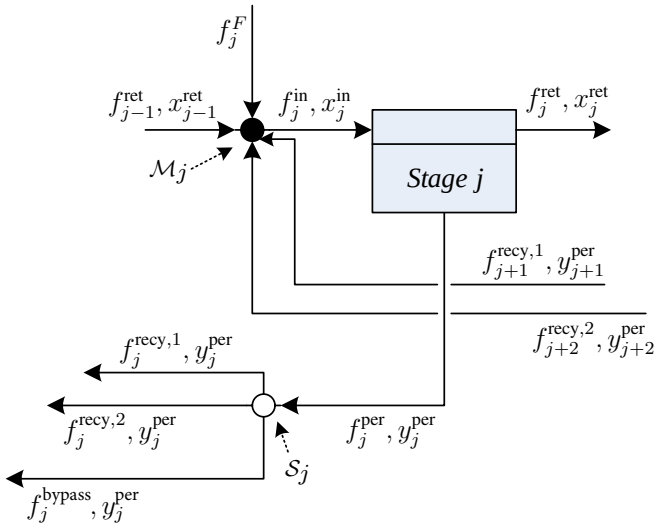

Fig. 1.8. A representative membrane module in the superstructure.

Table 1.2.

List of variables

Symbol	**Definition**
u	Auxiliary variable defined in (1.2a)
k	Auxiliary variable defined in (W12)
f_j^F	Molar flow rate along the arc connecting $\mathcal{F}$ and $\mathcal{M}_j$
f_j^{in}	Molar flow rate entering stage j from $\mathcal{M}_j$
f_j^{ret}	Molar flow rate of the retentate stream leaving stage j
f_j^{per}	Molar flow rate of the permeate stream leaving stage j
$f_j^{\text{recy},p}$	Molar flow rate along the arc connecting $\mathcal{M}_{j-p}$ and $\mathcal{S}_j$, $p = 1, 2$
f_j^{bypass}	Molar flow rate along the arc connecting $\mathcal{P}$ and $\mathcal{S}_j$
x_j^{in}	Mole fraction of component A in the inlet stream to stage j
x_j^{ret}	Mole fraction of component A in the retentate stream leaving stage j
y_j^{per}	Mole fraction of component A in the permeate stream leaving stage j
y_j^{in}	Local mole fraction of component A at the entrance of stage j on permeate side
y_j^{out}	Local mole fraction of component A at the exit of stage j on permeate side
$z_j^{\text{in}},\ z_j^{\text{out}}$	Auxiliary variables defined in (W14)
θ_j	Stage cut of stage j
ω_j^F	Binary variable introduced to regulate the flow along the arc connecting $\mathcal{F}$ and $\mathcal{M}_j$
$\omega_j^{\text{recy},p}$	Binary variable introduced to regulate the flow along the arc connecting $\mathcal{M}_{j-p}$ and $\mathcal{S}_j$, $p = 1, 2$
ω_j^{bypass}	Binary variable introduced to regulate the flow along the arc connecting $\mathcal{P}$ and $\mathcal{S}_j$

First, consider the separation of a gaseous mixture. In this case, the energy input is required to compress the outlet streams from splitters $\mathcal{S}_j$ to $r-$times its pressure (see Figure 1.5). We assume the compressor has an isothermal efficiency of E^{comp}. Then, the net power required for the cascade is,

$$W_G = \frac{RT}{E^{comp}} \left(\sum_{j=2}^{N} f_j^{\text{recy},1} + \sum_{j=3}^{N} f_j^{\text{recy},2} + \sum_{j=1}^{N} f_j^{\text{bypass}} \right) \ln r. \tag{1.10}$$

Next, consider the separation of a liquid mixture. We assume that the feed mixture and the product streams are at pressure P^{per}. In this case, the energy is supplied to pump the feed mixture from P^{per} to an intermediate pressure P^{TC}, and to pump the streams connecting $\mathcal{S}_j$ and mixers $\mathcal{M}_{j-1}$ and $\mathcal{M}_{j-2}$, for $j = 2, \ldots, N$, from P^{per} to P^{ret}. Thus, the net power required for the cascade,

$$W_L = \underbrace{\frac{V_{mix}}{E^{pump}} F \left(P^{TC} - P^{\text{per}}\right)}_{\text{to pump the feed}} + \underbrace{\frac{V_{mix}}{E^{pump}} \left[\sum_{j=2}^{N} f_j^{\text{recy},1} \left(P^{\text{ret}} - P^{\text{per}}\right) + \sum_{j=3}^{N} f_j^{\text{recy},2} \left(P^{\text{ret}} - P^{\text{per}}\right) \right]}_{\text{to pump the recycle streams}}, \tag{1.11}$$

where $V_{mix} = (V_A + V_B)/2$ and E^{pump} denote the average molar volume of the mixture and the pump efficiency, respectively. As mentioned earlier, the turbocharger pressurizes the feed further from P^{TC} to P^{ret} and expands the retentate product stream from P^{ret} to P^{per}. Let, E^{TC} denote the efficiency of the turbocharger. Then,

$$V_{mix}\, F \left(P^{\text{ret}} - P^{TC}\right) = E^{TC}\, V_{mix}\, f_N^{\text{ret}} \left(P^{\text{ret}} - P^{\text{per}}\right), \tag{1.12}$$

where the LHS denotes the work needed to pressurize the feed mixture, and the RHS excluding E^{TC} denotes the work produced due to the expansion of the retentate product stream. We substitute P^{TC} from (1.12) in (1.11) to obtain

$$W_L = \frac{V_{mix}}{E^{pump}} \left(F\,\Delta P^{trans} - E^{TC} f_N^{\text{ret}}\,\Delta P^{trans} + \sum_{j=2}^{N} f_j^{\text{recy},1}\,\Delta P^{trans} + \sum_{j=3}^{N} f_j^{\text{recy},2}\,\Delta P^{trans} \right). \tag{1.13}$$

From (1.10) and (1.13), we obtain a unified objective function that is applicable for both gaseous and liquid mixtures using (1.2a) as $D_0 u + D_1 \sum_{j=1}^{N} f_j^{\text{bypass}} \cdot u + \sum_{j=2}^{N} D_j f_j^{\text{recy},1} \cdot u + \sum_{j=3}^{N} D_j f_j^{\text{recy},2} \cdot u + D_{N+1} f_N^{\text{ret}} \cdot u$, where

$$D_0 = \begin{cases} 0, & \text{for a gaseous mixture} \\ \frac{V_{mix}\,F}{E^{pump}}, & \text{for a liquid mixture} \end{cases} \tag{1.14a}$$

$$D_1 = \begin{cases} \frac{RT}{E^{comp}}, & \text{for a gaseous mixture} \\ 0, & \text{for a liquid mixture} \end{cases} \tag{1.14b}$$

$$D_j = \begin{cases} \frac{RT}{E^{comp}}, & \text{for a gaseous mixture} \\ \frac{V_{mix}}{E^{pump}}, & \text{for a liquid mixture} \end{cases}, \quad j = 2, \ldots, N \tag{1.14c}$$

$$D_{N+1} = \begin{cases} 0, & \text{for a gaseous mixture} \\ -\frac{V_{mix}\,E^{TC}}{E^{pump}}, & \text{for a liquid mixture} \end{cases} \tag{1.14d}$$

1.4.3 MINLP formulation

Here, we present our mixed-integer nonlinear program (W) for identifying the optimal membrane cascade requiring at most N membrane stages. Consider the representative structure shown in Figure 1.8. Let $\mathcal{J} = \{1, \ldots, N\}$, and $\mathcal{K} = \mathcal{J} \setminus \{1\} = \{2, \ldots, N\}$. In the following, acronyms OMB and CMB stand for overall mass balance and mass balance of component A, $\delta_{(\cdot)} = \{1,$ if $(\cdot)$ is true; $0,$ otherwise$\}$, $(\cdot)^{\text{lo}}$ and $(\cdot)^{\text{up}}$ denote the lower and upper bounds on $(\cdot)$.

$$
\begin{aligned}
(\mathrm{W}): \quad \min \quad & D_0 u + D_1 \sum_{j=1}^{N} f_j^{\mathrm{bypass}} \cdot u + \sum_{j=2}^{N} D_j f_j^{\mathrm{recy},1} \cdot u \\
& + \sum_{j=3}^{N} D_j f_j^{\mathrm{recy},2} \cdot u + D_{N+1} f_N^{\mathrm{ret}} \cdot u, && \text{(Obj. Fun.)} \quad \text{(W1)} \\
\text{s.t.} \quad & \sum_{j=1}^{N} f_j^F = F, && \text{(OMB around } \mathcal{F}\text{)} \\
& && \text{(W2)} \\
\forall\, j \in \mathcal{J}, \quad & f_j^{\mathrm{in}} = f_{j-1}^{\mathrm{ret}} \delta_{j\geq 2} + f_{j+1}^{\mathrm{recy},1} \delta_{j\leq N-1} + f_{j+2}^{\mathrm{recy},2} \delta_{j\leq N-2} + f_j^F, && \text{(OMB around } \mathcal{M}_j\text{)} \\
& && \text{(W3)} \\
\forall\, j \in \mathcal{J}, \quad & f_j^{\mathrm{in}} x_j^{\mathrm{in}} = f_{j-1}^{\mathrm{ret}} x_{j-1}^{\mathrm{ret}} \delta_{j\geq 2} + f_{j+1}^{\mathrm{recy},1} y_{j+1}^{\mathrm{per}} \delta_{j\leq N-1} \\
& + f_{j+2}^{\mathrm{recy},2} y_{j+2}^{\mathrm{per}} \delta_{j\leq N-2} + f_j^F X^F, && \text{(CMB around } \mathcal{M}_j\text{)} \\
& && \text{(W4)} \\
\forall\, j \in \mathcal{J}, \quad & f_j^{\mathrm{per}} = f_j^{\mathrm{recy},1} \delta_{j\geq 2} + f_j^{\mathrm{recy},2} \delta_{j\geq 3} + f_j^{\mathrm{bypass}}, && \text{(OMB around } \mathcal{S}_j\text{)} \\
& && \text{(W5)} \\
\forall\, j \in \mathcal{J}, \quad & f_j^{\mathrm{per}} y_j^{\mathrm{per}} = f_j^{\mathrm{recy},1} y_j^{\mathrm{per}} \delta_{j\geq 2} + f_j^{\mathrm{recy},2} y_j^{\mathrm{per}} \delta_{j\geq 3} + f_j^{\mathrm{bypass}} y_j^{\mathrm{per}}, && \text{(CMB around } \mathcal{S}_j\text{)} \\
& && \text{(W6)} \\
\forall\, j \in \mathcal{J}, \quad & f_j^{\mathrm{in}} = f_j^{\mathrm{per}} + f_j^{\mathrm{ret}}, && \text{(OMB around stage } j\text{)} \\
& && \text{(W7)} \\
\forall\, j \in \mathcal{J}, \quad & f_j^{\mathrm{in}} x_j^{\mathrm{in}} = f_j^{\mathrm{per}} y_j^{\mathrm{per}} + f_j^{\mathrm{ret}} x_j^{\mathrm{ret}}, && \text{(CMB around stage } j\text{)} \\
& && \text{(W8)} \\
& f_N^{\mathrm{ret}} = F^{\mathrm{ret}},\ x_N^{\mathrm{ret}} = X^{\mathrm{ret}} && \text{(Retentate product)} \\
& && \text{(W9)} \\
& \sum_{j=1}^{N} f_j^{\mathrm{bypass}} = F^{\mathrm{per}} && \text{(OMB around } \mathcal{P}\text{)} \\
& && \text{(W10)} \\
& \sum_{j=1}^{N} f_j^{\mathrm{bypass}} y_j^{\mathrm{per}} = F^{\mathrm{per}} Y^{\mathrm{per}} && \text{(CMB around } \mathcal{P}\text{)} \\
& && \text{(W11)}
\end{aligned}
$$

$$(S-1)^2 k = (S-1) - \left(S e^{-C_A u} - e^{-C_B u}\right), \qquad \text{(Definition of } k\text{)} \tag{W12}$$

$$\forall\, j \in \mathcal{J}, \quad f_j^{\text{per}} = \theta_j f_j^{\text{in}}, \qquad \text{(Stage cut)} \tag{W13}$$

$$\left.\begin{aligned} & S \ln y_j^{\text{out}} - S \ln y_j^{\text{in}} - \ln(1 - y_j^{\text{out}}) + \ln(1 - y_j^{\text{in}}) \\ & - (S-1)^2 (k \ln z_j^{\text{out}}) + (S-1)^2 (k \ln z_j^{\text{in}}) \\ & = (S-1)^2 \left[k \ln(1-\theta_j)\right], \\ & z_j^{\text{in}} = y_j^{\text{in}} - x_j^{\text{in}}, \\ & z_j^{\text{out}} = y_j^{\text{out}} - x_j^{\text{ret}}, \\ & k + (S-1)(k y_j^{\text{in}}) - S\left[\frac{k}{S-(S-1)y_j^{\text{in}}}\right] = z_j^{\text{in}}, \\ & k + (S-1)(k y_j^{\text{out}}) - S\left[\frac{k}{S-(S-1)y_j^{\text{out}}}\right] = z_j^{\text{out}}, \end{aligned}\right\} \quad \forall\, j \in \mathcal{J}, \qquad \text{(Permeator Model)} \tag{W14}$$

$$\left.\begin{aligned} & 0 \le (\cdot) \le (\cdot)^{\text{up}}, \quad \forall\, (\cdot) \in \left\{ f_j^F, f_j^{\text{in}}, f_j^{\text{ret}}, f_j^{\text{per}}, \right. \\ & \qquad\qquad \left. f_j^{\text{recy},1}, f_j^{\text{recy},2}, f_j^{\text{bypass}} \right\} \\ & (\cdot)^{\text{lo}} \le (\cdot) \le (\cdot)^{\text{up}}, \quad \forall\, (\cdot) \in \left\{ u, k, \theta_j, x_j^{\text{in}}, x_j^{\text{ret}}, \right. \\ & \qquad\qquad \left. y_j^{\text{per}}, y_j^{\text{in}}, y_j^{\text{out}}, z_j^{\text{in}}, z_j^{\text{out}} \right\} \end{aligned}\right\} \quad \forall\, j \in \mathcal{J}, \qquad \text{(Bounds on variables)} \tag{W15}$$

$$\sum_{j=1}^{N} \omega_j^F = 1, \quad \omega_j^F \in \{0,1\}, \quad \forall\, j \in \mathcal{J}, \tag{W16}$$

$$\forall\, j \in \mathcal{J}, \quad f_j^F \le \omega_j^F (f_j^F)^{\text{up}}, \tag{W17}$$

$$\left.\begin{aligned} & \omega_j^{\text{recy},1} \delta_{j\ge 2} + \omega_j^{\text{recy},2} \delta_{j \ge 3} + \omega_j^{\text{bypass}} = 1, \\ & \omega_j^{\text{recy},1} \in \{0,1\}, \quad \omega_j^{\text{recy},2} \in \{0,1\}, \quad \omega_j^{\text{bypass}} \in \{0,1\} \end{aligned}\right\} \quad \forall\, j \in \mathcal{J}, \tag{W18}$$

$$\forall\, j \in \mathcal{K}, \quad f_j^{\text{recy},p} \le \omega_j^{\text{recy},p} (f_j^{\text{recy},p})^{\text{up}}, \quad p = 1, 2. \tag{W19}$$

$$\forall\, j \in \mathcal{J}, \quad f_j^{\text{bypass}} \le \omega_j^{\text{bypass}} (f_j^{\text{bypass}})^{\text{up}}, \; \omega_j^{\text{bypass}} = 0 \; \forall j > 2 \tag{W20}$$

The formulation of the objective function is described in the previous subsection. We now describe the formulation of constraints.

Mass balance constraints: (W2) models overall mass balance around the feed splitter $\mathcal{F}$ (see the superstructures of Figures 1.5-1.6). (W3), (W5), and (W7) (*resp.* (W4), (W6), and (W8)) model overall mass balance (*resp.* mass balance of component A) around mixer $\mathcal{M}_j$, splitter $\mathcal{S}_j$, and membrane stage j, respectively. Mass balances of component B are implied from the overall mass balances and the mass balances on component A, so we do not impose them explicitly. On the other hand, although (W6) is implied from (W5), we impose it explicitly, because it is not implied in the relaxation where the bilinear terms appear in relaxed form. Next, (W9) specifies the molar flowrate and the composition of the retentate product stream, and (W10) (*resp.* (W11)) models the overall mass balance (*resp.* the mass balance of component A) around mixer $\mathcal{P}$.

Permeator model constraints: (W12) is the same as (1.6) and it computes the value of k. (W13) computes the stage cut value needed for the permeator model. (W14) is the permeator model in (1.7)–(1.9). Observe that we introduced auxiliary variables z_j^{in} and z_j^{out} for $y_j^{\text{in}} - x_j^{\text{in}}$ and $y_j^{\text{out}} - x_j^{\text{out}}$ along with the constraints $(z_j^{\text{in}})^{\text{lo}} \leq z_j^{\text{in}}$ and $(z_j^{\text{out}})^{\text{lo}} \leq z_j^{\text{out}}$ (see (W15)), where $0 < (z_j^{\text{in}})^{\text{lo}}$ and $0 < (z_j^{\text{out}})^{\text{lo}}$. The choice of the lower bounds will be discussed shortly. Without the auxiliary variables and the bound constraints, BARON reports an error since it cannot infer $y_j^{\text{in}} - x_j^{\text{in}} > 0$ and $y_j^{\text{out}} - x_j^{\text{out}} > 0$ needed for $\ln(y_j^{\text{in}} - x_j^{\text{in}})$ and $\ln(y_j^{\text{out}} - x_j^{\text{out}})$ terms (see (1.7)). Further, we have *disaggregated* all log terms *i.e.*, each log term is expressed as $\ln(y_j^{\text{out}}/y_j^{\text{in}}) = \ln y_j^{\text{out}} - \ln y_j^{\text{in}}$. Without disaggregation, a typical factorable relaxation procedure first introduces an auxiliary variable for the fraction $y_j^{\text{out}}/y_j^{\text{in}}$, and then relaxes the log term over the range of $y_j^{\text{out}}/y_j^{\text{in}}$. Such a relaxation tends to be weaker.

Bounds on variables: (W15) constrains all variables to lie in a hyperrectangle in the positive orthant. Since the total flowrate along the arcs connecting $\mathcal{F}$ and mixer $\mathcal{M}_j$ cannot exceed the flowrate of the feed, we choose $(f_j^F)^{\mathrm{up}} = F$. Similarly, since the total flowrate along the arcs connecting $\mathcal{S}_j$ and $\mathcal{P}$ cannot exceed the flowrate of the permeate product, we choose $(f_j^{\mathrm{bypass}})^{\mathrm{up}} = F^{\mathrm{per}}$. However, a natural upper bound does not exist on the remaining flow variables. It is essential to have finite bounds on all flow variables in order to construct a valid convex relaxation. Therefore, we choose a sufficiently large number as the upper bound on the remaining flow variables. Alternatively, one could find a feasible point to MINLP (W) using local solvers and use optimality-based bound tightening techniques or shell balances around different stages to rigorously bound the flow variables.

For a gaseous (*resp.* liquid) mixture, let the admissible range of operating pressure ratio (*resp.* trans-membrane pressure difference) for the chosen membrane be $[r^{\mathrm{lo}}, r^{\mathrm{up}}]$ (*resp.* $[(\Delta P^{trans})^{\mathrm{lo}}, (\Delta P^{trans})^{\mathrm{up}}]$). Then, we choose the following as the lower and upper bounds on u.

$$u^{\mathrm{lo}} = \begin{cases} \ln r^{\mathrm{lo}}, & \text{for a gaseous mixture} \\ (\Delta P^{trans})^{\mathrm{lo}}, & \text{for a liquid mixture} \end{cases} \tag{1.15a}$$

$$u^{\mathrm{up}} = \begin{cases} \ln r^{\mathrm{up}}, & \text{for a gaseous mixture} \\ (\Delta P^{trans})^{\mathrm{up}}, & \text{for a liquid mixture} \end{cases} \tag{1.15b}$$

We obtain the lower and upper bounds on k by substituting $u = u^{\mathrm{lo}}$ and $u = u^{\mathrm{up}}$ in (1.6), respectively. For gases, it can be shown easily that k increases monotonically with u, thereby justifying the choice. On the other hand, for liquids, numerical values of C_A, C_B and S are needed to mathematically show the monotonic behavior. Instead, we use a physical argument to justify the choice. For a given mixture, the local composition of the most permeable component on the permeate side increases with an increase in the trans-membrane pressure difference. Therefore, for a given y, we

want x to decrease with increase in u in (1.5). This is possible only if k increases as u increases, thereby demonstrating the validity of the monotonic behavior for liquids.

By definition, stage cut is the fraction of the total feed permeating through a membrane module, so $\theta_j \in [0, 1]$. However, when $\theta_j = 1$, $\ln(1-\theta_j)$ (see (W14)) is not well-defined. Therefore, we choose $\theta_j^{\text{lo}} = 0$ and $\theta_j^{\text{up}} = 1 - \epsilon_\theta$. For all our computations in this article, we choose $\epsilon_\theta = 10^{-3}$.

The choice of lower and upper bounds on mole fractions is listed in (1.16). Since the mole fraction of component A is the lowest in the retentate stream of stage N, X^{ret} (see (W9)) is a valid lower bound on all mole fractions of component A. Nevertheless, we obtain a tighter lower bound on y_j^{in} (*resp.* y_j^{out}) using (1.8) (*resp.* (1.9)) and the bounds on x_j^{in} (*resp.* x_j^{ret}) and u. It can be shown using (1.5) that the local mole fraction on permeate side (y) increases monotonically with the mole fraction on the retentate side (x) and with u. Therefore, we obtain $(y_j^{\text{in}})^{\text{lo}}$ (*resp.* $(y_j^{\text{out}})^{\text{lo}}$) by substituting $x_j^{\text{in}} = X^{\text{ret}}$ (*resp.* $x_j^{\text{ret}} = X^{\text{ret}}$) and $u = u^{\text{lo}}$ in (1.8) (*resp.* (1.9)), and solving for y_j^{in} (*resp.* y_j^{out}). This procedure is symbolically represented as $y|_{x=X^{\text{ret}}, u=u^{\text{lo}}}$ in (1.16b). Next, we recognize that the net permeate composition (y_j^{per}) from each stage is always greater than the local permeate composition y_j^{out} at the exit, so we choose $(y_j^{\text{per}})^{\text{lo}} = (y_j^{\text{out}})^{\text{lo}}$. On the other hand, intuitively, it is expected that, in the optimal solution, the mole fraction of component A in the permeate decreases from stage 1 through N. Since the final permeate product is a mixture of permeate from the first stage, and possibly, from the second stage (will be discussed shortly), the mole fraction of the permeate product lies in between the mole fraction of the permeate streams from first and second stages. Thus, we set $(y_j^{\text{per}})^{\text{up}} = Y^{\text{per}}$ for all $j \geq 2$. Furthermore, since the composition of the feed entering the membrane (x_j^{in}) and the local composition on the permeate side near the exit (y_j^{out}) are always less than the net permeate composition, we choose $(x_j^{\text{in}})^{\text{up}} = (y_j^{\text{out}})^{\text{up}} = Y^{\text{per}}$ for all $j \geq 2$. We note that for y_1^{per}, x_1^{in}, and y_1^{out} there is no guarantee that the latest upper bound

would be valid. While a value of one is a natural upper bound for any mole fraction, $\ln(1 - y_1^{\text{out}})$ (see (W14)) is not well-defined when $y_1^{\text{out}} = 1$. Therefore, we choose $y_1^{\text{out}} = 1 - \epsilon$. This upper bound is also imposed on x_1^{in} and y_1^{per}, as well as for all y_j^{in}. For all computations in this article, we employed $\epsilon = 10^{-3}$. For all $j \geq 2$, we determine the upper bound on x_j^{ret} (see (1.16e)) using (1.9) and the upper bound on y_j^{out}. For x_1^{ret}, we impose its upper bound equal to $(1 - \epsilon)$, as a tighter bound is not available.

$$(x_j^{\text{in}})^{\text{lo}} = (x_j^{\text{ret}})^{\text{lo}} = X^{\text{ret}} \tag{1.16a}$$

$$(y_j^{\text{in}})^{\text{lo}} = (y_j^{\text{out}})^{\text{lo}} = (y_j^{\text{per}})^{\text{lo}} = y|_{x=X^{\text{ret}},\, u=u^{\text{lo}}} \tag{1.16b}$$

$$(x_j^{\text{in}})^{\text{up}} = (y_j^{\text{out}})^{\text{up}} = (y_j^{\text{per}})^{\text{up}} = \begin{cases} 1 - \epsilon, & \text{if } j = 1 \\ Y^{\text{per}}, & \text{otherwise} \end{cases} \tag{1.16c}$$

$$(y_j^{\text{in}})^{\text{up}} = 1 - \epsilon \tag{1.16d}$$

$$(x_j^{\text{ret}})^{\text{up}} = \begin{cases} 1 - \epsilon, & \text{if } j = 1 \\ x|_{y=Y^{\text{per}},\, u=u^{\text{lo}}}, & \text{otherwise} \end{cases} \tag{1.16e}$$

Lastly, we obtain the bounds on z_j^{in} and z_j^{out} by analyzing the behavior of (1.8) and (1.9), respectively. It can be verified that in the interval $[0, 1]$, the RHS of both the equations is concave, evaluates to zero at $y = 0$ and $y = 1$, and goes through a maxima at $y = \frac{S-\sqrt{S}}{S-1}$. This leads to the choice of bounds in (1.17). As before, $z|_{y=(y_j^{\text{in}})^{\text{lo}},u=u^{\text{lo}}}$ represents that the value of z is obtained by substituting $y = (y_j^{\text{in}})^{\text{lo}}$ and $u = u^{\text{lo}}$ in (1.8).

$$(z_j^{\text{in}})^{\text{lo}} = \min\left\{ z|_{y=(y_j^{\text{in}})^{\text{lo}},u=u^{\text{lo}}},\ z|_{y=(y_j^{\text{in}})^{\text{up}},u=u^{\text{lo}}} \right\} \tag{1.17a}$$

$$(z_j^{\text{out}})^{\text{lo}} = \min\left\{ z|_{y=(y_j^{\text{out}})^{\text{lo}},u=u^{\text{lo}}},\ z|_{y=(y_j^{\text{out}})^{\text{up}},u=u^{\text{lo}}} \right\} \tag{1.17b}$$

$$(z_j^{\text{in}})^{\text{up}} = \begin{cases} z|_{y=(y_j^{\text{in}})^{\text{up}},u=u^{\text{up}}}, & \text{if } (y_j^{\text{in}})^{\text{up}} \leq \frac{S-\sqrt{S}}{S-1} \\ k^{\text{up}}(\sqrt{S}-1)^2, & \text{if } (y_j^{\text{in}})^{\text{lo}} \leq \frac{S-\sqrt{S}}{S-1} \leq (y_j^{\text{in}})^{\text{up}} \\ z|_{y=(y_j^{\text{in}})^{\text{lo}},u=u^{\text{up}}}, & \text{if } \frac{S-\sqrt{S}}{S-1} \leq (y_j^{\text{in}})^{\text{lo}} \end{cases} \tag{1.17c}$$

$$(z_j^{\text{out}})^{\text{up}} = \begin{cases} z|_{y=(y_j^{\text{out}})^{\text{up}},u=u^{\text{up}}}, & \text{if } (y_j^{\text{out}})^{\text{up}} \leq \frac{S-\sqrt{S}}{S-1} \\ k^{\text{up}}(\sqrt{S}-1)^2, & \text{if } (y_j^{\text{out}})^{\text{lo}} \leq \frac{S-\sqrt{S}}{S-1} \leq (y_j^{\text{out}})^{\text{up}} \\ z|_{y=(y_j^{\text{out}})^{\text{lo}},u=u^{\text{up}}}, & \text{if } \frac{S-\sqrt{S}}{S-1} \leq (y_j^{\text{out}})^{\text{lo}} \end{cases} \tag{1.17d}$$

Restricting flows along specific arcs: As mentioned in §1.4.1, we are interested in the solutions where the feed mixture is fed to only one mixer. To model this requirement, we define binary variables $\omega_j^F = \{1, \text{ if the feed is fed to mixer } \mathcal{M}_j,\ 0,\ \text{otherwise}\}$, for every $j \in \{1, \ldots, N\}$ such that they satisfy (W16). (W17) suppresses material flow along the arc connecting $\mathcal{F}$ and $\mathcal{M}_j$ when $\omega_j^F = 0$. In a similar manner, we define binary variables $\omega_j^{\text{bypass}} = \{1, \text{ if the permeate from stage } j \text{ is sent to mixer } \mathcal{P};$ 0, otherwise$\}$, and for $p = 1, 2$, $\omega_j^{\text{recy},p} = \{1, \text{ if the permeate from stage } j \text{ is recycled to}$ mixer $\mathcal{M}_{j-p}$; 0, otherwise$\}$, for every j such that they satisfy (W18). Finally, (W19) and (W20) suppress material flows along appropriate arcs, when the corresponding binary variable is zero. In (W20), we set $f_j^{\text{bypass}} = 0$, for $j = 3, \ldots, N$, by setting their corresponding binary variables to zero. We impose this restriction for two reasons. First, we did not find any evidence in the literature supporting that a non-zero flow along these arcs help in reducing the energy consumption of the cascade. Second, we performed preliminary optimization tests on some separations considered in this work, and did not find any energy benefit in allowing a non-zero flow along these arcs.

1.4.4 Additional cuts

Here, we derive additional cuts that aid global solvers, such as BARON, in expediting the convergence of branch-and-bound algorithm. Most of the cuts are derived by exploiting the mathematical properties of nonlinear constraints in (W14). While

these constraints are redundant to MINLP (W), they are not implied in the relaxation where the nonlinear constraints appear in a relaxed form. Providing these constraints explicitly helps global solvers in constructing tighter relaxations of MINLP (W). The remaining cuts derived here are based on physical insights.

In the following, we state the properties used in the derivation of additional cuts to MINLP (W):

P1 The mole fraction of component A on the retentate side decreases along the length of the membrane module. Mathematically, this can be readily shown using (1.4).

P2 The mole fraction of component A in the permeate stream of each membrane module is at least as high as the mole fraction in the feed to the membrane module. Mathematically, from (W8) and (W13), x_j^{in} can be expressed as a convex combination of x_j^{ret} and y_j^{per} *i.e.*, $x_j^{\text{in}} = (1-\theta_j)x_j^{\text{ret}} + \theta_j y_j^{\text{per}}$ and $\theta_j \geq 0$. Since $x_j^{\text{ret}} \leq x_j^{\text{in}}$ from P1, $y_j^{\text{per}} \geq x_j^{\text{in}}$.

P3 The local mole fraction of component A on the permeate side (y) and the corresponding mole fraction on the retentate side (x) are related by (1.5). These compositions satisfy the following (A mathematical proof is included in the Appendix).

P3-1 $y \geq x$, and y increases monotonically with x.

P3-2 The ratio $(y-x)/y$ decreases monotonically with y.

P4 In an optimal solution, the mole fraction of the most permeable component in the inlet, retentate and permeate streams decrease from stage 1 through N *i.e.*, $x_1^{\text{in}} \geq \cdots \geq x_N^{\text{in}}$, $x_1^{\text{ret}} \geq \cdots \geq x_N^{\text{ret}}$, and $y_1^{\text{per}} \geq \cdots \geq y_N^{\text{per}}$. This is based on empirical observations and physical insights. A mathematical proof for its validity to MINLP (W) is not available.

We derive the following inequalities based on the above properties.

$$\forall\, j \in \mathcal{J}, \quad x_j^{\text{ret}} \le x_j^{\text{in}} \le y_j^{\text{per}}, \tag{W21}$$

$$\forall\, j \in \mathcal{J}, \quad y_j^{\text{out}} \le y_j^{\text{per}} \le y_j^{\text{in}}, \tag{W22}$$

$$\forall\, j \in \mathcal{K}, \quad x_j^{\text{in}} \le x_{j-1}^{\text{in}}, \quad x_j^{\text{ret}} \le x_{j-1}^{\text{ret}}, \quad y_j^{\text{per}} \le y_{j-1}^{\text{per}} \tag{W23}$$

$$\forall\, j \in \mathcal{K}, \quad y_j^{\text{in}} \le y_{j-1}^{\text{in}}, \quad y_j^{\text{out}} \le y_{j-1}^{\text{out}} \tag{W24}$$

$$Y^{\text{per}} \le y_1^{\text{per}} \tag{W25}$$

$$\forall\, j \in \mathcal{J}, \quad \left.\begin{aligned} &\ln(z_j^{\text{in}}) = \ln\left[(S-1)^2 k\right] + \ln y_j^{\text{in}} + \ln(1-y_j^{\text{in}}) - \ln\left[S-(S-1)y_j^{\text{in}}\right] \\ &\ln(z_j^{\text{out}}) = \ln\left[(S-1)^2 k\right] + \ln y_j^{\text{out}} + \ln(1-y_j^{\text{out}}) - \ln\left[S-(S-1)y_j^{\text{out}}\right] \end{aligned}\right\} \tag{W26}$$

$$\forall\, j \in \mathcal{J}, \quad \left.\begin{aligned} &\ln y_j^{\text{out}} \le \ln y_j^{\text{in}} \\ &\ln\left(1-y_j^{\text{in}}\right) \le \ln\left(1-y_j^{\text{out}}\right) \\ &\ln\left[S-(S-1)y_j^{\text{in}}\right] \le \ln\left[S-(S-1)y_j^{\text{out}}\right] \end{aligned}\right\} \tag{W27}$$

$$\forall\, j \in \mathcal{K}, \quad \left.\begin{aligned} &\ln y_j^{\text{in}} \le \ln y_{j-1}^{\text{in}} \\ &\ln y_j^{\text{out}} \le \ln y_{j-1}^{\text{out}} \\ &\ln\left(1-y_{j-1}^{\text{in}}\right) \le \ln\left(1-y_j^{\text{in}}\right) \\ &\ln\left(1-y_{j-1}^{\text{out}}\right) \le \ln\left(1-y_j^{\text{out}}\right) \\ &\ln\left[S-(S-1)y_{j-1}^{\text{in}}\right] \le \ln\left[S-(S-1)y_j^{\text{in}}\right] \\ &\ln\left[S-(S-1)y_{j-1}^{\text{out}}\right] \le \ln\left[S-(S-1)y_j^{\text{out}}\right] \end{aligned}\right\} \tag{W28}$$

$$\forall\, j \in \mathcal{J}, \quad \left.\ln(z_j^{\text{in}}) - \ln(y_j^{\text{in}}) \le \ln(z_j^{\text{out}}) - \ln y_j^{\text{out}} \right\} \tag{W29}$$

$$\forall\, j \in \mathcal{K}, \quad \left.\begin{aligned} &\ln(z_{j-1}^{\text{out}}) - \ln(y_{j-1}^{\text{out}}) \le \ln(z_j^{\text{out}}) - \ln(y_j^{\text{out}}) \\ &\ln(z_{j-1}^{\text{in}}) - \ln(y_{j-1}^{\text{in}}) \le \ln(z_j^{\text{in}}) - \ln(y_j^{\text{in}}) \end{aligned}\right\} \tag{W30}$$

(W21) is derived using the properties P1 and P2. (W22) follows from the following arguments. P1 in conjunction with P3-1 implies that the local mole fraction of component A on the permeate side decreases monotonically along the length of the membrane module *i.e.*, $y_j^{\text{in}} \ge y_j^{\text{out}}$. Further, the net permeate stream is the aggregate

of the fluxes through differential elements of the membrane module (see Figure 1.1). Therefore, its composition would lie in between y_j^{in} (the highest value possible for the local composition) and y_j^{out} (the lowest value possible for the local composition). (W23) follows from P4, and (W24) follows from (W23) and P3-1. To derive (W25) we use the following reasoning. From (W23), we have that $y_1^{\text{per}} \geq y_2^{\text{per}}$. This implies that the composition of the permeate product (Y^{per}) must be lower or equal than y_1^{per} as the permeate product is formed from the permeate exiting the first stage, and possibly, from the permeate exiting the second stage.

To obtain (W26), we express the RHS of (1.8) and (1.9) as $k(S-1)^2 y(1-y)/[S-(S-1)y]$, replace $y-x$ on the LHS with the auxiliary variable z, take natural log on both sides, and disaggregate the log terms. To derive the remaining inequalities, we make use of the following property. Let $g(v)$ be a monotonically increasing function of v. Then, $g(v_1) \leq g(v_2)$ for every v_1, v_2 satisfying $v_1 \leq v_2$. (W27) (*resp.* (W28)) is derived from (W22) (*resp.* (W24)) using the monotonically increasing nature of ln. From P3-2, the function $(y-x)/y$ decreases monotonically with y *i.e.*, $(y_j^{\text{in}} - x_j^{\text{in}})/y_j^{\text{in}} \leq (y_j^{\text{out}} - x_j^{\text{ret}})/y_j^{\text{out}}$ because $y_j^{\text{out}} \leq y_j^{\text{in}}$ from (W22). We replace $y-x$ with the auxiliary variable z, and use the monotonically increasing nature of ln to obtain (W29). Similarly, we derive (W30) from P3-2, (W24), and utilizing the monotonically increasing nature of ln. Finally, we remark that the nonlinear constraints in (W26)–(W30) make the local search more difficult, as local solvers fail to converge when they are included in the model. Since they are redundant in the presence of (W14) and (W21)–(W24), and are needed only for the construction of a relaxation, we provide (W26)–(W30) to BARON using the '`relaxation_only_equations`' construct (see [42, 43]).

1.4.5 Computational experiments

Here, through numerical experiments, we demonstrate that the proposed MINLP (W) is able to identify the optimal membrane cascade within a relative tolerance of 5%. In addition, we show the effectiveness of the cuts derived in Section 1.4.4 in expediting the convergence of the branch-and-bound algorithm by solving (W) with and without (W21)–(W30). For our numerical experiments, we considered a *test set* of 13 cases shown in Table 1.3. The values of the remaining parameters are reported in the caption. Note that instead of the flowrate and the composition of permeate and retantate product streams, we have reported the composition (Y^{per}) and the recovery (γ_A) of component A in the permeate product stream. Recovery of a component is defined as the ratio of its molar flowrate in the permeate product stream to that in the feed mixture. The values of the former parameters needed in (W9)-(W11) are obtained from the latter using (1.18).

$$\gamma_A = \frac{F^{\text{per}} \cdot Y^{\text{per}}}{F \cdot X^F}, \tag{1.18a}$$

$$F = F^{\text{per}} + F^{\text{ret}}, \tag{1.18b}$$

$$F \cdot X^F = F^{\text{per}} \cdot Y^{\text{per}} + F^{\text{ret}} \cdot X^{\text{ret}}. \tag{1.18c}$$

(1.18a) is the definition of the recovery of component A. (1.18b) is the overall mass balance on the cascade, and (1.18c) is the mass balance of component A on the cascade. For all gaseous (*resp.* liquid) mixtures, we choose the admissible range of operating pressure ratio (*resp.* trans-membrane pressure difference) to be $[1.1, 9]$ (*resp.* $[30 \text{ bar}, 107 \text{ bar}]$) *i.e.*, $r^{\text{lo}} = 1.1$ and $r^{\text{up}} = 9$ (*resp.* $(\Delta P^{trans})^{\text{lo}} = 30$ bar and $(\Delta P^{trans})^{\text{up}} = 107$ bar).

Table 1.3.
Test set for computational experiments. Note that the mole fractions correspond to the most permeable component.

Case	Mixture	Feed Pressure (bar)	Feed Composition (% mol)	Permeate Purity (% mol)	Molar Recovery (%)	Membrane perm-selectivity
			Gaseous Mixtures			
1	CO_2/CH_4	20	60	95	98.7	25
2		20	10	95	81.7	25
3		20	10	69	82.4	12
4		55	30	86.7	93.2	21
5	H_2/CO_2	28	21.5	99	98.2	38
6	propylene / propane	9	80	90	90	5
7		9	70	99.6	97.8	35
8		9	70	92	97.8	35
			Liquid Mixtures			
9	p-xylene / pseudocomponent	1	65	99.5	90	50
10		1	65		99	
11		1	90		90	
12		1	90		99	
13		1	23.6		97.5	

We use BARON 18.5.8 on GAMS 25.1 to solve the MINLP (W). All BARON options except `pDo` were left at their default values. `pDo` was set to -1. We set the relative tolerance for convergence (ϵ_r) to 5% and the time limit to 80 h as the termination criteria. All computations are performed on a Dell Optiplex 5040 with 16 GB RAM, which has Intel Core i7-6700 3.4 GHz processor and is running 64-bit Windows 10. The computational results are summarized in Table 1.4.

The second (*resp.* third) column in Table 1.4 lists the computational performance when the MINLP (W) is solved without (*resp.* with) (W21)–(W30). Clearly, when the additional cuts are not included, none of the cases converge even after 80 hours. The remaining duality gap (defined as (Best known upper bound − Best known lower bound)/Best known upper bound) at the end of 80 hours is as high as 97% in some cases. On the other hand, with the inclusion of (W21)–(W30), we could solve all 13 cases to 5%-optimality within 80 hours.

1.5 Case studies

Here, we examine Case 8: separation of propylene/propane mixture and Case 12: separation of p-xylene/(o-xylene+m-xylene) mixture in Table 1.4 in more detail. In particular, we determine the optimal membrane cascades requiring at most four stages along with the optimal operating conditions using the MINLP (W). Additionally, we describe constrains to limit the number of compressors/pumps in the optimal cascade. All optimization problems in this section are solved to 5%-optimality.

We note that, unless otherwise stated, when referring to a stream concentration in the following discussion, we refer to the most permeable component, which is p-xylene or propylene in the studied separations.

1.5.1 propylene/propane separation

The separation of propylene/propane is of great relevance at industrial level as propylene is an important precursor to produce a wide variety of chemicals such as polypropylene, propylene oxide, acryl acid, acrylonitrile, and isopropanol [44]. The current process employed to separate the mixture propylene/propane is distillation, which is usually operated at sub-ambient conditions and at a mild pressure close to 9 bar [45, 46]. Since the demand of propylene is very high, it is typically separated with a high recovery that ranges between 97.8 % to 99 % [47, 48]. On the other hand,

Table 1.4.
Results from the computational experiments. The input parameters are set to $N = 4$, $F = 250$ mol/s, $E^{comp} = 0.75$, $E^{pump} = 0.75$, $E^{TC} = 0.8$, $V_A = 1.233 \times 10^{-4}$ m^3/mol, $V_B = 1.215 \times 10^{-4}$ m^3/mol, and $T = 303.15$ K. Molar volumes are determined using Aspen Plus v8.6, and the reported V_B is the average of molar volumes of o-xylene and m-xylene. All cases were solved with BARON 18.5.8 in GAMS 25.1 with a time limit of 80 hours. Except `epsr` and `pDo`, all other BARON options were left at their default values. We choose `epsr` = 0.05 and `pDo` = -1. TL indicates that the time limit was reached, and the number in parenthesis is the remaining duality gap at the end of 80 hours. I/T correspond to number of BARON iterations/computational time (in hours) to reach 5%-optimality.

Case	Without (W21)–(W30) I/T	With (W21)–(W30) I/T
Gaseous Mixtures		
1	TL (67%)	91,175 / 77.4
2	TL (85%)	8,281 / 2.8
3	TL (83%)	12,899 / 3.9
4	TL (30%)	13,729 / 4.8
5	TL (88%)	22,675 / 5.7
6	TL (54%)	41,613 / 12.1
7	TL (78%)	147,803 / 79.6
8	TL (11%)	55,929 / 47.8
Liquid Mixtures		
9	TL (63%)	7,765 / 3.0
10	TL (88%)	4,331 / 1.2
11	TL (48%)	42,679 / 26.0
12	TL (47%)	8,997 / 2.8
13	TL (97%)	1,909 / 0.4

the final purity of the propylene product varies according to its use downstream. In general, propylene is separated at a very high purity greater than 99.5 % for the synthesis of polymers, or at a moderate purity of about 92 % for some other chemical applications such as the production of 2-propanol [44, 49].

For our case study, we consider the separation of a 70%/30% mixture of propylene/propane to produce *chemical grade propylene* at 92% purity and 97.8% recovery. These feed composition and product recovery, which were taken from [47], are in good agreement with those encountered in industry [50]. In addition, we assume the molar flow rate of the feed mixture to be 250 mol/s, and that it is available at 9 bar. Lastly, we assume that all the membranes in the cascade have a perm-selectivity of 35 [47] (note that propylene is the most permeable component).

Optimum four-stage cascade

The optimum four-stage membrane cascade for the separation of the propylene/propane mixture is shown in Figure 1.9. In this cascade, the feed mixture is located at the first stage. This is not surprising given that the degree of enrichment of the most permeable component in the permeate product stream is not too high. Thus, one stage is sufficient to achieve the required purity specification. It is also because of this reason, the optimal cascade does not recycle the permeate stream of stage 2 to stage 1. This helps in reducing the energy requirement as it avoids compressing extra material flow. Clearly, in this case, a single membrane stage is sufficient to produce propylene at the desired purity. Nevertheless, a single stage is not sufficient to recover the desired amount of propylene while maintaining the purity. As shown in Figure 1.9, the optimal arrangement employs three additional stages for stripping propylene from the retentate stream leaving the first stage.

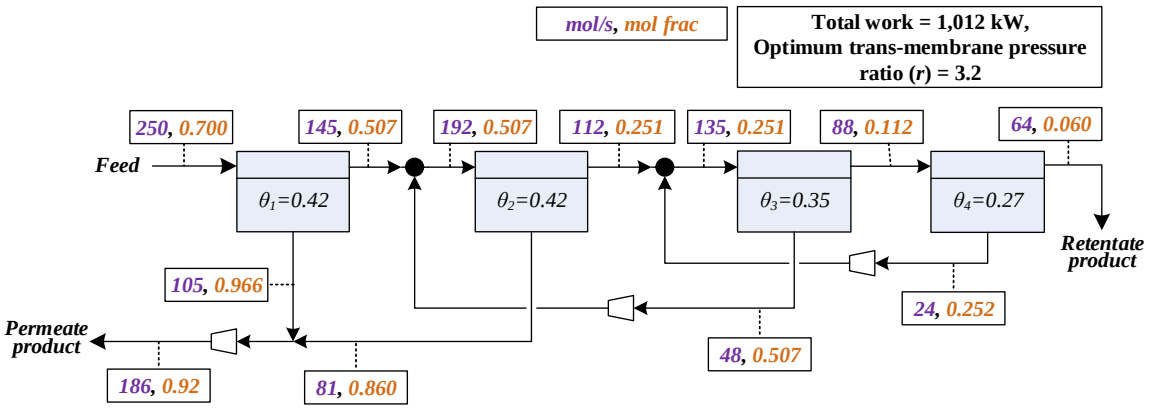

Fig. 1.9. Optimum four-stage cascade for the separation of propylene/propane. All mole fractions shown in the box-legends refer to propylene. Any mismatch in the mass balances is due to the rounding of the flow and the composition values shown in the above labels

Optimum cascade with only one intermediate compressor

As shown in Figure 1.9, the optimum four-stage cascade has two intermediate compressors, and one compressor to pressurize the permeate product stream. Owing to high capital cost and maintenance issues associated with compressors, process designers often seek cascades with a fewer number of compressors. In the following, we formulate constraints which can be appended to the MINLP (W) to obtain cascades that have limited number of compressors.

Excluding the compressor needed to compress the permeate product stream, the total number of compressors, M_{comp}, in a cascade can be determined from the binary variables $\omega_j^{\text{recy},1}$ and $\omega_j^{\text{recy},2}$ as

$$\sum_{j=2}^{N} \omega_j^{\text{recy},1} + \sum_{j=3}^{N} \omega_j^{\text{recy},2} - \sum_{j=3}^{N} \omega_{j-1}^{\text{recy},1} \omega_j^{\text{recy},2} = M_{comp}, \tag{1.19}$$

The first (*resp.* second) term in the above equation accounts the compressor along the arc connecting the splitter $\mathcal{S}_j$ and mixer $\mathcal{M}_{j-1}$ (*resp.* $\mathcal{M}_{j-2}$) (see Figure 1.5). In cases where the material flow from both $\mathcal{S}_{j-1}$ and $\mathcal{S}_j$ is sent to mixer $\mathcal{M}_{j-2}$, both the streams can be mixed before compressing, thereby reducing the number of compressors needed in the cascade. Thus, the third term in the above equation reduces the number of compressors by one, when both $\omega_{j-1}^{\text{recy},1} = 1$ and $\omega_j^{\text{recy},2} = 1$. We linearize (1.19) by introducing an auxiliary variable h_{j-1} for the product, and relax $h_{j-1} = \omega_{j-1}^{\text{recy},1}\omega_j^{\text{recy},2}$ by replacing the bilinear term with its convex and concave envelopes over $[0,1]^2$. This results in the following constraints

$$\sum_{j=2}^{N} \omega_j^{\text{recy},1} + \sum_{j=3}^{N} \omega_j^{\text{recy},2} - \sum_{j=3}^{N} h_{j-1} = M_{comp}, \tag{1.20}$$

$$\forall\, j \in \{3,\ldots,N\}, \quad \begin{cases} h_{j-1} \le \omega_{j-1}^{\text{recy},1}, \quad h_{j-1} \le \omega_j^{\text{recy},2} \\ h_{j-1} \ge 0, \quad h_{j-1} \ge \omega_{j-1}^{\text{recy},1} + \omega_j^{\text{recy},2} - 1, \end{cases} \tag{1.21}$$

Since $\omega_{j-1}^{\text{recy},1}$ and $\omega_j^{\text{recy},j}$ are binary, it can be easily verified that the feasible solutions to (1.20) and (1.21) are the same as that of (1.19).

We now append (1.20) and (1.21) to (W) and solve the resulting MINLP by substituting $M_{comp} = 1$. This yields the optimal cascade requiring only one intermediate compressor. As shown in Figure 1.10, the optimal solution requires only three stages. The optimizer bypasses material flow through a stage by setting its stage cut to zero. This cascade requires only 1.3% more energy than the one shown in Figure 1.9. Since the capital cost of a compressor is significant, the small increase in energy cost may be dominated by the reduction in the overall capital cost making this arrangement more economical. Since the main purpose of this example is to illustrate the application of constraints (1.20) and (1.21) in identifying attractive cascades requiring fewer number of compressors, a quantitative cost benefit analysis of the cascade of Figure 1.10 over the cascade of Figure 1.9 is beyond the scope of our case study.

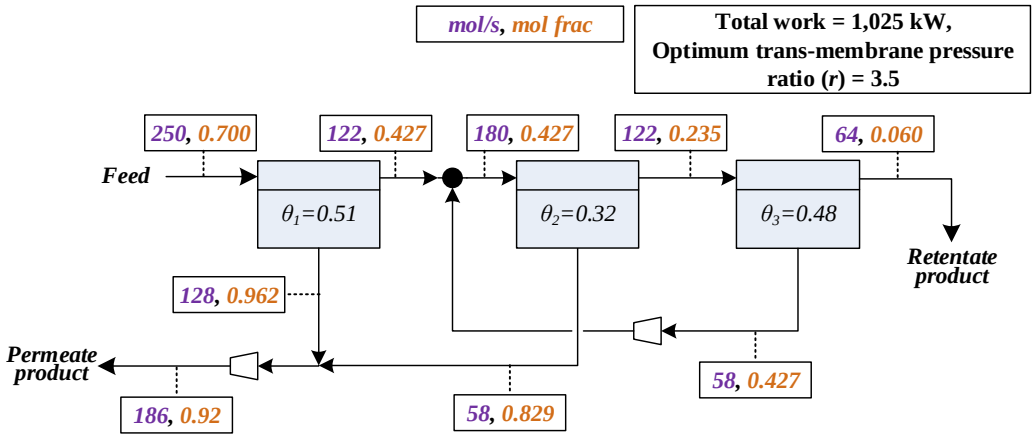

Fig. 1.10. Optimum cascade for the separation of propylene/propane derived under the additional constraint of operating with only one intermediate compressor. The number of stages in the optimization problem was set to four but the resulting optimum solution eliminates one membrane stage. Thus, the shown configuration has only three membrane stages. All mole fractions shown in the box-legends refer to propylene. Any mismatch in the mass balances is due to the rounding of the flow and the composition values shown in the above labels

We note that a two-stage cascade with only one intermediate compressor (see Figure 1.11) would consume similar amount of energy as the three-stage cascade of Figure 1.10. Thus, it appears that a suitable cascade with a few compressors can be alternatively obtained by solving the MINLP (W) with just lower number of stages, instead of solving the MINLP by appending (1.20) and (1.21). However, this is a coincidence. As we shall demonstrate with the next case study, in general, solving the MINLP with (1.20) and (1.21) yields better solutions than simply solving the MINLP with fewer number of stages.

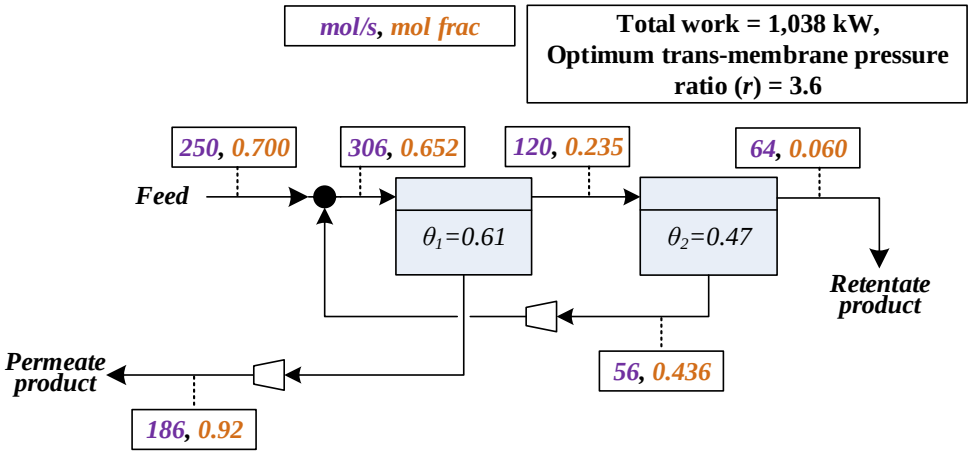

Fig. 1.11. Optimum two-stage cascade for the separation of propylene/propane. All mole fractions shown in the box-legends refer to propylene. Any mismatch in the mass balances is due to the rounding of the flow and the composition values shown in the above labels

1.5.2 p-xylene separation

Xylenes are important compounds used in the manufacturing of many products ranging from plastics, paint solvents, resins, inks and plasticizers [51]. Among all the isomers, p-xylene has the highest commercial demand. One of the major applications of p-xylene is the synthesis of terephthalic acid, which is used as the building block for the manufacturing of polymers such as polyethylene terephthalate (PET) and polybutylene terephthalate (PBT) [52]. The production of p-xylene comes primarily from the catalytic reforming of naphtha, but it is also produced through other routes, such as the toluene disproportionation process. As compared to the catalytic reforming, the latter process offers the advantages that p-xylene is produced at higher concentration and that ethylbenzene (EB) is practically absent [51]. In the reforming process, p-xylene is produced in a concentration of $\sim$ 20 mol%, based on the C8 cut composed by p-xylene, o-xylene, m-xylene and EB, whereas in the toluene disproportionation process, the concentration of p-xylene in the C8 fraction is around 90% [53, 54].

Currently, simulated moving bed and crystallization are the major technologies employed to separate the p-xylene from the C8 cut. Nevertheless, the inherent energy intensive nature of this separation due to the similarities in the physical and structural properties of the molecules that compose the mixture keeps active the research in this field with the aim of finding more efficient separation options. Here, we explore an example of the separation of p-xylene through a membrane cascade. For this example, we consider that the mixture subject to separation comes from the toluene disproportionation process, and for this reason, we assume that EB is not contained in the mixture. Furthermore, we assume that all the membranes that compose the cascade are more selective to p-xylene than o-xylene and m-xylene. This assumption is consistent with permeation experiments that have been carried out with polymeric membranes [55, 56]. Although the C8 mixture obtained from the toluene disproportionation process is multicomponent, we treat it as a binary mixture that is composed by p-xylene and a pseudo-component that groups the least permeable constituents, which are o-xylene and m-xylene.

All the results discussed for the current study case are based on a liquid feed at ambient conditions (30 °C and 1 bar) with a flow of 250 mol/s and a concentration of 90% p-xylene. Since downstream uses require high purity and p-xylene is a valuable chemical, we set the final purity and recovery of p-xylene equal to a typical value of 99.5% mol and 99% respectively [54]. The perm-selectivity of p-xylene (most permeable component) at all the membranes in the cascade was assumed to be 50. This value is in the same order of magnitude as experimental selectivities measured by Koh et al. for the liquid separation of p-xylene/o-xylene through a polymeric membrane [55]. Finally, we let the admissible operating range of the trans-membrane pressure difference be 30 bar – 107 bar.

Optimum two-stage cascade

According to the superstructure of Fig. 1.6, there are two possible cascades with two stages, each of which differs only in the feed location. Figure 1.12 shows the optimum two-stage cascade with the minimum energy consumption for the analyzed separation. This configuration has the feed located at the second stage, and operates at 107 bar, which is the maximum permissible trans-membrane pressure difference. It is interesting to note that the optimum stage cuts are very unbalanced as the stage cut of the first stage (θ_1) is very small, but in contrast, the stage cut of the second stage (θ_2) is very high, which results in the pumping of a large recycle flow.

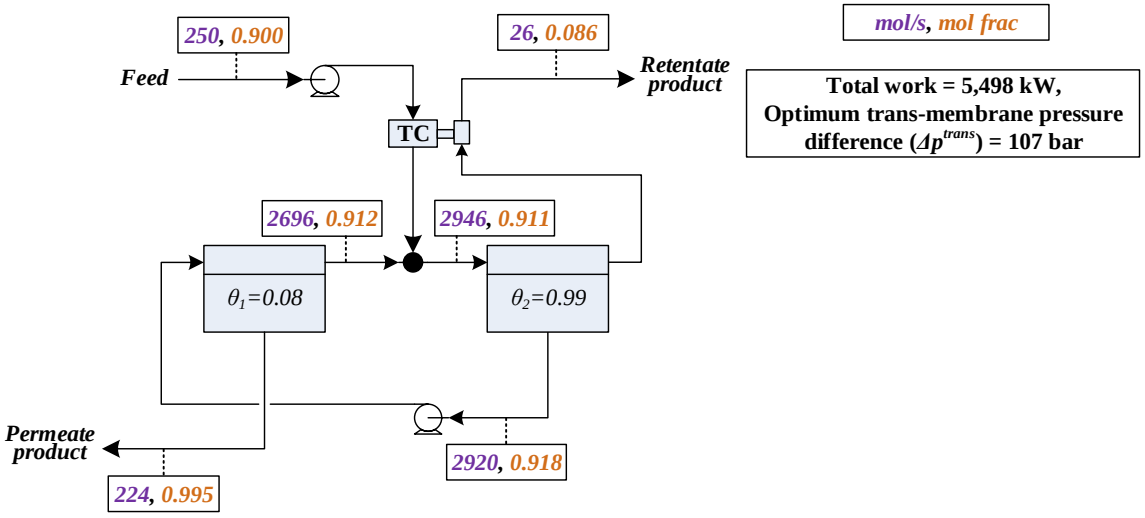

Fig. 1.12. Optimum two-stage cascade for the separation of p-xylene. All mole fractions shown in the box-legends refer to p-xylene. Any mismatch in the mass balances is due to the rounding of the flow and the composition values shown in the above labels

The energy consumption of the cascade could be further reduced if decreasing θ_2. However, the current upper bound imposed on the trans-membrane pressure difference makes infeasible such an operation. Let us explain in more detail why this happens. A reduction of θ_2 would require to lower the inlet concentration to the second stage to still produce a retentate with a molar fraction in p-xylene of 0.086,

otherwise, the net retentate product will exceed this concentration. Since a reduction of θ_2 lowers the inlet flow to the first stage, θ_1 needs to be increased to maintain the required amount of the net permeate product. With a higher stage cut at the first stage, the concentration of the inlet flow to this stage needs to be increased in order to achieve the final purity of 0.995 that is required in the permeate product. Although the reduction of θ_2 would tend to increase the inlet concentration to the first stage, this effect is counteracted by the concentration reduction in the feed of the second stage, which finally causes a net decrease in the concentration of the stream entering the first stage, and consequently, makes unfeasible to satisfy the required p-xylene purity in the permeate product.

The only ways to make feasible to operate the two-stage cascade with a reduced θ_2 is by increasing the trans-membrane pressure difference, or by using more selective membranes. These strategies would enhance the separation driving force and would make possible to achieve the target purity of the permeate product, despite of a reduction of the concentration in the feed of the first stage and an increase of θ_1. Operating the cascade under a lower value of θ_2 is favorable because as it is observed from Table 1.5, it helps to reduce markedly the overall energy consumption. Nevertheless, with the considered membrane, which we assumed that has similar properties as the membranes developed by Kho et al. [55], it might be not possible to operate the cascade with a trans-membrane pressure difference above 107 bar, as it is likely that the membranes would suffer from compaction and would considerably reduce their selectivity to p-xylene[1]. Therefore, to improve the energy efficiency of the membrane cascade without adding more stages, further research should be directed on developing membrane materials which not only have improved selectivity, but also, which can be operated at higher trans-membrane pressure differences without suffering from considerable compaction.

[1]We infer that membrane compaction is likely to taking place above 107 bar of trans-membrane pressure difference from the data presented on Fig. 2E, Figs. S28-S29 and Table S6 from the work of Koh et al. [55]

Table 1.5.
Optimum stage cuts and power consumption of a two-stage cascade for the analyzed separation of p-xylene under various values of ΔP^{trans} and membrane permselectivity

Δp^{trans} (bar)	Membrane permselectivity	Optimum θ_1	Optimum θ_2	Total power (kW)
107	50	0.077	0.991	5,498
125		0.154	0.982	3,425
150		0.233	0.965	2,306
175		0.336	0.941	1,843
200		0.428	0.913	1,638
107	100	0.135	0.982	2,861
	500	0.296	0.951	1,283
	1000	0.332	0.942	1,141

It is interesting to note that contrary to the optimal two-stage cascade for the separation of p-xylene/o-xylene shown in Figure 1.12, the configuration of Figure 1.11 for the separation of propylene/propane does not operate with a very high θ_1 and very low θ_2, but instead, both stage cuts have moderate magnitudes. This happens due to the following reasons. As compared to the separation of p-xylene/o-xylene, in the separation of propylene/propane the stream entering the last stage has a more diluted concentration of the most permeable component (propylene), which allows to achieve the target purity of the retentate product without operating the last stage with a very high value of θ_2. Handling a relatively low concentration of propylene in the inlet to the last stage is possible because the permeate recycle from this stage does not need to be high as it is not required to produce ultra pure propylene in the net permeate. Of course, since θ_2, and consequently the amount of flow recycled to the first stage are not very high, θ_1 can not be very small, but instead, has to be moderate as the first stage needs to permeate a significant amount of flow to satisfy the high recovery of propylene in the permeate product.

Optimum three-stage cascade

Fig. 1.13 shows the optimum three-stage cascade. This configuration is similar to the configuration of Fig. 1.12 in the sense that the permeate stream from each membrane, except the net permeate product, is pumped and fed to the high pressure side of the previous membrane. However, as compared to the two-stage cascade, the optimum three-stage cascade operates the last stage with a lower stage cut, which helps to decrease the flow recycled to the previous stage, and consequently decreases the overall energy consumption. As we mentioned, reducing the stage cut of the last stage causes a reduction in the concentration of the feed and permeate streams of this stage, something that we discussed that would make unfeasible the operation of the two-stage cascade with the considered membrane permselectivity and the imposed restriction on trans-membrane pressure difference. Nevertheless, such an operation is feasible with the three-stage cascade as the intermediate stage provides an additional media to enhance sufficiently the concentration of the stream entering the first stage to produce the permeate product with the required purity and recovery of p-xylene.

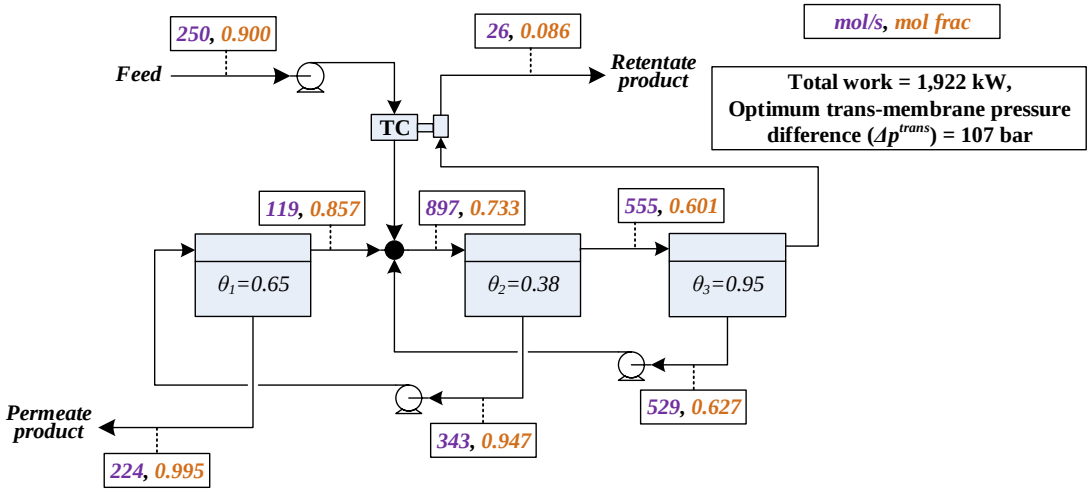

Fig. 1.13. Optimum three-stage cascade for the separation of p-xylene. All mole fractions shown in the box-legends refer to p-xylene. Any mismatch in the mass balances is due to the rounding of the flow and the composition values shown in the above labels

Optimum four-stage cascade

Fig. 1.14 shows the optimum membrane cascade derived from the superstructure of Fig. 1.6 with four stages. Once again, the increase in the number of stages helps reducing the total energy consumption. Nevertheless, it is important to note that the reduction obtained by increasing the number of stages from three to four is lower than that obtained when going from two to three stages. This observation is in agreement with the work of Pathere and Agrawal [17], which shows that the benefit of adding more stages in the membrane cascade becomes less relevant as the number of stages grows up. Since operating the cascade with more stages implies an increment of pumps, membrane housing and other auxiliary equipment, it is likely that the addition of more stages beyond a certain limit would be economically unattractive as the small reduction of energy consumption might not justify the accompanied increase of capital cost due to more equipment.

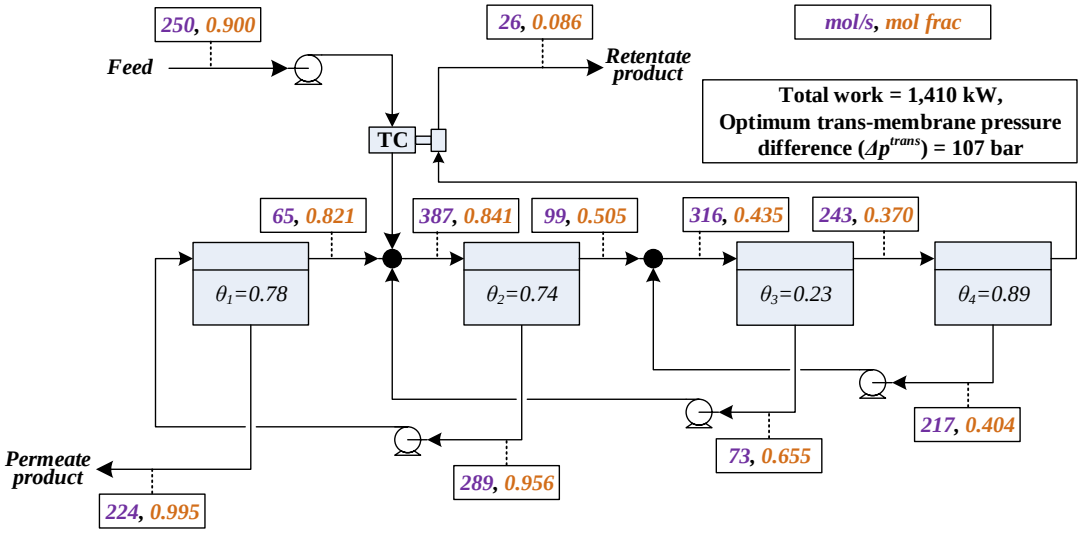

Fig. 1.14. Optimum four-stage cascade for the separation of p-xylene. All mole fractions shown in the box-legends refer to p-xylene. Any mismatch in the mass balances is due to the rounding of the flow and the composition values shown in the above labels

Another interesting observation to note is that when increasing the number of stages from two to up to four, the corresponding optimum cascades allocate the extra stages in the stripping section (to the right of the feed) rather than in the enriching section (to the left of the feed). This mainly happens because the feed is already enriched in the most permeable component (90 % p-xylene), and thus, there is no much gain from adding more stages in the enriching section as the permeate leaving the feed stage has a purity relatively close to the target value of 99.5 % p-xylene required in the net permeate product. In contrast, it is more beneficial to add more stages in the stripping section as they provide additional media to purify the retentate that exits the feed stage, which concentration is still far from the target purity of 91.4% o-xylene required in the net retentate product. If the extra stages were located in the enriching section, the stage cut of the last stage would have to be increased to complete the high level of purification needed for the retentate, but as was mentioned before, this would increase the recycling flow from the last stage, resulting in a net increase of the energy consumption.

Optimum four-stage cascade with two intermediate pumps

Unlike compressors, pumps are relatively cheap and easy to operate. Thus, the number of pumps used for liquid separations is not a major concern. Nevertheless, operating a cascade beyond a certain number of pumps may not be economically attractive. In such cases, one can append (1.20) and (1.21) to the MINLP in order to obtain attractive cascades with limited number of pumps.

For the xylene mixture, we determine the optimal cascade requiring only two intermediate pumps *i.e.*, $M_{comp} = 2$. Solving (W) after appending (1.20) and (1.21) yields the solution shown in Figure 1.15. Similar to Figure 1.14, the feed mixture is fed at the second stage in Figure 1.15. However, in the latter arrangement, the permeate streams from both the second and third stages are mixed and recycled to

the first stage. At optimum operation, this cascade requires 13% more energy than the one in Figure 1.14. A detailed economic analysis enables us to determine whether the reduction in the capital cost due to elimination of a pump is beneficial compared to the increase in operating cost due to the increase in energy consumption.

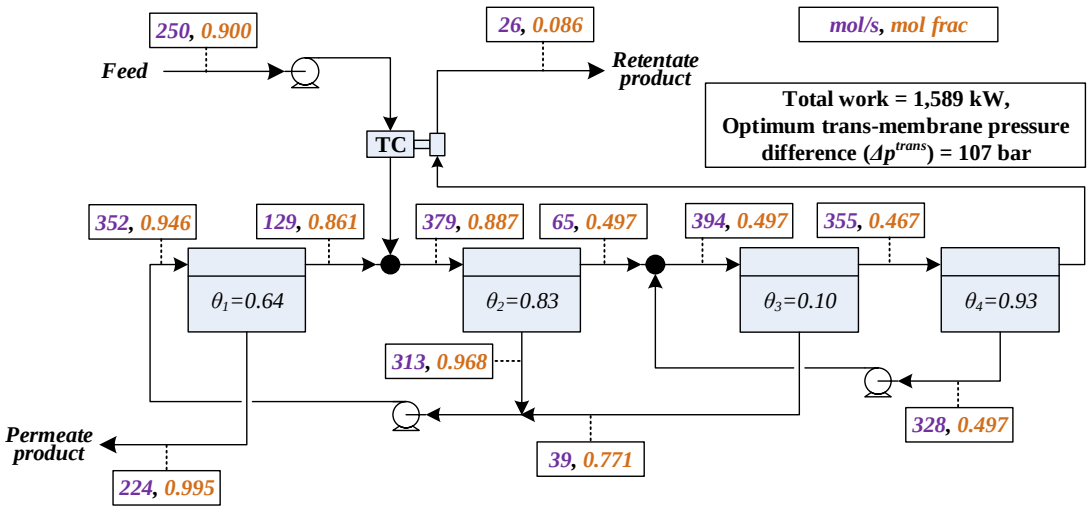

Fig. 1.15. Optimum four-stage cascade for the separation of p-xylene subject to the constraint of operating with only two pumps. All mole fractions shown in the box-legends refer to p-xylene. Any mismatch in the mass balances is due to the rounding of the flow and the composition values shown in the above labels

This example demonstrates that solving the MINLP with (1.20) and (1.21) often leads to better solutions than simply solving (W) with a fewer number of stages. As we showed for the xylene separation, a cascade with only two intermediate pumps can also be designed by solving (W) with $N = 3$ (see Figure 1.13). In this case, the maximum pumps permissible in all the cascades embedded in the superstructure is two. Interestingly, we observe that the optimal three-stage cascade consumes significantly higher energy than the cascade in Figure 1.15 even though both the arrangements require the same number of pumps. This example illustrates the utility of (1.20) and (1.21) in finding energy efficient cascades with limited number of pumps/compressors which are not easy to obtain directly by solving the MINLP (W).

1.6 Concluding remarks

In this article, we presented a new optimization model to find energy efficient membrane cascades for the separation of binary mixtures in liquid or gaseous phase through dense membranes. The introduced optimization model was formulated as MINLP based on a superstructure that embeds several possible multistage membrane configurations. Thus, for a given liquid or gaseous binary mixture, the solution of the proposed MINLP allows to find in one step the optimum membrane cascade along with the optimum operating conditions that minimize the overall energy consumption.

The main highlights of our membrane cascade optimization model are the following. First, we employed a permeator model that, as shown here and in other works, predicts with good accuracy the separation of diverse mixtures. This model is originally given as a differential algebraic equation (DAE). While an approximated solution of this model has been used previously in other optimization formulations, we propose, for the first time, to use an exact solution of it within the cascade optimization problem. This strategy eliminates any error that might arise from alternatively discretizing the DAE. Second, we reformulated the permeator model in a way that allows its application for both liquid and gaseous separations. Third, we derived several linear and non-linear cuts into the complete optimization model. Finally, we tested the performance of our formulation with several separation examples. Our results show that the introduced linear and non-linear cuts help remarkably to expedite global optimality convergence using the commercial global solver BARON.

We remark that our proposed optimization model is not only helpful to identify membrane cascades with enhanced energy efficiency that could be potentially used for existing or new separations, but also, it can be used to compare the optimum energy consumption of a multistage membrane process against alternative separations methods, and aid in the decision of whether or not to use a membrane system.

2. SYSTEMATIC ANALYSIS REVEALS THERMAL SEPARATIONS ARE NOT NECESSARILY MOST ENERGY INTENSIVE

2.1 Introduction

Molecular separations are needed across many types of industries, including oil & gas, food, pharmaceutical, and chemical industries. They play an important role in the manufacturing of a vast variety of products, such as fuels, plastics, therapeutic drugs, and so forth. Among the available separation technologies, thermal processes (see Note 1 in Appendix B), such as distillation, that vaporize one or more constituent components, have traditionally been preferred in chemical and petrochemical plants. Just in the U.S., it is estimated that over 90-95% of all fluid separations in chemical plants and refineries are performed by distillation [57]. Nevertheless, recent literature claims that thermal methods involving vaporization (simply referred as thermal methods in the rest of this chapter) are inherently highly energy intensive and if replaced by alternative methods in the separation of various chemical mixtures, will lead to huge energy savings [57–62].

While detailed energy analyses have demonstrated the energy benefits brought by non-thermal membranes for water desalination [63–66], the relative energy intensity between thermal and non-thermal processes in the separation of chemical mixtures has not been deeply studied in the literature. In contrast, we highlight that most of the publications stating in general that thermal processes are highly energy intensive, do not even provide an energy comparison or any other concrete evidence that supports the claim. Furthermore, some studies that attempt to explain or demonstrate the apparent energy-intensive nature of thermal processes, through energy compar-

isons or conceptual arguments, base their analysis on ad-hoc assumptions or insufficient rationale. For example, in a recent research agenda published by the National Academies of Sciences, Engineering and Medicine [59], thermal methods are ranked as the most energy intensive. The rationale provided is that "thermal processes are energy-intensive because they are based on the enthalpy of vaporization of at least one component". However, we will argue that this rationale is insufficient to support the claim that any process that separates a mixture by vaporization would consume more energy than other mechanisms. More specifically, we show that the energy intensity of a thermal process is not solely determined by the enthalpy of vaporization. For example, even when a thermal process must supply a large amount of heat for vaporizing the mixture, the energy intensity of the process could be low if the heat source is at a low temperature. This is because the quality of heat is determined by the temperature.

Another argument that is eroding the interest in thermal methods hinges on a direct comparison of heat requirement of a thermal method with work requirement of a non-thermal alternative. For instance, a recent study reported that replacing thermal methods with non-thermal counterparts could reduce the energy intensity by a factor of ten [58]. This estimate is not well-founded for the following reasons. First, the analysis focuses on a particular separation process concerning water desalination whose attributes are atypical among industrial chemical separations. Specifically, in the desalting of water, the molar concentration of water in the feed is very high ($>$ 97%). Therefore, even when producing water with $\geq$ 99.9% purity, the level of purity enhancement of the water relative to its feed concentration is relatively small. This is in contrast to most separations in the chemical industry. Also, chemical products are usually separated at high recoveries due to their high value. However, in water desalination, purified water is only recovered at around 50%. Second, it compares heat consumed by a multistage flash with electrical work consumed by reverse osmosis. Since work and heat are different forms of energy, the comparison does not

correctly reflect the energy intensity of the processes. This is because the second law of thermodynamics shows that a given amount of work is more valuable than the same amount of heat. In other words, the reduction in energy intensity, even in the context of water desalination cannot be adequately measured in the absence of a comprehensive framework that accounts for such issues.

In this chapter, we focus on introducing a comprehensive framework that allows for a proper energy comparison of different separation processes using different forms of energy. We then use this framework to test the belief that thermal separation processes are energy intensive. Towards this end, we compared two relevant separations, p-xylene/o-xylene and propylene/propane, by analyzing both a thermal and a non-thermal separation process. These separations are often touted as examples of energy-intensive distillation [60, 67]. Our results show that the perception that thermal methods are generally the most energy intensive is not well-founded. We demonstrate that, in the absence of a thorough comparison, thermal processes are likely to appear energy intensive. Therefore, technology selection that is not based on comprehensive analysis of the energy requirements can lead to significantly sub-optimal implementation, which will not only adversely affect the energy needs of the process, but by consuming more fuel, will increase the carbon footprint of the process to the detriment of the environment. Furthermore, continuing the misperception that thermal methods are generally the most energy intensive, can divert resources and effort from further improving the efficiency of distillation and other thermal based processes [68, 69].

2.2 A framework to compare separation processes

Frequently, thermal and non-thermal separation processes consume different forms of energy. Non-thermal processes, consume electrical work, whereas thermal processes, usually consume heat, which is available in a wide range of temperatures.

Therefore, to understand their energy intensity, it is not sufficient to compare the heat and electricity consumed by the process candidates. Observe that these energies are typically derived from a fuel source and, by the second law of thermodynamics, the amount of fuel needed to produce a certain amount of work is often markedly different from that to produce the same amount of heat. Therefore, a better way to compare thermal and non-thermal processes is to calculate the amount of primary fuel consumed by each process. This strategy has been used to compare the energy requirements of thermal-based processes and RO for water desalination [63]. In our work, we also use this approach to compare the relative energy intensity of the analyzed processes. We note that the discussion presented in this research is in the context where the separation processes are powered by fossil fuels.

Alternatively, the use of exergy efficiency is a plausible approach to compare separation processes that consume different types of energy [15, 70]. In the field of water desalination, the exergy method has been used not only for comparing thermal and non-thermal processes, but also to identify the main sources of inefficiencies [71–74]. An exergy analysis assigns an exergy value to each material and energy stream in a process, which is quantified in terms of "maximum work extractable". Thus, it assumes that rejected heat has an exergy benefit. But in reality, not all heat streams are practically useful for producing work or for another task. Furthermore, even when rejected heat is reused, it is not always possible to utilize the exergy to its full extend. As a result, the exergy efficiency is not a universal metric to compare different separation processes under all the operating conditions. To identify the separation alternative that is most energy efficient in a given implementation, it is necessary to compare the process candidates by analyzing a system that accounts for the multiple alternatives that may be available with the uses of heat at a given plant site. This form of analysis is essential because, in addition to all the inefficiencies linked to the separation unit, the amount of fuel consumed by a separation process strongly depends on how its supplied energy is obtained, and how the rejected heat is utilized.

The framework of Fig. 2.1 depicts the energy interactions we consider. When the separation process consumes heat, this energy could come from steam that is directly generated by burning fuel (line 1), or from a co-generation power plant (line 2). A power plant can be operated to produce both electricity and steam at different levels of temperature and pressure. Alternatively, the required heat for the separation could come from waste heat rejected from another process unit (line 3) within a chemical or petrochemical plant. On the other hand, when the separation process consumes electricity, typically, the required energy is produced at a power plant (line 4). A possible alternate route is to extract electrical work from a rejected heat stream (line 5). When feasible, rejected heat from the separation unit could also be used to directly supply heat to another process (line 6) or to generate electricity (line 7). Distillation, as well as some other separation processes, are often heat integrated with other processing units within the same plant. Tools such as pinch analysis [75] are commonly employed to identify suitable heat integration schemes that help to reduce the overall energy demand.

As can be seen in Fig. 2.1, the total energy from the fuel combustion is distributed across the entire plant. This distribution can be direct if the fuel is physically divided and sent to different processes or can be indirect if the fuel energy is first generated as heat at a high temperature which is then cascaded along different processing units. Henceforth, we will refer to the fuel utilized directly or indirectly to provide the energy needed by the separation unit as the *effective fuel*. For example, when a separation unit uses steam that is co-generated by a power plant, one can calculate the additional fuel that would be needed by the power plant to restore the power loss due to the supply of co-generated steam to provide *effective fuel* used by the separation.

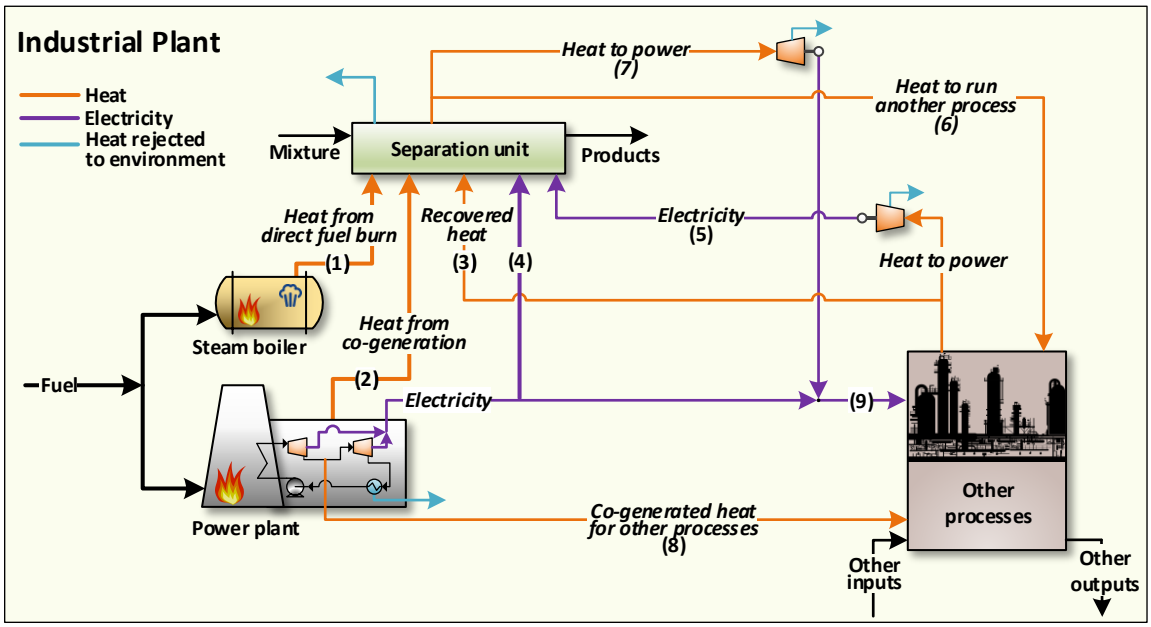

Fig. 2.1. Different ways to energy integrate a separation unit with the rest of the plant.

2.2.1 Understanding heat duty of an energy-intensive distillation

The following example illustrates the importance of evaluating the energy performance of a separation process at a system-level. The analyzed case is the separation of a liquid mixture of p-xylene/o-xylene. p-xylene is a valuable feedstock that is used in the manufacturing of important polymers such as polyethylene terephthalate (PET). Currently, simulating moving bed (SMB) and crystallization are the major technologies for separating xylene mixtures. Nevertheless, distillation is still employed in combination with SMB or crystallization when co-production of o-xylene is needed [76]. For several years, the separation of p-xylene through membranes (a non-thermal method) has been studied by a number of researchers [55, 67, 77, 78]. These researchers have used mixture of p-xylene/o-xylene as a test case. Typical mixture compositions used in these studies are 50% to 90% p-xylene and rest o-xylene. The studies are mainly motivated from the perception that the use of membranes could

bring high energy savings for this separation [79]. However, as we shall show later through an example of 50% p-xylene and 50% o-xylene, this expectation seems very optimistic since even with highly selective membranes, distillation consumes lower fuel than membranes. In the next section, we will add more details on this discussion about the fuel required by membranes for the separation of p-xylene/o-xylene and how they compare with distillation, but before that, we carefully review in this section the fuel required solely by distillation.

To simulate the separation of p-xylene/o-xylene through distillation, we consider a feed with a molar concentration of 50% in p-xylene. Since downstream uses require high purity and p-xylene is a valuable chemical, it is desirable that the separation process recover most of p-xylene from the mixture [54]. For this reason, we set the final purity and recovery of p-xylene equal to a typical value of 99.5% mol and 99% respectively (see Note 2 in Appendix B for a precise definition of purity and recovery).

In our analysis, we assumed that the distillation unit is part of a chemical plant, that has a power plant to supply various needs or co-generated steam is available from a nearby power plant. One scenario to utilize the energy released by fuel combustion in the power plant is to use the heat at the highest temperature level for producing electricity and extract heat at low temperature to perform the separation. Besides this possibility, we will calculate and analyze the effective fuel consumption of the distillation unit under various other scenarios that use different routes to supply the required energy. These scenarios were identified using Fig. 2.1. For brevity, and in order to avoid cases which could inherently favor distillation, we will assume that the energy does not come from a rejected waste heat stream from the plant (lines 3 and 5), and the heat rejected from the separation unit is not utilized downstream (lines 6 and 7).

Scenario 1- Using steam produced by directly burning fuel

When the distillation column is operated with heat input, the energy required at the reboiler can be supplied through steam directly produced from fuel combustion (line 1, Fig. 2.1). Figure 2.2a) shows the specific flowsheet that we simulated for heat supplied distillation.

Scenario 2 - Using steam co-generated in a power plant

The required steam to run the distillation scheme of Fig. 2.2a) can alternately be co-generated in a power plant (line 2, Fig. 2.1). For this case, we consider the extraction of saturated steam at 6 bar from the power plant. At this pressure, the steam saturation temperature is 159 °C, which is sufficient to perform the required heat transfer at the reboiler ($T_{reb} = 146$ °C).

Scenario 3- Using electricity from a power plant

The reuse of the heat from the distillation condenser ($T_{cond} = 138$ °C) could significantly reduce the fuel consumption for the separation. One way to reuse this heat is to transfer it to the reboiler with the aid of a heat pump. Figure 2.2b) shows a variant of heat pump distillation that we simulated for the analyzed separation. Under this approach, all the energy required to run distillation is supplied in the form of electricity, rather than in the form of heat. This energy comes from the power plant (line 4, Fig. 2.1).

Table 2.1 summarizes the energy requirements for all three evaluated scenarios. See section 2.5 for details on how the energy requirements were calculated. In Scenario 1, fuel is directly burned to produce extremely high temperature heat, which is then used to generate the steam supply for the distillation reboiler. Not surprisingly, the use of fuel in this way is very inefficient since the distillation column does not require an extremely high temperature heat as $T_{reb} = 146$ °C. In Scenario 2, the fuel, all of which is sent to a power plant, is utilized more efficiently as the combustion heat

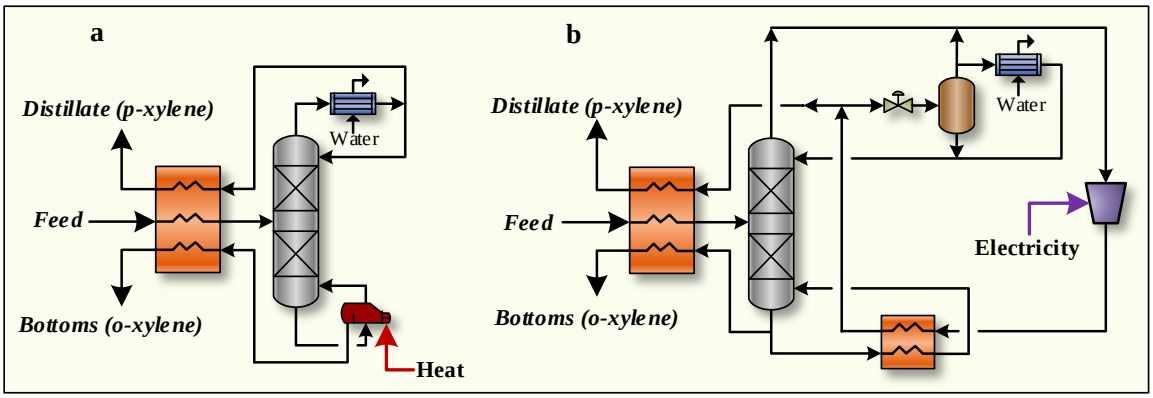

Fig. 2.2. Simulated configurations for the distillation of p-xylene/o-xylene. Distillate is 99.5% p-xylene and bottoms product is 99.0% o-xylene. **a-b**, Heat supplied distillation (**a**), Heat pump distillation (**b**). The heat integration between the feed and the product streams shown in both configurations has the purpose of preheating the feed up to its bubble point before it enters the column. This strategy helps to reduce the amount of external heat needed in configuration (**a**) and to reduce the amount of compression work needed in configuration (**b**).

is cascaded to produce electricity, and then heat at a moderate temperature. This synergy lowers the total fuel required by the entire plant, which is reflected in the amount of fuel that is effectively consumed for the separation. As we note, although the heat transferred to the reboiler in both Scenarios 1 and 2 is the same, the effective fuel used for distillation is 59% lower when using steam from co-generation and is the more preferred option for this distillation when it is heat driven. In Scenario 3, only electricity generated from the power plant is used for distillation. Interestingly, the effective fuel for distillation is, in this case, nearly on-tenth of that for Scenario 2, although once again, the heat exchanged at the reboiler is the same.

Table 2.1.
Energy requirements (kWhr/lb p-xylene in the feed) to distill 99.5% mol purity and 99% recovery of p-xylene from a 50%/50% mixture of p-xylene/o-xylene

Simulated scenarios	**ΔH_{vap} at reboiler**	**Supplied heat**	**Supplied electricity**	**Effective fuel heat**
Scenario 1- Steam from direct fuel burn	0.631	0.631	0	0.742
Scenario 2- Co-generated steam	0.631	0.631	0	0.303
Scenario 3- Heat pump distillation	0.631	0	0.018	0.036

The huge benefit from heat pump distillation can be understood intuitively by considering the temperature difference between the reboiler temperature of 146 °C and the condenser temperature of 138 °C. Since this difference is small, a low compression ratio, and, therefore, only a small quantity of electrical energy is needed to upgrade and deliver the heat collected at the condenser to the reboiler at the higher temperature. We note that when energy is the only metric for evaluation, heat pump consumes an order of magnitude lower energy than heat and a proper comparison with alternate methods requires careful examination of the mode in which this distillation need to be considered.

These results clearly demonstrate that the effective fuel consumption of a separation process depends significantly on how the energy is supplied and integrated with the rest of the plant. Thus, a systems level analysis is necessary to correctly evaluate its energy performance.

2.3 Thermal methods are not necessarily the most energy intensive

In addition to the previous calculations for distillation (thermal method), we calculated the energy requirements to separate the mixture p-xylene/o-xylene through reverse osmosis, which is a non-thermal method. This separation method consumes electricity, which we assume is supplied by a power plant (line 4, Fig. 2.1). It is important to mention that, for this separation, a single membrane is insufficient to meet the purity and recovery specifications. For this reason, we considered the use of a multistage membrane system similar to the one shown in Fig. 2.3. We formulated and solved an optimization model aimed at finding the optimum multistage membrane configuration and operating conditions that minimize the electrical work required for this separation (see section 2.5 for the calculation details). This optimum scheme also accounts for energy recovery from the high pressure of the net retentate stream.

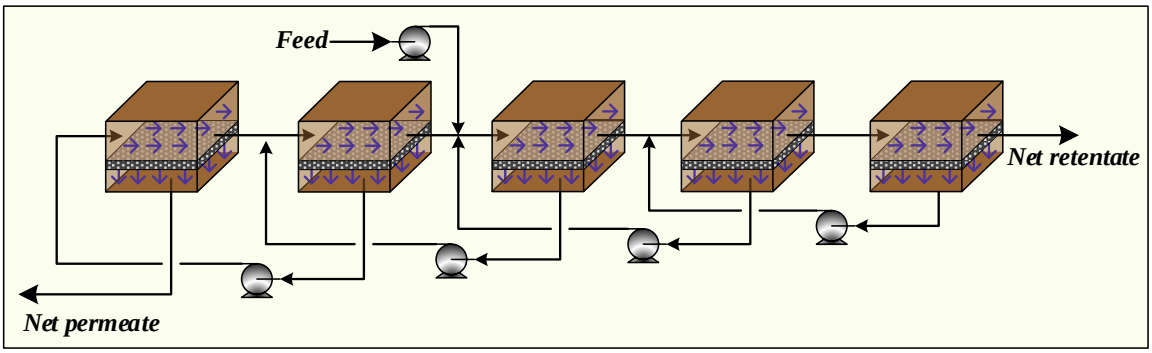

Fig. 2.3. Membrane cascade. The permeate stream (discharge stream at low pressure) from each membrane stage, except the p-xylene (net permeate) product stage, is pumped and fed to the high pressure side of the previous membrane stage. The retentate stream (the discharge stream at high pressure) from each membrane stage, except the o-xylene (net retentate) product stage, is fed to the high pressure side of the next membrane stage. For the 50%/50% p-xylene/o-xylene mixture, the net permeate stream is 99.5% p-xylene and the net retentate stream is 99.0% o-xylene.

Table 2.2 shows the energy consumed by a six-stage membrane cascade for various values of membrane permselectivity, which is defined as permeabilities ratio between the most (p-xylene) and the least permeable (o-xylene) components. Interestingly, these results show that even with very high permselectivity, the membrane cascade consumes over 2.9 times more fuel than heat pump distillation (see Table 2.1).

Table 2.2.
Energy requirements (kWhr/lb p-xylene in the feed) to permeate 99.5% mol purity and 99% recovery of p-xylene from a 50%/50% mixture of p-xylene/o-xylene through a six-stage membrane cascade

Permselectivity	**Supplied electricity**	**Effective fuel heat**
100	0.073	0.146
1,000	0.056	0.111
10,000	0.053	0.107

We highlight that to the best of our knowledge, the permselectivity employed in this comparison is very optimistic as the current highest permselectivity exhibited at lab scale for this separation through reverse osmosis is about 130 [55]. It is worth noting that due to practical considerations, the lab-scale permselectivity often declines when scaled to an industrial scale operation [80,81]. These factors include for instance concentration polarization, membrane aging, and the presence of membrane defects formed during the fabrication of membranes at commercial scale. This reduction in permselectivity translates into an increased fuel consumption for the separation. Besides the previous observations, it is important to point out that the separation efficiency of the heat pump distillation for the discussed example is 21% (see section 2.5 for the calculation details). Therefore, it is thermodynamically impossible for an alternative separation process to cut the energy intensity of the distillation by a factor of 10 as suggested by Sholl & Lively [58].

The systematic comparison results discussed so far clearly disprove the general perception that thermal processes are the most energy intensive. Now let us examine the general perception that thermal processes that entail vaporization of one or more components are more energy intensive than non-thermal counterparts that do not require phase change. As is observed from Table 2.1, the heat of vaporization incorrectly quantifies the energy performance. For the separation example of p-xylene/o-xylene, the total heat of vaporization at the reboiler is about thirty-five times higher than the electricity needed for the heat pumped option. In addition, the magnitude of fuel heat is much lower when co-generated steam is used or when the distillation is run with a heat pump. We also emphasize that a misperception exists, such as reflected in the following statement, in considering that the separation of close boiling point components through distillation is unattractive from an energy standpoint.

> "The similar size and boiling points of the various xylene isomers make them difficult to separate by conventional methods such as distillation. Advances in membranes or sorbents could reduce the energy intensity of these processes" [58].

In the case of the mixture p-xylene/o-xylene, both components have close boiling points, and yet distillation is less energy intensive than non-thermal membranes. Certainly, the close boiling points involved in this separation makes the internal heat transferred at the reboiler very high, but the actual fuel required by heat pump distillation is just a small fraction of this value [82].

We now discuss how some of the comparisons in the literature are deficient and how they have derived incorrect conclusions. Some of these studies have erroneously directly compared the quantities of heat and electricity consumed by thermal and non-thermal processes [83]. For instance, Koros & Lively [83] compared the heat for multistage flash distillation (50 kWhr-m^{-3}) against the electrical work needed in reverse osmosis (4.5 kWhr-m^{-3}) for water desalination. They concluded that membranes

consume more than an order of magnitude less energy than distillation. However, this comparison approach is misleading since heat and work are different forms of energy and should not be compared directly.

Coming back to our example of p-xylene/o-xylene, a direct comparison of the amount of heat supplied to distillation in Table 2.1 vis-a-vis the work for membrane with permselectivity of 10,000 in Table 2.2, would have lead to the incorrect conclusion that distillation is roughly 12 times more energy intensive relative to the six-stage membrane cascade. But, in reality, the fuel consumed by distillation is only 2.8 times the fuel consumed by the membrane cascade when the heat is supplied using a co-generated steam. We highlight that the fuel required by heat supplied distillation can be much lower if the heat rejected from the condenser, which is at significantly high temperature of 138 °C, is reused. For instance, the condenser heat could be used to generate steam and then extract electrical work from it using a condensing turbine. In this case, the effective fuel consumed by the distillation unit would be much lower than the value of 0.303 kWhr/lb p-xylene reported in Table 2.1. We remind that the use of heat pump distillation is one of the alternatives that overcomes the inefficiency of rejecting the high temperature condenser heat to the environment. As we illustrated in our example of p-xylene/o-xylene, heat pump distillation greatly reduces the fuel requirements, going even below than the fuel consumed by the six-stage membrane cascade with the extremely high permselectivity of 10,000.

Another method employed to compare a process that consumes heat versus another that consumes electricity consists in converting the corresponding electricity into an equivalent heat. Then, the resulting heat is compared to that needed for the thermal process. The idea is to determine how much heat is required in a power plant to produce the electricity. For the p-xylene/o-xylene example, under this approach, effective fuel heat of 0.107 kWh/lb p-xylene from Table 2.2 would be compared with either 0.631 kWhr/ lb p-xylene or 0.742 kWhr/lb p-xylene from Table 2.1.

However, the last comparison method often leads to incorrect conclusions since it implies that the heat consumed by the thermal method is always directly produced from combustion of fuel as in scenario 1 of Table 2.1, which is at a very high temperature. But this is frequently not true. Instead, as we illustrated before in the example of p-xylene/o-xylene, the heat employed in a separation process can come from a much lower temperature source, e.g. co-generation, which helps to reduce the fuel requirements. Furthermore, there could be other efficient modes of operation such as heat pump. This example stresses that in addition to following a consistent framework to perform an energy comparison among processes that consume different forms of energies, it is paramount to ensure that each of the compared processes is at its optimal mode. This includes in the case of a multi-component separation through distillation, finding the optimum arrangement of distillation columns that is most energy efficient as it has been shown that for a given separation, there could exist millions of possible configurations that can be used, but they have different energy requirements [68, 84]. In the literature, it has been reported sophisticated optimization models that can be used for this purpose [84–87]. Similar optimization models for multi-component separations through membranes or other alternative separation methods need to be developed to accurately compare their energy consumption against other processes.

The previous misconceptions over thermal methods are also prevalent for separations other than that of p-xylene and o-xylene. For instance, consider the separation of propylene and propane. It was reported [60] that distillation consumes over three times more energy than that reported for a three-stage membrane cascade with a permselectivity of 35 [47]. This estimate compares the reboiler heat of distillation with the combustion heat that, in a power plant, would produce the work needed for membrane-based separation. As we discussed before, this comparison assumes that the heat required by distillation is of the same quality (at the same temperature) as the one used to produce electricity in a power plant. However, this is clearly not a reasonable assumption since, in practice, for this application, the reboiler is at a

temperature close to the ambient temperature, $T_{reb} = 23$ °C at 9 bar. Therefore, this separation is in reality operated without using an external heat source. Instead, it is operated using a heat pump [48, 88].

The difference in the relative performance of distillation and membrane-based separation is staggering when one accounts for the quality of heat. This is apparent from our calculations in Table 2.3, where we use a propylene/propane permselectivity of 100 (with propylene being more permeable component), instead of 35 as used previously, a change that should make membrane-based separation even less energy intensive than claimed before. Instead, we find that such an optimized three-membrane cascade separation consumes 40% more fuel than heat pump distillation (Fig. 2.4), where the separation is of a propylene/propane feed, with 70 mol% propylene. The separation parameters were set at a purity of 99.6 mol% and 97.8% recovery in propylene. These feed and product compositions, which are the same as the ones employed by Colling et al. [47], are in agreement with typical industrial settings [50]. An important remark to be mentioned for this separation is that the thermodynamic efficiency of distillation is 27% (see section 2.5 for the calculation details). Therefore, as in the separation of p-xylene/o-xylene, a factor of ten reduction in energy intensity as suggested by Sholl & Lively [58] is thermodynamically infeasible.

Through our analysis, we have demonstrated that thermal methods often consume similar or even lower energy, than their non-thermal counterparts. Nevertheless, it should not be assumed that thermal separation processes are always the most energy efficient option. For example, in the separation of propylene/propane mixture under consideration, a single membrane stage with a propylene/propane permselectivity greater than 24 would consume lower fuel than heat pump distillation if only 50% of propylene needs to be recovered with 90% purity (see section 2.5 for the calculation details). In other words, lower product recovery at somewhat lower purity of propylene prefers membranes. Energy consumption by membrane water desalination plants

Table 2.3.
Energy requirements (kWhr/lb propylene in the feed) to separate propylene with 99.6% purity and 97.8% recovery from a 70%/30% mixture of propylene/propane through distillation, and a three-stage membrane cascade

Separation process	**ΔH_{vap} at reboiler**	**Supplied electricity**	**Primary fuel heat**
Heat pump distillation	0.468	0.021	0.042
Membrane cascade	Not applicable	0.030	0.059

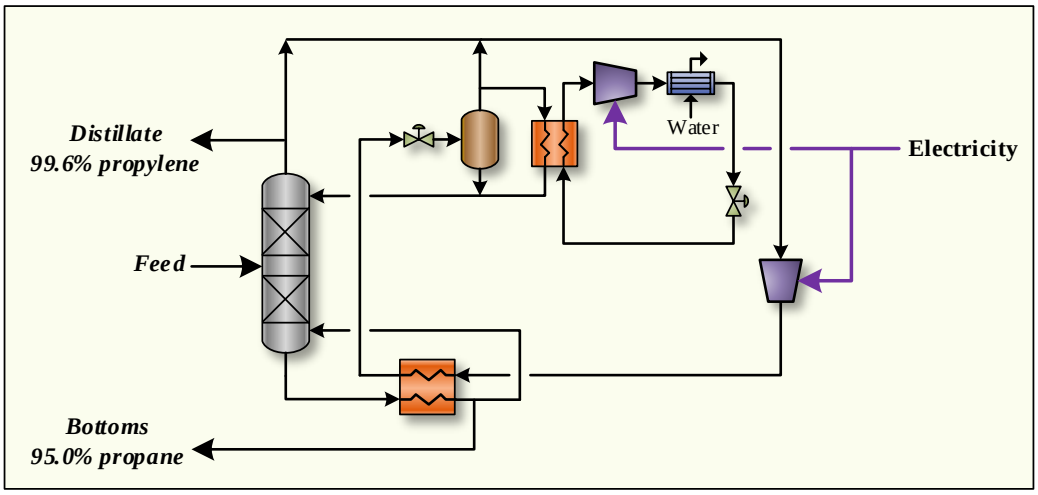

Fig. 2.4. Simulated configuration for the sub-ambient temperature distillation of 70%/30% propylene/propane mixture.

also benefits from the small level of purification of water relative to its molar feed-concentration, and the low recovery of water which is often in the neighborhood of 50%. These examples further demonstrate that one must carefully analyze the separation technologies to determine which of them will be most efficient for the separation at hand. Therefore, to derive reasonable estimates of relative performance

it is imperative to perform comparisons that follow a structural approach such as the one proposed here using Fig. 2.1.

2.4 Final remarks

In this chapter, we have shown conclusively that, despite the widely-held belief [58, 59], thermal separations are not necessarily the most energy intensive separation processes. Instead, this conclusion varies with the application at hand and can only be drawn following a system-level analysis that accounts for all energy interactions or else the claims are neither meaningful nor informative. To address this issue, we propose such a disciplined system-level analysis approach and show that, with such an approach, the conclusion drawn in the literature often reverses completely. For example, we showed that a thermal process previously claimed to be more energy-intensive than its non-thermal counterpart is actually significantly more efficient than the latter, even when the latter is accorded significant privileges that are not yet industrially feasible. We also showed that prior conclusions are sometimes at odds with the basic laws of thermodynamics, an undesirable outcome that can be prevented by following our structured comparison approach. Moreover, we also highlight that it is important to recognize that the most efficient way to operate a thermal process may not be using an external high temperature heat source. Rather, it may be much more efficient to use heat pumps.

In the absence of a structured comparison approach, there could be some consequences. First, more energy-intensive processes may be chosen for deployment. Second, the research is likely to ignore avenues that have the most potential and the chosen directions may be misguided leading to a significant waste of resources. Third, if deployed, the more energy-intensive process will significantly increase the system-wide release of CO_2 and other greenhouse gases, a growing concern of this economy. Therefore, it is important to carry out careful energy comparisons before selecting or

dismissing the use of a separation technology, and not just relying on perceptions, no matter how widely spread they are. Furthermore, since our conclusion is that neither thermal nor non-thermal processes always dominate the other, a balanced research portfolio would make advances on both fronts and be informed by structured comparison approaches like the one suggested in this work. This would help the chemical industry remain competitive and sustainable in the future.

2.5 Calculation methods

In this section, we describe the calculation methods employed to generate the results discussed in this chapter.

2.5.1 Fuel calculations

We employed the following methods to calculate the fuel heat effectively consumed by a separation process. These calculations are defined according to the specific energy utility supplied to the separation unit. Refer Fig. 2.1 for the entire system that captures relevant energy interactions of the separation unit with the rest of the plant.

Steam produced by directly burning fuel (line 1, Fig. 2.1): In this scenario, the fuel heat (Q_{fuel}) released from the combustion of fuel is transferred to water to produce steam, which carries the heat (Q) that is supplied to the separation process. The value of Q_{fuel} is calculated, as in equation (2.1), by dividing Q by the corresponding fuel-to-steam boiler efficiency, ($\eta_{fuel\ to\ steam}$), where the latter was assumed to be 85% [89].

$$Q_{fuel} = Q/\eta_{fuel\ to\ steam} \tag{2.1}$$

Steam co-generated in a power plant (line 2, Fig. 2.1): The fuel heat associated with co-generated steam is calculated as follows. If the heat supplied to the separation unit (Q) was not withdrawn from the power plant, an extra work W_{eq} would have

been produced. Then, we let Q_{fuel} denote the amount of heat required in the power plant to produce only W_{eq}. This value is calculated in equation (2.2) by dividing W_{eq} by the efficiency of the power plant when it is operated to solely generate electricity. The power plant efficiency ($\eta_{power\ plant}$) was assumed to be 50%.

$$Q_{fuel} = W_{eq}/\eta_{power\ plant} \tag{2.2}$$

Since the amount of work extracted from a certain quantity of heat increases with the heat temperature [90], the value of W_{eq}, and consequently, the fuel effectively consumed for separation, depends on the temperature at which heat is utilized by separation. We obtained, via simulation the ratio η, between W_{eq} and Q, for different temperature and pressure-levels of co-generated steam. More especifically, we simulated in Aspen Plus the flowsheet of Fig. 2.5 to estimate the equivalent work associated with co-generated heat in a power plant. In this scheme, super high pressure steam at 100 bar and 500 °C is expanded in three turbines connected in series to produce electrical work. All turbines were assumed to have an overall isentropic efficiency of 80%. The dotted orange lines represent the possibility of co-producing steam at different conditions (high pressure steam-HS, medium pressure steam-MS, and low pressure steam-LS). Normally, the extracted vapor later undergoes total condensation to provide heat to a process unit within the plant under consideration. The condensers shown in Fig. 2.5 are intended to represent these steps.

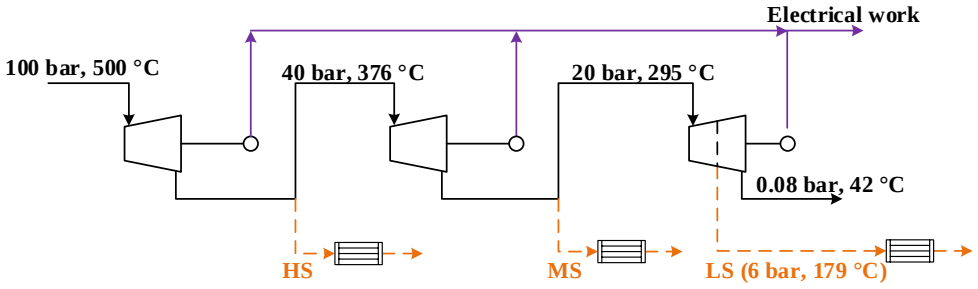

Fig. 2.5. Simulated flowsheet to calculate the equivalent work associated to co-generated heat in a power plant.

For those simulations where low pressure steam (LS) was not co-produced, the last turbine was operated as a condensing turbine with an outlet pressure of 0.08 bar. Under this condition, the stream leaving such turbine has 88% vapor (and 12% condensate). When LS steam was produced, the exhaust pressure of the last turbine was set to 6 bar. The equivalent work associated with the extracted vapor is then the electrical work that would be produced in subsequent turbines if the vapor was not withdrawn. The heat-to-work conversion factor ($\eta = W_{eq}/Q$) associated with the co-generated heat is then calculated by dividing the equivalent work by the heat released as the steam condenses. Table 2.4 shows a summary of these results.

Table 2.4.
Typical conditions and associated heat-to-work conversion factors (η) for co-generated steam.

P (bar)	**Tsat (°C)**	$\boldsymbol{\eta = W_{eq}/Q}$	**Steam classification**
40	250	0.42	HS-high pressure steam
20	212	0.34	MS-medium pressure steam
6	159	0.24	LS-low pressure steam

Electricity (line 4, Fig. 2.1): When the separation unit requires electricity, the corresponding fuel heat is calculated using equation (2.3), simply, by taking the ratio between the electrical work (W) and the power plant efficiency, which is, as before, assumed to be 50% so that

$$Q_{fuel} = W/\eta_{power\ plant}. \tag{2.3}$$

2.5.2 Simulation models for distillation

The separations of p-xylene/o-xylene and propylene/propane through distillation were simulated in Aspen Plus V8.6 using the rigorous equilibrium model RADFRAC. The equations of state selected for these simulations were the Soave-Redlich-Kwong (SRK) equation for the separation of p-xylene/o-xylene, and the Peng-Robinson equation in combination with Wong-Sandler mixing rules (PRWS) for the separation of propylene/propane [91–93]. As it is observed from Figure 2.6, there is a good agreement between experimental data of the vapor liquid equilibrium for both of the analyzed mixtures, and the predictions through the aforementioned equations of state.

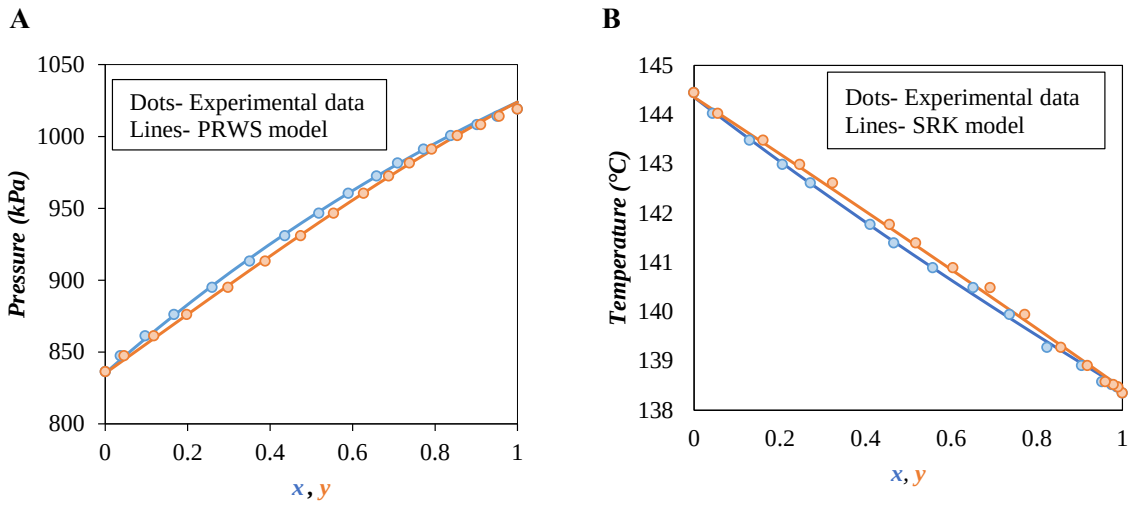

Fig. 2.6. Comparisons between predicted data and experimental data [94, 95] for the VLE of the mixtures p-xylene/o-xylene and propylene/propane. (A) VLE of the mixture propylene/propane at 30 °C. (B) VLE of the mixture p-xylene/o-xylene at 1 bar. x represents the molar fraction of p-xylene (resp. propylene) in the liquid phase, whereas y represents the molar fraction of p-xylene (resp. propylene) in the vapor phase.

Table 2.5 and Table 2.6 shows a summary of the feed and product conditions for all simulated cases of distillation. Figure 2.2 shows the complete configurations for heat supplied distillation and heat pump distillation for the separation case of

p-xylene/o-xylene. In these schemes, the feed is preheated up to its saturation point by performing heat integration with the product streams. This strategy helps to reduce the reboiler heat. For the separation of propylene/propane, we simulated the flowsheet shown in Fig. 2.4, which includes a refrigeration system to condense the vapor generated after the throttling valve in the heat pump system. The pressure drop inside the distillation column for the configurations of Fig. 2.2 and Fig. 2.4 was taken equal to 0.30 mbar/tray. This value is in good agreement with commercial structured packing such as MELLAPAK [96].

Table 2.5.
Feed and product conditions for the simulated separation of p-xylene/o-xylene through heat supplied distillation

Mixture	**p-xylene recovery in distillate (%)**	**Stream**	**Mol fraction (p-xylene)**	**Temperature (°C)/ pressure (bar)**	**Phase**
p-xylene/ o-xylene	99	Feed	0.500	30 / 1	Liquid
		Net distillate	0.995	30 / 1	
		Net bottoms	0.010	30 / 1	

Table 2.6.
Feed and product conditions for the simulated separations of p-xylene/o-xylene, and propylene/propane through heat pump distillation

Mixture	**p-xylene or propylene recovery in distillate (%)**	**Stream**	**Mol fraction (p-xylene or propylene)**	**Temperature (°C)/ pressure (bar)**	**Phase**
p-xylene/ o-xylene	99	Feed	0.500	30 / 1	Liquid
		Net distillate	0.995	35 / 1	
		Net bottoms	0.010	35 / 1	
Propylene/ propane (case 1)	97.765	Feed	0.700	17 / 9	Vapor
		Net distillate	0.996	15 / 9	
		Net bottoms	0.050	23 / 9	
Propylene/ propane (case 2)	50	Feed	0.700	17 / 9	Vapor
		Net distillate	0.900	16 / 9	
		Net bottoms	0.573	18 / 9	

NOTE: The feed propylene/propane is at saturated conditions for the two cases simulated

For each separation case, we calculated the total number of theoretical trays and feed tray location for the distillation column using the following procedure:

1. Estimate the minimum reflux ratio (RR_{min}) by simulating in Aspen Plus a column with a large number of trays (keeping the pressure along the column constant and equal to the pressure of the feed). In addition, from the simulation results, obtain the value of relative volatility at the feed tray location. The values of RR_{min} and relative volatility are used in the next step.

2. Calculate the optimum number of trays and feed tray location using the equations proposed by Underwood [97]. This approach requires the specification of the composition of the feed and product streams, feed quality, relative volatility, and the reflux ratio, which was taken as $1.1RR_{min}$.

3. Simulate in Aspen Plus the column designed in step 2. If the reflux ratio obtained through rigorous simulation is $1.1RR_{min}$, accept the design. Otherwise increase or reduce the number of trays while maintaining constant the relation between the feed tray location and total number trays until the reflux ratio gets close to $1.1RR_{min}$.

Additional considerations for heat pump distillation:

As mentioned before, the only input energy to the heat pump distillation schemes shown in Fig. 2.2b and Fig. 2.4 is the electricity supplied to the compressors. To reduce the compressor work, the temperature difference at the boiler/condenser, which exchange heat between the bottoms liquid and the compressed vapor must be maintained to the lowest possible value because such a design reduces the work done by the compressor. Modern highly efficient heat exchangers allow temperature differences as low as 0.5 °C [98]. In this work, we have used a conservative value of 1.0 °C. This temperature difference was also imposed at the boiler/condenser within the refrigeration cycle used in the separation of propylene/propane. To account for pressure losses that may be present in a real operation, we assumed that the vapor that exits the

top of the column undergoes a pressure loss of 0.1 psi for each pipeline located before and after the compressor. The pressure drop at the boiler/condenser was neglected since highly efficient heat exchangers practically eliminate such a pressure drop [99]. Finally, all compressors were assumed to have overall isentropic efficiencies of 75%.

Each heat pump distillation flowsheet was embedded into an optimization framework formulated in Aspen Plus with the objective of minimizing the compressor power. The outlet pressure of the compressor, and the fraction of the vapor flow (out of the separator) recycled to the compressor were taken as the decision variables. The amount of heat exchanged by the boiler/condenser was constrained to match the external heat required for the same separation by heat supplied distillation.

2.5.3 Optimization of the membrane cascade

For some of the separation cases discussed in this paper, a single membrane is not enough to achieve both high purity and recovery. Multistage membrane separation is a suitable solution. However, finding the optimum configuration and operating conditions is not straightforward, as there are many designs that fulfill the separation requirements, but consume different amounts of energy. To handle this task, we solved the optimization model developed in Chapter 1 with the goal of identifying the membrane cascade with the least energy input. For the liquid separation of p-xylene/o-xylene, the energy input is pump work, and for the gaseous separation of propylene/propane, the energy input is compressor work. Figure 1.6 shows the multistage membrane superstructure that was optimized for the liquid separation of p-xylene/o-xylene. This arrangement includes a turbocharger (TC) which helps to reduce the energy consumption by transferring part of the hydraulic energy from the final retentate stream to the feed stream. We assumed that the efficiency of the turbocharger was 80 %, and that the efficiencies of the pumps were 75%. Table 2.7 shows the operating conditions of the feed and product streams.

Table 2.7.
Stream conditions in the separation of p-xylene/o-xylene through a membrane cascade

p-xylene recovery in the net permeate (%)	Stream	Mol fraction (p-xylene)	Temperature (°C)/ pressure (bar)	Phase
99	Feed	0.500	30 / 1	Liquid
	Net permeate	0.995		
	Net retentate	0.010		

For the gaseous separation of propylene/propane, we optimized the superstructure shown in Fig. 1.5. The propylene/propane feed, which is saturated vapor at 17 °C, was heated up to 30 °C before entering the cascade by transferring heat from the environment. This preheating stage was considered to avoid capillarity condensation inside the membrane. The quantity of heat utilized in this stage was not included in the total amount of energy that was compared against the energy consumed by heat pump distillation. This is because the heat supplied to the feed is *free* as it is taken from the environment. Table 2.8 shows a summary of the conditions for the feed and product streams in the separation cases that we evaluated. Observe that because of the preheating stage, the products streams from the membrane cascade are at a higher temperature than the products from heat pump distillation (Table 2.6). At first glance, it might appear that having the membrane products at a higher temperature is advantageous from an energy perspective as it could be possible to extract work from sensible heat, and thus, decrease the net work consumption. Nevertheless, this is practically infeasible since the products are already at ambient temperature (30 °C). In addition to the previous observation, we note that the final permeate was compressed up to 9 bar, which is the same pressure as that of the feed and retentate streams, as well as that of all the streams simulated in the alternative separation through heat pump distillation. The compression of the permeate stream was considered as it is needed for its transportation and because some downstream applications require moderate pressure conditions (e.g. the Unipol process for polypropylene

production operates between 25-30 bar [100]).The power of the compressors in the cascades were calculated using an isothermal efficiency of 75%.

Table 2.8.
Feed and product conditions in all the evaluated cases for the separation of propylene/propane through a membrane cascade

Case	Propylene recovery in the net permeate (%)	Stream	Mol fraction (propylene)	Temperature (°C)/ pressure (bar)	Phase
1	97.765	Feed	0.700	17 / 9	Vapor
		Net permeate	0.996	30 / 9	
		Net retentate	0.050		
2	50	Feed	0.700	17 / 9	Vapor
		Net permeate	0.900	30/9	
		Net retentate	0.573		

The number of stages of a membrane cascade is usually determined by economic factors. In the case of the gaseous separation of propylene/propane, we considered a maximum of three stages with two intermediate compressors. Multistage membrane gas separations are often limited to this number due to the high cost of the compressors [11, 101]. Observe that if we account for the compressor to pressurize the net permeate stream, a three-stage cascade has more compressors than those needed for the sub-ambient distillation with a heat pump. Thus, in terms of only capital cost associated to compressors, distillation might be more advantageous. In the case of a liquid separation, the cost associated with pumping is lower than the compression of gases. Thus, a higher number of stages in the membrane cascade may be allowed. In this work, we employed six stages for the liquid separation of p-xylene/o-xylene.

To solve the corresponding optimization problems for the separations of propylene/propane, and p-xylene/o-xylene, we used the global optimum solver BARON [33]. For the separation of propylene/propane, we proved global optimality within an optimality gap of 5%. With respect to the separation of p-xylene/o-xylene, preliminary calculations showed that the optimal power consumption of the six-stage

cascade decreases as the trans-membrane pressure difference (Δp^{trans}) is increased. For this reason, we first fixed Δp^{trans} at 115 bar, which is the highest Δp^{trans} value reported in Kho et al. [55], and then optimized the cascade (global optimality was also guaranteed within an optimality gap of 5%).

2.5.4 Calculation of separation efficiency

The efficiency reported for the separation of p-xylene/o-xylene and propylene/propane through heat pump distillation was calculated according to equation (2.4) [82]. In this expression, W_{min} is the thermodynamic minimum work of separation, which corresponds to the amount of work required if the separation is performed using a reversible process [90]. This value is a lower limit of the work energy needed to separate a mixture. The magnitude of W_{min} is equal to the change in Gibbs free energy (ΔG) between the products and the feed at ambient conditions (taken as 30°C and 1 bar in this work). We calculated the value of ΔG in Aspen Plus V8.6. For these calculations, we employed the SRK equation of state in the case of the separation of p-xylene/o-xylene, and the PRWS equation of state in the case of the separation of propylene/propane. As we mentioned before, these models predicts well the vapor liquid equilibrium of the corresponding mixtures.

The remaining term in equation (2.4), W_{dist}, is the amount of electrical work needed to run the corresponding distillation flowhseet shown in either Fig. 2.2b) or Fig. 2.4. As mentioned, this value was calculated through rigorous simulation in Aspen Plus. We point out that the calculation of W_{dist} accounts for most irreversibilities encountered in practice, which include compressor inefficiencies, pressure drop, and finite temperature differences in heat exchangers.

$$\eta_{sep} = \frac{W_{min}}{W_{dist}} \tag{2.4}$$

3. WHICH SEPARATION METHOD TO USE: MEMBRANES OR DISTILLATION?

3.1 Introduction

Mixture separations play a crucial role in the production of a large number of chemicals and purified products that have improved our lives. Among the separation technologies, distillation, which is a thermally driven process, has remained the preferred choice at many types of industries. To give an insight of the scale of utilization of distillation, just in the U.S., it is estimated that more than 90% of all fluid separations in chemical and petrochemical plants are performed with distillation columns [57], which consume all together about 3% of the total energy consumption in the U.S [102].

Although distillation and other commercial separation technologies fulfill most of the current separation needs, the energy-intensive nature of many molecular separations, and the growing concern of reducing CO_2 emissions has led to intense research to seek for more energy-efficient separation processes. Among the separation alternatives portfolio, there is a special attention in the use of membranes. The increasing interest towards expanding the range of separations through membranes has been influenced significantly from the widespread perception that membranes are markedly less energy intensive than distillation. This perception comes primarily from the rationale that distillation is inherently more energy intensive because it requires the vaporization of at least one component [59]. However, as we showed in Chapter 2, inferring the energy intensity of distillation based solely on the enthalpy of vaporization is misleading and incorrect. In reality, distillation has the potential to operate with similar or even lower energy intensity than membranes. Nevertheless, this does not

imply that distillation is always the most energy efficient option, but instead, there are applications where distillation is superior to the membrane processes and there are applications where membranes are better.

Since neither membranes nor distillation is always the best, research efforts and future technological developments should be directed at both of these separation methods. To make a better utilization of financial resources and efforts to research or design potential separation applications with either membranes or distillation, it is deemed important to understand under which operating conditions the use of each of these two processes is likely to be more favored from an energy standpoint. This chapter is focused on that purpose. More clearly, in this research we introduce a comparative study of the energy requirements of both membranes and distillation under different separation conditions, given in terms of feed composition, and target purity and recovery. This study aids to demarcate when it is more energy efficient to use membranes or distillation.

3.2 Previous works

Some works that compare the energy consumption of membranes and distillation have been reported before, but unlike our study, those works do not explore a wide range of recovery of the component of interest, as well as most of them only analyze a single feed composition and target purity. Moreover, some of those studies provide misleading conclusions. Koros & Lively [83] directly compared the heat for distillation against the electrical work needed in reverse osmosis for water desalination. The conclusion reached in this study was that membranes consume more than an order of magnitude less energy than distillation. However, as it was pointed out in Chapter 2, the direct comparison of heat vis-a-vis electrical work energy does not provide meaningful information of the energy intensity of these processes. This is because the second law of thermodynamics dictates that a given amount of work is more valuable

than the same amount of heat. Furthermore, the energy needed for membranes or distillations usually comes from a fuel source, and under this scenario, a consequence of the second law of thermodynamics is that the relative difference between the heat and the electrical work required by these processes can be quite different than the corresponding difference of fuel utilization. Therefore, the direct comparison of heat vs work is misleading as it may not be consistent with the corresponding difference in terms of fuel, which is the primary source of energy.

Koros [60] analyzed the energy required by distillation and a membrane process for the separation of propylene/propane in gaseous phase. They reported that membranes consume over three times less energy than distillation based on the comparison of the reboiler heat of distillation with the combustion heat that, in a power plant, would produce the work needed for the membrane process. Nevertheless, as we detailed in Chapter 2, this comparison approach, and consequently, the conclusion reached is misleading because they assume that the heat required by distillation always comes from a high temperature source, such as the heat used to produce electricity in a power plant. But in reality, the heat for distillation can come from a lower temperature source, such as steam co-generated in a power plant, which helps to reduce the effective fuel utilized for the separation.

Furthermore, modern distillation plants that perform the separation of propylene/propane are not even operated with heat, but in contrast, they operate with a heat pump, which require solely electrical work energy. The comparison of the membrane work vs the work for heat pump distillation completely reverses the previous conclusion, showing that the evaluated membrane process consumes roughly 40% more energy than distillation for the production of 99.6% pure propylene with 97.8 % recovery from a 70%/30% mixture of propylene/propane. As we observe, a confusion often arises when comparing membranes and distillation because these processes use different forms of energy. In Chapter 2, we introduced a framework that resolves

the aforementioned issues, and allow to correctly compare processes that consume different types of energies.

It is worthy to highlight that for some separations, such as in the separation of propylene/propane, it is more energy efficient to operate a distillation process with the aid of a heat pump, which requires the supply of electrical work, rather than operating it with external heat input. Unfortunately, the use of heat pump distillation seems to be absent in most current published comparisons between membranes and distillation, which may not allow to conclusively identify whether membranes are more energy efficient than distillation.

Among the few works that we found which compare the energy performance of heat pump distillation (HP-Distillation) and membranes, Ma et al. [103] studied the separation of propylene/propane through a single membrane and HP-Distillation. These authors concluded that the replacement of distillation by a membrane for the current separation seems challenging to achieve as even a hypothetical membrane with an extremely high selectivity of 500, would only recover 80% of propylene at a purity of 99.7%, which is significantly lower than the target recovery of 99.6% currently achieved through distillation at the same purity. Notwithstanding, they showed that the operation of a hybrid system that combines a distillation column and a single membrane could provide about 10% of energy savings as compared to the standalone distillation process. This study opens a new possibility of improving the energy efficiency of this separation. Nevertheless, it is important to note that the simulated heat pump distillation flowsheet operates at a suboptimal temperature difference of 5 °C at the boiler/condenser. Modern heat exchangers allow to operate at temperature differences as low as 0.5 °C [98], which helps to reduce the net work consumed by the heat pump. This leaves unanswered whether the proposed hybrid distillation with a membrane is more energy attractive than an optimized heat pump distillation. In this work, we provide further knowledge regarding this separation by comparing the

energy requirements between an optimized heat pump distillation process with an optimized membrane process under different conditions of purity and recovery.

Another comparative analysis of the energy requirements of a single membrane and heat pump distillation is found in the work of Belaissaoui [104], who studied the separation of O_2 from air. They compared the electrical work consumption for both distillation and membranes at a fixed stage cut of 10% (defined as the flow ratio of the enriched O_2 product stream and the feed flow), but under different target purity values of O_2, which range from low to very high values. Under these purity values and the considered stage cut, the corresponding O_2 recovery ranges between 14 to 48%. It was found that when O_2 is required at a high purity, a single membrane consumes more energy than heat pump distillation, even if using a membrane with a much higher selectivity than current commercial membranes. Nevertheless, when only a moderate O_2 purity of around 65 to 85% is needed, it appears promising that future membranes with improved selectivity could offer a more energy efficient alternative as compared to current heat pump distillation.

In the area of molecular liquid separations, reported comparisons between distillation and membranes concentrate mainly on applications of water desalination. Darwish et al. [64] showed that reverse osmosis consumes less energy than multi-stage flash distillation to desalt seawater. As we shall show later, this observation is in agreement with the trend found in our results for other separations which shows that membranes are more energy attractive than distillation-based processes when the feed is highly concentrated in the most permeable component and the recovered amount of most permeable component in the permeate product is moderate. Energy consumption by membrane water desalination plants benefits from the high molar concentration of water (most permeable component) in the feed and the low recovery of water which is usually less than 50%. Additional studies that analyze thermal and membrane based separation for water desalination have been reported. Among those

works, Al-Karaghouli & Kazmerski [65] evaluated the energy consumption of Reverse Osmosis (RO) and the energy required for different distillation based processes, which include multi-effect distillation (MED). These authors reported that the work energy required for RO (4-6 kWh/m^3) is lower than the equivalent work needed for MED (14.45-21.35 kWh/m^3). However, we note that this comparison is not accurate because the purity requirement considered for reverse osmosis (400-500 ppm of salt) was less stringent than the one employed for distillation (10 ppm of salt). Similar inconsistencies are found in the work of Mabrouk et al. [72] and Kempton et al. [71]. To obtain accurate conclusions, it is important to ensure that the same separation requirements are used for all evaluated processes.

In this chapter, we analyze and compare the energy consumed by membranes and distillation for the separation of two different mixtures. The first of them is the liquid mixture of p-xylene/o-xylene, whereas the second is the gaseous mixture of propylene/propane. In our analysis we optimize both membrane and distillation processes, and contrast their energy consumption under different values of feed composition, and target purity and recovery of the component of interest.

3.3 State of art of the analyzed separations

In this section we provide further information regarding the mixture separations that we study in this chapter.

p-xylene/o-xylene

p-xylene is a very important compound used in the production of diverse chemicals, including terephthalic acid, which is subsequently used as a building block for the manufacturing of important polymers such as polyethylene terephthalate (PET) and polybutylene terephthalate (PBT) [52].

The primary route to synthesize p-xylene is the catalytic reforming of naphtha, which produces p-xylene in a concentration close to 20% based on the C8 cut [53]. Alternatively, p-xylene is produced via other routes such as toluene disproportionation or transalkylation. It is worthy to highlight that the toluene disproportionation process has the advantage that p-xylene is produced at a high concentration of around 90%, which facilitates its separation [54]. The major technologies commercially available to separate p-xylene include simulated moving bed (SMB) and crystalization. Nevertheless, distillation is still employed in combination with SMB or crystalization when co-production of o-xylene is needed [76]. Usually, the reformate is separated in a first fractionator, and then, the obtained liquid enters a xylene splitter that partially separates o-xylene from p-xylene and the other isomers contained in the C8 cut. The latest mixture is sent to a p-xylene extraction unit, which can be SMB, crystallization or a combination of both, to finally produce p-xylene with a purity and recovery close to 99.5% and 99% respectively [105]. In general, SMB is preferred over crystallization as it has a higher p-xylene recovery per pass (95%) than the latter process (60-65%) [106].

We clarify that although in reality the mixture that contains p-xylene and o-xylene is multi-component, for the purpose of this study, we assume that it is composed only by p-xylene and o-xylene.

Propylene/propane

Propylene is the second most produced feedstock in the petrochemical industry after ethylene [107]. It is the precursor to produce a wide variety of chemicals such as polypropylene, propylene oxide, acryl acid, acrylonitrile, cumene, and isopropanol [44]. It is also employed in refining processes for alkylation, catalytic polymerization, and dimerization for gasoline blends [108].

The production of propylene comes mainly from two sources; as a coproduct in the ethylene process by steam cracking and as a byproduct in the Fluid Catalytic Cracking (FCC) within a refinery, being the first source the most important one [108]. The effluent from either of these two processes is separated by means of a series of fractionators [48]. The feed concentration of the mixture that enters the propylene/propane splitter has a concentration of 70% mol in propylene, however, other separation cases have been reported with a value close to 50% [45, 50, 109]. In general, propylene is produced in three purity levels; 70% for refinery applications, 92-96% for chemicals and 99.6 % for polymer grade [108]. Since the demand of propylene is very high, it is separated with a high recovery close to 99%.

To the best of our knowledge, there are no commercially available membrane processes for both of the separations described above; p-xylene/o-xylene and propylene/propane. Nevertheless, it is frequently perceived that the use of membranes could introduce significant energy savings for these separations, which has led to a lot of research in this area. Different types of membranes have been proposed, which include polymeric, zeolite and facilitated transport membranes, among others [55,67,77,78,103,110–113]. As we shall show in our analysis, membranes certainly provide a promising route to save energy for these separations, but only in a narrow region of feed composition, and target purity and recovery.

3.4 Methodology

3.4.1 Simulated conditions

For the separation of p-xylene/o-xylene, we assumed a liquid feed at 1 bar and 30 °C (ambient conditions). Moreover, the feed flow was assumed to be 250 mol/s, which is in a similar order of magnitude than the treated flow at the industrial scale. We perform several sensitivities in terms of feed composition, and target purity and recovery of p-xylene. Table 3.1 shows a summary of these values. The feed composition

of 0.20 and 0.90 capture the concentration of p-xylene typically encountered in the output from the naphtha reforming and from the toluene disproportionation processes respectively. On the other hand, the intermediate composition of 0.65 was included to simulate a stream that comes from a partial separation through SMB [114]. The p-xylene recovery in the product stream (which becomes enriched in p-xylene) was varied from 50% up to 99% (where the latter is near to the typical industrial recovery).

For the separation of propylene/propane, the feed was assumed to be saturated vapor at 9 bar. The feed flowrate and its corresponding molar fraction of propylene were assumed to be 250 mol/s and 0.65 respectively. The target purity and recovery of propylene were varied according to the values shown in Table 3.1. The simulated feed composition of 0.65 is within the range found in the real industrial separation. Also, the target purity values of 0.995 and 0.91 are similar to those needed in the production of polymeric and chemical grade propylene respectively, which as we said before, is typically accompanied by a propylene recovery close to 99 %. We highlight that to get a better understanding of the relative energy intensity between membranes and distillation, the feed concentration, recovery, and purity values evaluated in this study do not only capture the conditions commonly encountered in the industry for such separations, but they also cover a much wider operating spectrum.

Table 3.1.
Simulated conditions in the separation of p-xylene/o-xylene, and propylene/propane. All compositions and recovery range shown above refer to either p-xylene or propylene.

Mixture	**Phase**	**Mole fraction of p-xylene or propylene in the feed**	**Purity of p-xylene or propylene in the final product***	**Molar recovery range (%)****
p-xylene/ o-xylene	Liquid	0.20	0.80, 0.995	50-99
		0.65	0.91, 0.995	
		0.90	0.97, 0.995	
Propylene/ propane	Gas	0.65	0.91, 0.995	50-99

* The reported purity values are given as mol fractions in the distillate or permeate product streams.
** The molar recovery is calculated as the ratio between the molar flow of p-xylene (resp. propylene) in the distillate (resp. in the permeate) stream, and the corresponding amount of the same component in the feed.

3.4.2 Evaluated distillation processes

To obtain insightful conclusions from our comparative analysis between membranes and distillation, we attempt to evaluate both of these processes at their most energy efficient conditions (within some practical constrains). This includes in the case of distillation, operating it with a heat pump, since as we show in Appendix C, the close boiling points of the components that comprise the studied mixtures make more energy efficient to use heat pump distillation rather than heat supplied distillation.

Heat pump distillation schemes

The separations of p-xylene/o-xylene and propylene/propane through distillation were simulated in Aspen Plus V8.6 using the rigorous equilibrium model RADFRAC. Fig. 3.1a shows the specific heat pump distillation flowsheet that we simulated for the separation of p-xylene/o-xylene. In this scheme, the vapor that comes out from the top of the column, which is at a lower temperature than the reboiler, is com-

pressed to upgrade its temperature and being able to deliver all the heat needed at the reboiler. Thus, under this approach, no external heat needs to be supplied to the distillation process, but instead, all the required energy is supplied in the form of electricity, which is consumed by the compressor. It is important to mention that in the flowsheet of Fig. 3.1a, the liquid feed is preheated up to its saturation point by performing heat integration with the distillate and bottom product streams. This strategy helps to reduce the vapor traffic inside the column, which results into a reduction of the amount of work needed for the compressor.

For the separation of propylene/propane we simulated the flowsheet shown in Fig. 3.1b. This configuration does not include any heat transfer between the feed, distillate and bottoms streams as the feed is already at saturated conditions. Since the vapor that is produced after the throttling valve is at sub-ambient temperature ($\sim$ 15 °C), we incorporate a refrigeration cycle. Finally, we should note that to maintain the same phase conditions in the product streams as those simulated for the membrane process, both the distillate and the bottoms products are withdrawn in vapor phase.

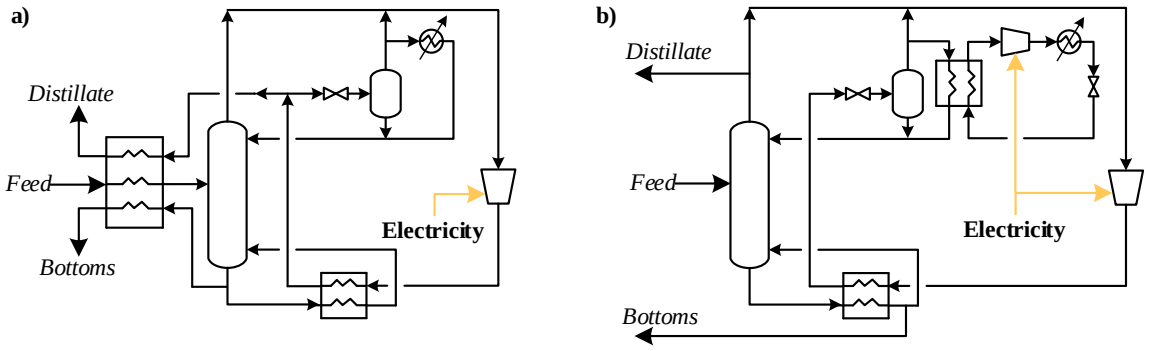

Fig. 3.1. Simulated heat pump distillation configurations. **a-b**, Simulated scheme for the separation of p-xylene/o-xylene (**a**), Simulated scheme for the separation of propylene/propane (**b**).

For each combination of feed composition, target purity and recovery considered for the separation of either p-xylene/o-xylene or propylene/propane, we designed and simulated a distillation column with a total number of theoretical trays and feed tray location such that it operates at 1.1 of its minimum reflux ratio. To make more realistic the simulations, the effect of pressure drop along the column was incorporated by setting a ΔP =0.30 mbar/stage, which is in good agreement with commercial structured packing such as MELLAPAK [96]. In addition, we assumed that the vapor that exits the top of the column, and which later undergoes its compression, has a pressure loss of 0.1 psi due to its transportation at each pipeline located before and after the compressor. Lastly, we assumed that all compressors that take part of the simulated heat pumps have an overall isentropic efficiency of 75%.

When operating a heat pump, it is crucial to maintain the lowest possible temperature difference between the streams at the boiler/condenser since operating at higher temperature differences increases the compressor power. In this work we have considered a minimum temperature difference of 1.0 °C at both ends of the heat exchanger. This temperature difference was also imposed at the boiler/condenser within the refrigeration cycle used in the separation of propylene/propane. We highlight that modern heat exchangers allows to operate with temperature differences as low as 0.5 °C [98]. The pressure drop at each boiler/condenser was neglected because optimized heat exchangers such as downflow type allow to practically eliminate pressure losses [99]. The evaluated heat pump distillation flowsheets were embedded into an optimization framework formulated in Aspen Plus with the objective of minimizing the total compression power. The pressure out the compressor, and the fraction of the vapor flow (out of the separator) recycled to the compressor, were taken as the decision variables. The optimization model was constrained to exchange the same amount of heat at the main boiler/condenser than the heat that would be supplied to the reboiler in conventional heat supplied distillation.

Heat pump distillation schemes with an intermediate reboiler

In addition to the configurations of Fig. 3.1, we simulated the improved heat pump distillation flowsheets shown in Fig. 3.2, which include an intermediate boiler/condenser. The use of an intermediate boiler/condenser allows to compress part of the vapor that leaves the column at a lower pressure ratio, which decreases the net compression work.

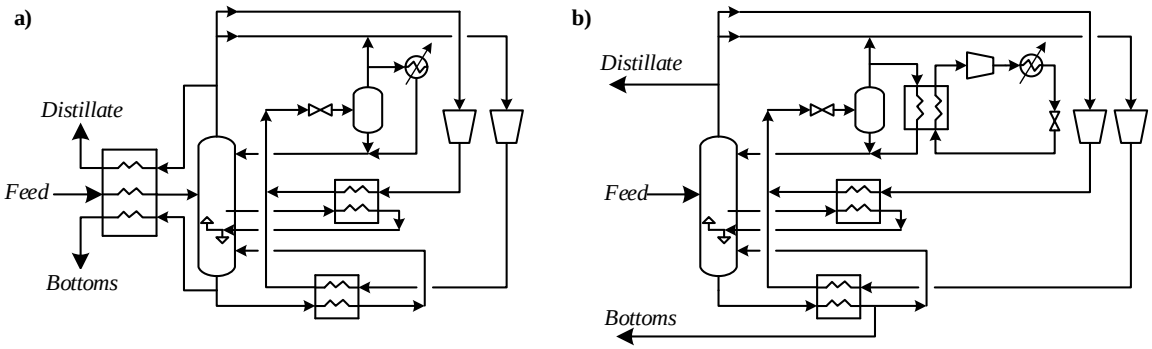

Fig. 3.2. Simulated heat pump distillation configurations with an intermediate boiler/condenser. **a-b**, Simulated scheme for the separation of p-xylene/o-xylene (**a**), Simulated scheme for the separation of propylene/propane (**b**).

When using an intermediate boiler/condenser in heat pump distillation, it is very important to optimize the tray location of the withdrawn liquid and the corresponding degree of vaporization as these variables strongly affect the compressor's work. Agrawal & Herron [115] developed a reliable shortcut method based on exergy analysis to find the optimum location and the fraction of vaporization of the withdrawn liquid. We employed this method to obtain an initial guess for the location of the intermediate boiler/condenser. Then, we varied the location around this guess in the rigorous simulation model until finding the optimum position. We should mention that for each tested location, we solved an optimization problem formulated within Aspen Plus with the objective of minimizing the total compression work. The chosen decision variables were the pressure ratio out of each compressor, the fraction of

the vapor flow (out of the separator) recycled to the main compressor, and the split fraction of the vapor stream that is distributed to both compressors.

3.4.3 Evaluated membrane processes

To evaluate the energy requirements for the analyzed separations through membranes we employ a multistage membrane cascade. This choice was taken because for many of the simulated separations, a single membrane was insufficient to meet the purity and recovery specifications, a limitation that was overcome through the use of a cascade.

Although a membrane cascade offers a suitable solution, its design is challenging as usually exits many possible cascades that fulfill the separation requirements, but consume different amounts of energy. To perform a proper comparison of the energy requirements of a membrane cascade against distillation, we solved an optimization problem with the goal of identifying the membrane cascade that consumes the least energy input. Figure 3.3 shows the multistage membrane superstructure that we optimized for each of the study cases corresponding to the liquid separation of p-xylene/o-xylene. This network includes a turbocharger (TC) which helps to reduce the net energy consumption by transferring part of the hydraulic energy from the final retentate stream to the feed stream. We assumed that the efficiency of the turbocharger was 80 %, and that the efficiencies of the pumps were 75%.

On the other hand, for each study case concerning the gaseous separation of propylene/propane, we optimized the superstructure shown in Figure 3.4. We note that the final permeate was compressed up to 9 bar, which is the same pressure as that of the feed and retentate product. This was made to maintain the same pressure conditions as those simulated for the same separation through heat pump distillation and because the propylene product needs to be pressurized for its transportation and

for some downstream applications that require moderate pressure (e.g. the Unipol process for polypropylene production operates between 25-30 bar [100]).

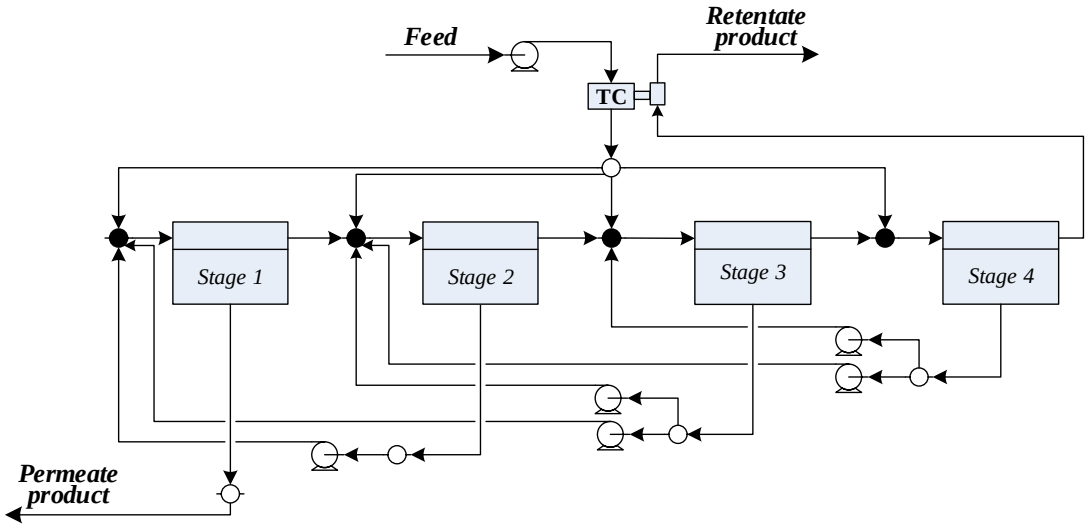

Fig. 3.3. Optimized cascade superstructure for the separation of p-xylene/o-xylene. TC means turbocharger

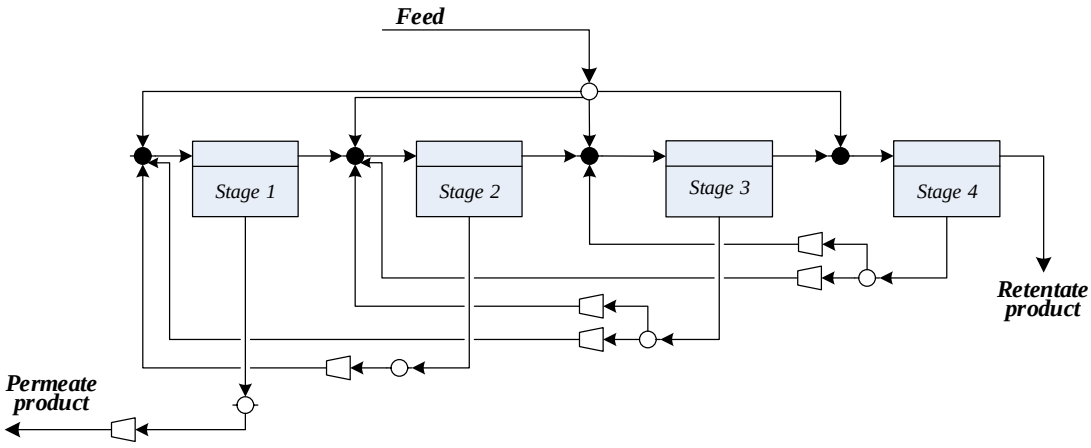

Fig. 3.4. Optimized cascade superstructure for the separation of propylene/propane

All membranes used in the cascades for either the liquid separation of p-xylene/o-xylene, or for the gaseous separation of propylene/propane were assumed to be dense membranes with a permeation mechanism described by the solution diffusion theory [39]. The complete membrane cascade optimization model for either the superstructure of Fig. 3.3 or Fig. 3.4 was formulated as MINLP as described in Chapter 1. The solution of this model allows to find in one step the optimum cascade structure (stream connections and number of stages), as well as the optimum operating conditions that yield to the minimum energy consumption, which include the optimum values of stream flows, compositions, and trans-membrane pressure difference (or trans-membrane pressure ratio). We clarify that according to the solution diffusion model embedded in the optimization formulation, the component fluxes across each membrane in the liquid separation of p-xylene/o-xylene depend on the trans-membrane pressure difference, whereas in contrast, for the gaseous separation of propylene/propane, they depend on the trans-membrane pressure ratio instead. We restricted the trans-membrane pressure difference to be less or equal than 107 bar, which is near the maximum trans-membrane pressure difference tested in the permeation experiments of Koh et al. [55] for the separation of p-xylene/o-xylene through reverse osmosis. With respect to the membranes in the superstructure of Fig. 3.4, we restricted them to operate at a trans-membrane pressure ratio less or equal than 9. The maximum number of stages allowed for any of the optimized superstructures was restricted to four. All postulated optimization problems were solved using the global optimum solver BARON 18.5.8 [33].

Membrane permselectivity

An important parameter needed when desigining a membrane separation process is the membrane permselectivity, which is defined as the permeability ratio between the most permeable component (p-xylene or propylene in this work) and the least permeable component (o-xylene or propane in this work). The value of this parameter, which depends on the membrane material, has a direct impact on the process energy

efficiency. In our study, we assume a permselectivity of 50 for all membranes that compose the simulated membrane cascades for the separation of p-xylene/o-xylene or propylene/propane. This value is in the same order of magnitude as the permselectivity exhibited by state of art membranes developed at laboratory scale [55, 103].

3.5 Comparison results between membranes and distillation

Since both heat pump distillation and membranes consume the same type of energy (electrical work), we performed the energy comparison between these processes by directly comparing their input energy. For convenience, in this and the following sections, we have employed the convention that when referring to composition or recovery, we refer to the most permeable and most volatile component (which is p-xylene or propylene in our work), unless otherwise is stated. The recovery of p-xylene (resp. propylene) is defined as the ratio of its molar flowrate in the permeate or distillate product stream to that in the feed mixture. Moreover, we represent the composition of p-xylene (resp. propylene) in the feed with the symbol $x_{px,f}$ (resp. $x_{propy,f}$), and the target purity of p-xylene (resp. propylene) at either the permeate or distillate stream with the term y^o_{px} (resp. y^o_{propy}).

3.5.1 p-xylene/o-xylene separation

Low concentration of the most permeable/most volatile component in the feed ($x_{px,f}$=0.20)

Fig. 3.5 plots the ratio between the electrical work energy consumed by HP-Distillation and a four-stage membrane cascade with a perm-selectivity of 50 under two different values of p-xylene purity and several values of p-xylene recovery. As we observe, the membrane cascade consumes more energy than distillation within the entire simulated range of purity and recovery when the feed has a concentration of 20% p-xylene, which represents the typical p-xylene concentration in the naphtha reformate (the main source of p-xylene at industrial scale). This energy difference

becomes higher as both the target purity and recovery grow up, being the energy consumed by the optimum membrane cascade roughly 86 times higher than that needed for heat pump distillation when p-xylene is separated with 99.5% purity and 99.0 % recovery.

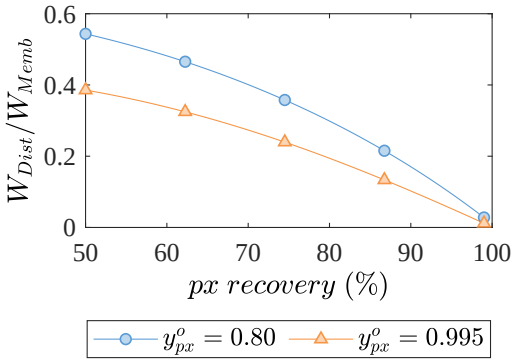

Fig. 3.5. Ratio of the electrical work consumed by HP-Distillation and a four-stage membrane cascade (with a perm-selectivity of 50) for different target p-xylene purity (y^o_{px}) and recovery values. The feed concentration was 20% p-xylene

The low concentration of the most permeable component (p-xylene) in the feed lessens the membrane separation driving force, which yields to a low energy performance of the overall separation. This effect can be better observed by analyzing the separation through a single membrane. Fig. 3.6 plots the p-xylene purity in the permeate stream separated through a single membrane-stage under a fixed permselectivity of 50, but under different values of feed composition, recovery, and trans-membrane pressure difference. As we observe, when the feed has a low concentration (e.g. 20% p-xylene), the concentration difference between the permeate and the feed is very small (see arrows in Fig. 3.6), even with a high trans-membrane pressure difference (ΔP^{trans}), which reflects the low separation driving force. Nevertheless, as the feed becomes more enriched in p-xylene, the separation driving force enhances, and thus, a higher increment in concentration relative to the feed is achieved in the

permeate. While the use of a membrane cascade helps to achieve both high purity and recovery even when the feed has a dilute concentration in the most permeable component, it requires the pumping of large recycle flows, which drives to a high energy consumption.

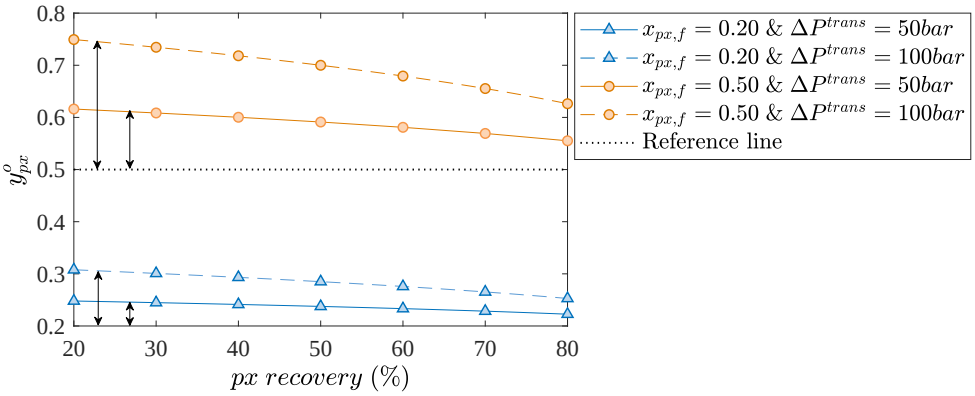

Fig. 3.6. p-xylene concentration in the permeate stream separated through a single membrane under various values of feed composition ($x_{px,f}$), p-xylene recovery, and trans-membrane pressure difference (ΔP^{trans}). A perm-selectivity of 50 was employed for these calculations

The poor energy performance of membranes when the feed is diluted in the most permeable component can be alternatively inferred from the magnitude of the osmotic pressure (Π). This thermodynamic function, which is proportional to the logarithm of the concentration of the most permeable component in the feed ($x_{f,A}$) as defined in Eq. (3.1), represents the minimum pressure difference that needs to be applied across a single membrane to produce an infinitesimal amount of pure permeate. For the discussed feed with 20% p-xylene, the osmotic pressure is 329 bar, which indicates the high level of energy consumption that would be needed for its separation. We note that in Eq. (3.1), V_A represents the molar volume of the most permeable component, R is the universal gas constant, and T is the absolute temperature.

$$\Pi = -\frac{RT}{V_A} \ln\left(x_{A,f}\right) \tag{3.1}$$

A membrane cascade allows to still achieve a high purity with a much lower trans-membrane pressure difference than the osmotic pressure. For instance, the optimum membrane cascade that was found for the separation of a feed with 20% p-xylene to produce a p-xylene product with 99.5% purity and 99% recovery, operates at ΔP^{trans} =107 bar. Nevertheless, the recycle flows that need to be pumped to achieve the target separation requirements are very large, and thus, a high amount of input energy is needed.

On the other hand, in the case of HP-distillation, the close boiling points between p-xylene and o-xylene drives to a small temperature difference across the column, which helps to reduce the input energy because the compression ratio needed to pump the heat from the top to the bottom of the column is small. For instance, when distillation is employed to produce p-xylene at 99.5% purity and with 99% recovery, the required compression ratio is only 1.3. We note that although the compressed vapor flow for the discussed separation is relatively high due to a high reflux ratio of 34, this flow is still markedly lower ($\sim$ 52 times lower) than the total amount of recycled flow that is pumped at the very high pressure difference of 107 bar in the optimized membrane cascade, which further explains why HP-distillation is more energy efficient.

Moderate and high concentration of the most permeable/most volatile component in the feed ($x_{px,f}$=0.65 and $x_{px,f}$=0.90)

Fig. 3.7 show the ratio between the electrical work needed to operate distillation and membranes when the concentration of p-xylene in the feed is 65% and 90% respectively. As it is observed, the use of membranes have more room to compete with distillation as the feed is more enriched in p-xylene. Once again, this behaviour can be anticipated from the reduction of osmotic pressure as the concentration of the most permeable component in the feed increases. For instance, for the feed streams with 65 % and 90% of p-xylene, the corresponding osmotic pressures are 88 bar and

22 bar respectively, which are evidently much lower than the value of 329 bar for the feed with 20 % p-xylene.

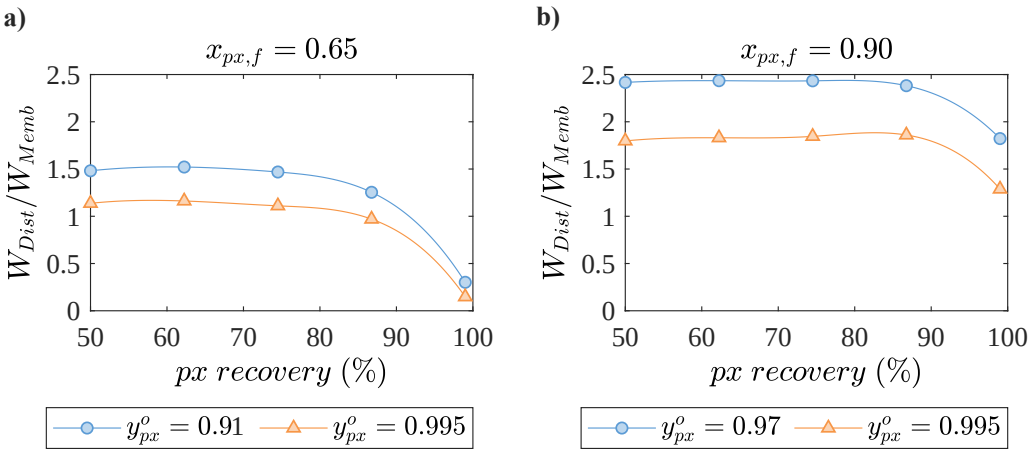

Fig. 3.7. Ratio of the electrical work consumed by HP-Distillation and an optimal membrane cascade with a maximum of four stages (and with a perm-selectivity of 50) for different values of feed compositions ($x_{px,f}$), and target p-xylene purity ($y^o_{px,f}$) and recovery. **a-b**, Simulations with a feed with 65 % p-xylene (**a**), Simulations with a feed with 90% p-xylene (**b**).

As it is seen from Fig. 3.7, when the feed has a moderate concentration of 65% of p-xylene and only a moderate amount of p-xylene less than 85-90% is recovered in the final product, an optimized four-stage membrane cascade with a perm-selectivity of 50 consumes less work energy than HP-Distillation. Furthermore, the ratio between the work energy consumed by HP-Distillation and the membrane cascade (W_{Dist}/W_{Memb}) increases as lower purity is needed in the p-xylene product stream, meaning that the use of membranes becomes more energy favored at such conditions. Nevertheless, as the recovery of p-xylene tends to a high value, the work ratio W_{Dist}/W_{Memb} decreases, going far below than one as approaching to 99% of recovery, which indicates that HP-Distillation is markedly more energy efficient in this separation region, and even more when p-xylene is produced at a very high purity (e.g. 99.5%).

The existence of a separation region where the use of membrane is more energy efficient, and another region where distillation is more energy favored is due to a trade-off between the amount of flow that is pumped or compressed, and its corresponding level of pressurization needed to perform a given separation through each of these processes. This trade-off is illustrated in Fig. 3.8, which corresponds to the separation of a feed with 65% p-xylene to produce p-xylene with 99.5% purity at different recoveries. Fig. 3.8a shows the amount of vapor flow that is compressed in HP-Distillation, and the total amount of flow that is pumped in the membrane cascade, which accounts for the feed and recycle streams. On the other hand, Fig. 3.8b shows the corresponding pressure ratio at which the compressor in HP-Distillation is operated, and the pressure differences at which the feed and recycles are respectively pumped in the membrane cascade. We note that although the compression ratio in HP-Distillation is small, and in contrast, the recycles in the membrane cascade are pumped at a high pressure difference, the amount of compressed flow in HP-Distillation is up to 2.3 times higher than the total pumped flow in the membrane cascade when the p-xylene recovery is moderate (*i.e.*, $\leq 87\%$), which drives to distillation to consume more energy in this region. However, when the p-xylene recovery increases to 99%, the total recycling flow that is pumped in the membrane cascade at the very high pressure difference of 107 bar rises up drastically, going far above than the compressed flow in HP-Distillation. In addition, as recovery increases, the net retentate flow decreases, which causes a reduction in the available energy that is recovered from the retentate product, and consequently, increases the pressure difference for the feed pump. These two effects, causes the membrane cascade to consume more energy than HP-Distillation at high recoveries of p-xylene.

In general, the trends observed in the curves of Fig. 3.7b, which corresponds to a feed with 90% p-xylene, are similar to those found in Fig. 3.7a in the sense that the work ratio W_{Dist}/W_{Memb} decreases as higher recovery and purity is needed. Nevertheless, for the scenario with the more enriched feed (90% p-xylene), an optimum

membrane cascade consumes less energy than distillation within the complete evaluated range of p-xylene recovery and purity. This happens because as we explained, having a feed more enriched in the most permeable component enhances the driving force for membranes, which derives into a significant reduction of the amount of flow that needs to be recycled in the cascade and the corresponding pressure difference at which it is pumped (compare Fig. 3.8 and Fig. 3.9). In contrast, the vapor flow for distillation as well as the compression ration remains almost unaltered when going from 65% to 90% (compare Fig. 3.8 and Fig. 3.9), meaning that the HP-Distillation flowsheet of Fig. 3.1a) does not benefit for a higher concentration of the most volatile component in the feed. Since the compressed flow for HP-Distillation is much higher than that pumped in the membrane cascade, the latter process consumes less energy.

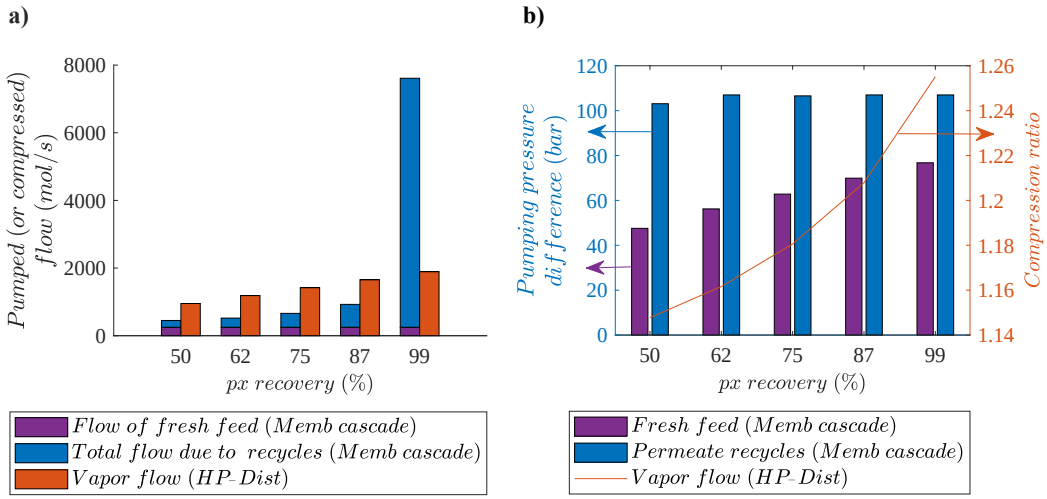

Fig. 3.8. Pumped (or compressed) flows and its corresponding level of pressurization required by a four-stage cascade and HP-Distillation to separate 99.5% pure p-xylene at different recoveries from a mixture with 65% p-xylene. **a-b**, Pumped flows in a four-stage membrane cascade and compressed flow in HP-Distillation (**a**), Pumping pressure difference required in the membrane cascade and compression ratio required in HP-Distillation (**b**).

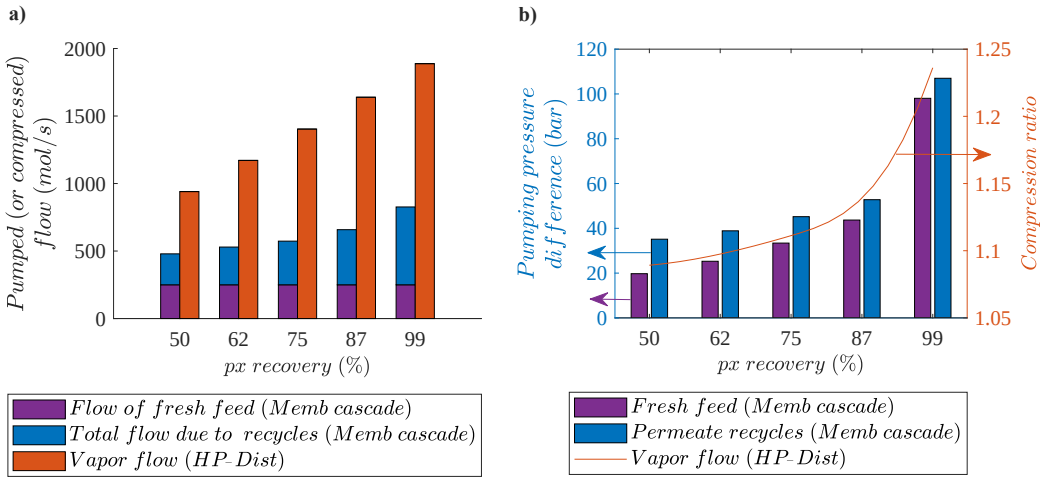

Fig. 3.9. Pumped (or compressed) flows and its corresponding level of pressurization required by a four-stage cascade and HP-Distillation to separate 99.5% pure p-xylene at different recoveries from a mixture with 90% p-xylene. **a-b**, Pumped flows in a four-stage membrane cascade and compressed flow in HP-Distillation (**a**), Pumping pressure difference required in the membrane cascade and compression ratio required in HP-Distillation (**b**).

Heat Pump Distillation with an Intermediate Boiler/Condenser

It can be noticed from the previous discussion that distillation seems to be less energy efficient as the feed becomes more enriched in the most volatile component. Nevertheless, it has been demonstrated that when the feed is enriched in the most volatile component, the energy efficiency of distillation can be notably enhanced by using an intermediate boiler/condenser [115, 116]. This situation coincides with two of the analyzed compositions in this work; $x_{px,f} = 0.65$ and particularly, $x_{px,f} = 0.90$. Therefore, we performed additional simulations for these feed conditions using the improved HP-distillation scheme shown in Fig. 3.2a that incorporates an intermediate boiler/condenser (IBC). The obtained results are shown in Fig. 3.10.

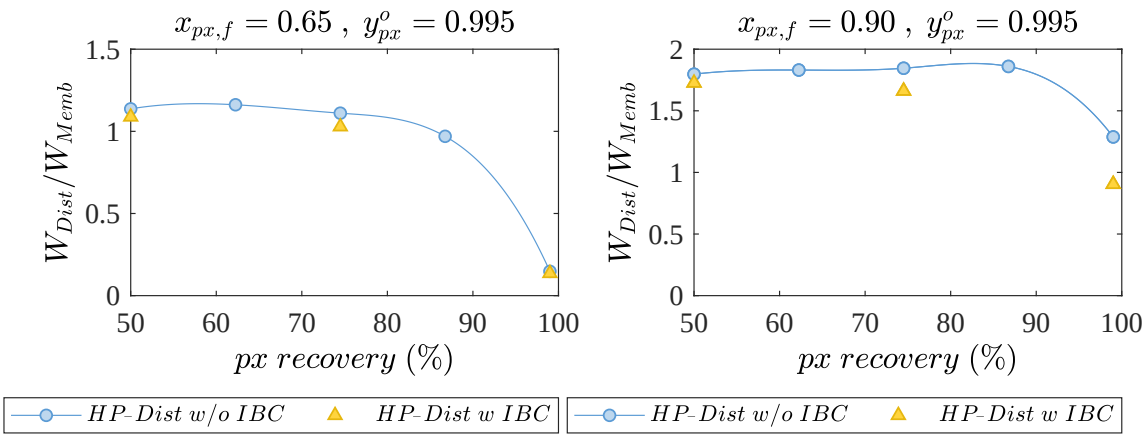

Fig. 3.10. Work input ratio between HP-distillation (w and w/o IBC) and membranes. IBC means Intermediate Boiler-Condenser. **a-b**, Simulations with a feed with 65 % p-xylene (**a**), Simulations with a feed with 90% p-xylene (**b**). The target purity of p-xylene was set to 0.995 for all the simulations.

As it can be seen from Fig. 3.10, the addition of an IBC helps to reduce the work consumption of HP-Distillation. This energy reduction is obtained because the intermediate boiler/condenser allows to compress part of the vapor flow at a lower pressure ratio. We should note that when looking at Fig. 3.10a, which corresponds to a feed of 65% p-xylene, it appears that the addition of the IBC does not bring any benefit for the maximum tested recovery as the ratio W_{Dist}/W_{mem} seems the same with or without an IBC. In reality, the IBC helps to achieve a non negligible work reduction of 8%. Nevertheless, the decrease in the ratio W_{Dist}/W_{Memb} is very small because the energy consumed by the membrane cascade is very large.

The energy savings from the use of an intermediate boiler/condenser becomes more significant as the feed is more enriched in the most permeable component, and higher recovery is needed. For instance, when the feed is 90% p-xylene, and p-xylene is produced with a purity and recovery of 99.5% and 99% respectively, the work needed for HP-Distillation decreases over 30% after adding an IBC, being the

net work slightly lower than the work consumed by membranes (see Fig. 3.10b). Nevertheless, as it is observed, in the moderate recovery range, membranes still look more competitive over distillation, even after the addition of an IBC.

3.5.2 propylene/propane separation

Fig. 3.11 shows the ratio between the work energy required by HP-Distillation and by the optimized membrane cascade for the separation of propylene/propane when the feed has a concentration of 65% propylene. We should note that from the total energy consumed by HP-Distillation, part of it is employed to operate the refrigeration cycle, and another part to operate the heat pump. Nevertheless, most of the input energy ($\sim$ 91%) is consumed by the heat-pump compressor (or compressors) that upgrade the temperature of the vapor utilized to provide the necessary heat at each boiler/condenser. The refrigeration system does not require a large amount of energy because the distillate is withdrawn in vapor phase and because part of the vapor generated after the throttling valve is recycled, which reduces significantly the amount of vapor that is condensed with the aid of the refrigerant.

Interestingly, the results for the separation of propylene/propane shown in Fig. 3.11 share similar patterns as those discussed before for the liquid separation of p-xylene/o-xylene (Fig. 3.7a and Fig. 3.10a). As it is observed from Fig. 3.11, the use of a membrane cascade is more energy favored than distillation when both the target purity and recovery of propylene is moderate. Nevertheless, in the contrary scenario, HP-Distillation consumes markedly less energy. For instance, when a 65% propylene feed is separated to produce polymeric grade propylene with 99.5% purity and 99.0% recovery (typical industrial recovery), HP-Distillation requires 45% less energy than the four-stage membrane cascade with a propylene permselectivity of 50. Moreover, if an intermediate boiler/condenser is used, the HP-Distillation work decreases about

22 %, making the energy input for HP-Distillation 57% lower than that needed for the membrane cascade.

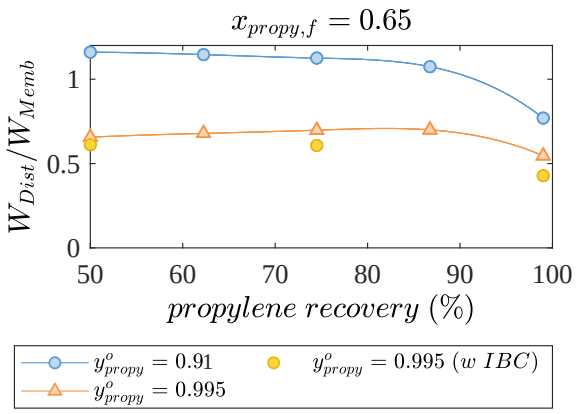

Fig. 3.11. Ratio of the electrical work needed by HP-Distillation and an optimal membrane cascade with a maximum of four stages (and with a perm-selectivity of 50) to separate propylene from a mixture of propylene/propane with 65% propylene at different values of target propylene purity (y^o_{propy}) and recovery. IBC indicates that an Intermediate Boiler Condenser was used for the heat pump distillation flowsheet.

3.6 Conclusions

A comparison of the energy required by a multistage membrane process and heat pump distillation is presented in this research. Both membranes and distillation processes are optimized as an attempt to evaluate them at their best operating conditions. The introduced energy comparison analysis was applied to two important separation examples; the separation of p-xylene/o-xylene, and propylene/propane. These mixtures are frequently perceived as potential candidates to be separated by membranes.

In general, our results showed that HP-distillation is more energy favored than membranes when the target purity and recovery of the most volatile (resp. most permeable) component in the distillate (resp. permeate) is high, and particularly when

the feed has a low concentration in the most volatile (resp. most permeable) component. On the other hand, when both the recovery and purity of the most volatile (resp. most permeable) component are required at moderate levels, and particularly when the feed is highly enriched in the most volatile (resp. most permeable) component, membranes show potential to save energy as compared with HP-Distillation. It should be noted that when the feed is highly enriched in the most volatile component, the energy consumption of distillation can be drastically reduced through the use of an intermediate boiler/condenser, but membranes still look more energy competitive at such feed conditions if only moderate purity and recovery are needed.

The growing concern of reducing the effects of anthropogenic pollution such as global warming and CO_2 emissions will undoubtedly foster in the near future the operation of more energy efficient processes. All those reasons make it necessary to carefully analyze which separation technology will provide the maximum energy benefits for a separation at hand. The comparison analysis between membranes and distillation presented in this work provides useful guidance to decide when it is more energy efficient to perform a separation with distillation or membranes.

REFERENCES

REFERENCES

[1] M. Galizia, W. S. Chi, Z. P. Smith, T. C. Merkel, R. W. Baker, and B. D. Freeman, "50th anniversary perspective: Polymers and mixed matrix membranes for gas and vapor separation: A review and prospective opportunities," Macromolecules, vol. 50, no. 20, pp. 7809–7843, 2017.

[2] L. S. White, "Development of large-scale applications in organic solvent nanofiltration and pervaporation for chemical and refining processes," Journal of Membrane Science, vol. 286, no. 1, pp. 26 – 35, 2006.

[3] R. Spillman, "Chapter 13 economics of gas separation membrane processes," ser. Membrane Science and Technology, R. D. Noble and S. A. Stern, Eds. Elsevier, 1995, vol. 2, pp. 589 – 667.

[4] R. Agrawal, "A simplified method for the synthesis of gas separation membrane cascades with limited numbers of compressors," Chemical Engineering Science, vol. 52, no. 6, pp. 1029 – 1044, 1997.

[5] R. Qi and M. Henson, "Optimization-based design of spiral-wound membrane systems for CO_2/CH_4 separations," Separation and Purification Technology, vol. 13, no. 3, pp. 209 – 225, 1998.

[6] E. L. Cussler and B. K. Dutta, "On separation efficiency," AIChE Journal, vol. 58, no. 12, pp. 3825–3831, 2012.

[7] M. M. Qiu, S. T. Hwang, and Y. K. Kao, "Economic evaluation of gas membrane separator designs," Industrial & Engineering Chemistry Research, vol. 28, no. 11, pp. 1670–1677, 1989.

[8] B. Bhide and S. Stern, "Membrane processes for the removal of acid gases from natural gas. I. Process configurations and optimization of operating conditions," Journal of Membrane Science, vol. 81, no. 3, pp. 209 – 237, 1993.

[9] ——, "A new evaluation of membrane processes for the oxygen-enrichment of air. I. Identification of optimum operating conditions and process configuration," Journal of Membrane Science, vol. 62, no. 1, pp. 13 – 35, 1991.

[10] H. Lababidi, G. A. Al-Enezi, and H. M. Ettouney, "Optimization of module configuration in membrane gas separation," Journal of Membrane Science, vol. 112, no. 2, pp. 185 – 197, 1996.

[11] J. Xu and R. Agrawal, "Gas separation membrane cascades I. One-compressor cascades with minimal exergy losses due to mixing," Journal of Membrane Science, vol. 112, no. 2, pp. 115 – 128, 1996.

[12] R. Agrawal and J. Xu, "Gas separation membrane cascades II. Two-compressor cascades," Journal of Membrane Science, vol. 112, no. 2, pp. 129 – 146, 1996.

[13] J. Hao, P. Rice, and S. Stern, "Upgrading low-quality natural gas with H_2S- and CO_2-selective polymer membranes: Part II. Process design, economics, and sensitivity study of membrane stages with recycle streams," Journal of Membrane Science, vol. 320, no. 1, pp. 108 – 122, 2008.

[14] F. Ahmad, K. Lau, A. Shariff, and G. Murshid, "Process simulation and optimal design of membrane separation system for CO_2 capture from natural gas," Computers & Chemical Engineering, vol. 36, pp. 119 – 128, 2012.

[15] J. Xu and R. Agrawal, "Membrane separation process analysis and design strategies based on thermodynamic efficiency of permeation," Chemical Engineering Science, vol. 51, no. 3, pp. 365 – 385, 1996.

[16] R. Agrawal and J. Xu, "Gas-separation membrane cascades utilizing limited numbers of compressors," AIChE Journal, vol. 42, no. 8, pp. 2141–2154, 1996.

[17] R. Pathare and R. Agrawal, "Design of membrane cascades for gas separation," Journal of Membrane Science, vol. 364, no. 1, pp. 263 – 277, 2010.

[18] K. Cohen, The Theory of isotope separation as applied to the large-scale production of U235. McGraw-Hill, 1951.

[19] F. P. McCandless, "Comparison of countercurrent recycle cascades with continuous membrane columns for gas separations," Industrial & Engineering Chemistry Research, vol. 29, no. 10, pp. 2167–2170, 1990.

[20] A. Aliaga-Vicente, J. A. Caballero, and M. J. Fernández-Torres, "Synthesis and optimization of membrane cascade for gas separation via mixed-integer nonlinear programming," AIChE Journal, vol. 63, no. 6, pp. 1989–2006, 2017.

[21] R. Qi and M. A. Henson, "Optimal design of spiral-wound membrane networks for gas separations," Journal of Membrane Science, vol. 148, no. 1, pp. 71 – 89, 1998.

[22] ——, "Membrane system design for multicomponent gas mixtures via mixed-integer nonlinear programming," Computers & Chemical Engineering, vol. 24, no. 12, pp. 2719 – 2737, 2000.

[23] R. V. S. Uppaluri, P. Linke, and A. C. Kokossis, "Synthesis and optimization of gas permeation membrane networks," Industrial & Engineering Chemistry Research, vol. 43, no. 15, pp. 4305–4322, 2004.

[24] M. Scholz, M. Alders, T. Lohaus, and M. Wessling, "Structural optimization of membrane-based biogas upgrading processes," Journal of Membrane Science, vol. 474, pp. 1 – 10, 2015.

[25] Álvaro A. Ramírez-Santos, M. Bozorg, B. Addis, V. Piccialli, C. Castel, and E. Favre, "Optimization of multistage membrane gas separation processes. Example of application to CO_2 capture from blast furnace gas," Journal of Membrane Science, vol. 566, pp. 346 – 366, 2018.

[26] A. M. Arias, M. C. Mussati, P. L. Mores, N. J. Scenna, J. A. Caballero, and S. F. Mussati, "Optimization of multi-stage membrane systems for CO_2 capture from flue gas," International Journal of Greenhouse Gas Control, vol. 53, pp. 371 – 390, 2016.

[27] R. E. Rosenthal, GAMS – A User's Guide, GAMS Development Corporation, Washington, DC, USA, 2014.

[28] J. Viswanathan and I. Grossmann, "A combined penalty function and outer-approximation method for MINLP optimization," Computers & Chemical Engineering, vol. 14, no. 7, pp. 769 – 782, 1990.

[29] R. V. Uppaluri, R. Smith, P. Linke, and A. C. Kokossis, "On the simultaneous optimization of pressure and layout for gas permeation membrane systems," Journal of Membrane Science, vol. 280, no. 1, pp. 832 – 848, 2006.

[30] M. Tawarmalani and N. V. Sahinidis, "A polyhedral branch-and-cut approach to global optimization," Mathematical programming, vol. 103, no. 2, pp. 225–249, 2005.

[31] V. S. Adi, M. Cook, L. G. Peeva, A. G. Livingston, and B. Chachuat, "Optimization of OSN Membrane Cascades for Separating Organic Mixtures," in 26th European Symposium on Computer Aided Process Engineering, ser. Computer Aided Chemical Engineering, Z. Kravanja and M. Bogataj, Eds. Elsevier, 2016, vol. 38, pp. 379 – 384.

[32] C. Kunde and A. Kienle, "Global optimization of multistage binary separation networks," Chemical Engineering and Processing - Process Intensification, vol. 131, pp. 164 – 177, 2018.

[33] M. R. Kılınç and N. V. Sahinidis, "Exploiting integrality in the global optimization of mixed-integer nonlinear programming problems with baron," Optimization Methods and Software, vol. 33, no. 3, pp. 540–562, 2018.

[34] X. Feng, J. Ivory, and V. S. V. Rajan, "Air separation by integrally asymmetric hollow-fiber membranes," AIChE Journal, vol. 45, no. 10, pp. 2142–2152, 1999.

[35] L. Tranchino, R. Santarossa, F. Carta, C. Fabiani, and L. Bimbi, "Gas separation in a membrane unit: Experimental results and theoretical predictions," Separation Science and Technology, vol. 24, no. 14, pp. 1207–1226, 1989.

[36] C. Y. Pan, "Gas separation by permeators with high-flux asymmetric membranes," AIChE Journal, vol. 29, no. 4, pp. 545–552, 1983.

[37] L. S. White, "Transport properties of a polyimide solvent resistant nanofiltration membrane," Journal of Membrane Science, vol. 205, no. 1, pp. 191 – 202, 2002.

[38] P. Silva, L. G. Peeva, and A. G. Livingston, "Organic solvent nanofiltration (OSN) with spiral-wound membrane elements—Highly rejected solute system," Journal of Membrane Science, vol. 349, no. 1, pp. 167 – 174, 2010.

[39] J. Wijmans and R. Baker, "The solution-diffusion model: a review," Journal of Membrane Science, vol. 107, no. 1, pp. 1 – 21, 1995.

[40] S. Weller and W. A. Steiner, "Separation of gases by fractional permeation through membranes," Journal of Applied Physics, vol. 21, no. 4, pp. 279–283, 1950.

[41] ——, "Erratum: Separation of gases by fractional permeation through membranes," Journal of Applied Physics, vol. 21, no. 12, pp. 1340–1340, 1950.

[42] N. Sahinidis and M. Tawarmalani, "Accelerating branch-and-bound through a modeling language construct for relaxation-specific constraints," Journal of Global Optimization, vol. 32, p. 259–280, 2005.

[43] N. Sahinidis, BARON user manual v. 2020.4.14, April 2020.

[44] H. Zimmermann, Propene. Wiley-VCH Verlag GmbH & Co. KGaA, 2013.

[45] J. R. Alcántara-Avila, F. I. Gómez-Castro, J. G. Segovia-Hernández, K.-I. Sotowa, and T. Horikawa, "Optimal design of cryogenic distillation columns with side heat pumps for the propylene/propane separation," Chemical Engineering and Processing: Process Intensification, vol. 82, pp. 112 – 122, 2014.

[46] F. Fábrega, J. Rossi, and J. d'Angelo, "Exergetic analysis of the refrigeration system in ethylene and propylene production process," Energy, vol. 35, no. 3, pp. 1224 – 1231, 2010.

[47] C. W. Colling, G. A. Huff Jr, and J. V. Bartels, "Processes using solid permselective membranes in multiple groups for simultaneous recovery of specified products from a fluid mixture," Patent, Jan., 2004, uS Patent 20040004040 A1.

[48] A. Górak and H. Schoenmakers, Distillation Operation and Applications. Boston: Academic Press, 2014.

[49] J. Klabunde, C. Bischoff, and A. J. Papa, Propanols. Wiley-VCH Verlag GmbH & Co. KGaA, 2018.

[50] D. R. Summers, P. J. McGuire, M. R. Resetarits, C. E. Graves, S. E. Harper, and S. J. Angelino, "High-capacity trays debottleneck Texas C_3 splitter," Oil and Gas Journal, vol. 93, no. 45, 1995.

[51] M. O. Daramola, Xylenes: Synthesis, Characterization and Physicochemical Properties. Nova Science Publishers, Incorporated, 2013.

[52] C. Perego and P. Pollesel, "Chapter 2 - advances in aromatics processing using zeolite catalysts," in Advances in Nanoporous Materials, ser. Advances in Nanoporous Materials, S. Ernst, Ed. Elsevier, 2010, vol. 1, pp. 97 – 149.

[53] M. T. Ashraf, "Analysis and optimization of p-xylene production process," Ph.D. dissertation, 2013.

[54] T.-C. Tsai, S.-B. Liu, and I. Wang, "Disproportionation and transalkylation of alkylbenzenes over zeolite catalysts," Applied Catalysis A: General, vol. 181, no. 2, pp. 355 – 398, 1999.

[55] D.-Y. Koh, B. A. McCool, H. W. Deckman, and R. P. Lively, "Reverse osmosis molecular differentiation of organic liquids using carbon molecular sieve membranes," Science, vol. 353, no. 6301, pp. 804–807, 2016.

[56] R. Chafin, J. S. Lee, and W. J. Koros, "Effects of casting and post casting annealing on xylene isomer transport properties of Torlon® 4000T films," Polymer, vol. 51, no. 15, pp. 3462 – 3471, 2010.

[57] Materials Research for Separation Technologies: Energy and Emission Reduction Opportunities. U.S. Department of Energy, 2005.

[58] D. S. Sholl and R. P. Lively, "Seven chemical separations to change the world," Nature, vol. 532, no. 7600, pp. 435–437, 2016.

[59] National Academies of Sciences, Engineering, and Medicine, A Research Agenda for Transforming Separation Science. Washington, DC: The National Academies Press, 2019.

[60] W. J. Koros, "Evolving beyond the thermal age of separation processes: Membranes can lead the way," AIChE Journal, vol. 50, no. 10, pp. 2326–2334, 2004.

[61] National Research Council, Sustainability in the Chemical Industry: Grand Challenges and Research Needs. Washington, DC: The National Academies Press, 2006.

[62] R. P. Lively and D. S. Sholl, "From water to organics in membrane separations," Nature materials, vol. 16, no. 3, p. 276–279, 2017.

[63] N. M. Wade, "Distillation plant development and cost update," Desalination, vol. 136, no. 1, pp. 3 – 12, 2001.

[64] M. Darwish, F. A. Asfour], and N. Al-Najem, "Energy consumption in equivalent work by different desalting methods: case study for kuwait," Desalination, vol. 152, no. 1, pp. 83 – 92, 2003.

[65] A. Al-Karaghouli and L. L. Kazmerski, "Energy consumption and water production cost of conventional and renewable-energy-powered desalination processes," Renewable and Sustainable Energy Reviews, vol. 24, pp. 343 – 356, 2013.

[66] H. Nassrullah, S. F. Anis, R. Hashaikeh, and N. Hilal, "Energy for desalination: A state-of-the-art review," Desalination, vol. 491, p. 114569, 2020.

[67] G. Xomeritakis, Z. Lai, and M. Tsapatsis, "Separation of xylene isomer vapors with oriented mfi membranes made by seeded growth," Industrial & Engineering Chemistry Research, vol. 40, no. 2, pp. 544–552, 2001.

[68] V. H. Shah and R. Agrawal, "A matrix method for multicomponent distillation sequences," AIChE Journal, vol. 56, no. 7, pp. 1759–1775, 2010.

[69] Z. Jiang and R. Agrawal, "Process intensification in multicomponent distillation: A review of recent advancements," Chemical Engineering Research and Design, vol. 147, pp. 122 – 145, 2019.

[70] R. Agrawal and D. Woodward, "Efficient cryogenic nitrogen generators: An exergy analysis," Gas Separation & Purification, vol. 5, no. 3, pp. 139 – 150, 1991.

[71] R. Kempton, D. Maccioni, S. M. Mrayed, and G. Leslie, "Thermodynamic efficiencies and GHG emissions of alternative desalination processes," Water Supply, vol. 10, no. 3, pp. 416–427, 2010.

[72] A. A. Mabrouk, A. Nafey, and H. Fath, "Thermoeconomic analysis of some existing desalination processes," Desalination, vol. 205, no. 1, pp. 354 – 373, 2007.

[73] M. A. Al-Weshahi, A. Anderson, and G. Tian, "Exergy efficiency enhancement of msf desalination by heat recovery from hot distillate water stages," Applied Thermal Engineering, vol. 53, no. 2, pp. 226 – 233, 2013.

[74] M. H. Sharqawy, J. H. Lienhard V, and S. M. Zubair, "On exergy calculations of seawater with applications in desalination systems," International Journal of Thermal Sciences, vol. 50, no. 2, pp. 187 – 196, 2011.

[75] B. Linnhoff and E. Hindmarsh, "The pinch design method for heat exchanger networks," Chemical Engineering Science, vol. 38, no. 5, pp. 745 – 763, 1983.

[76] P. Wantanachaisaeng and K. O'Neil. (2007) Capturing opportunities for para-xylene production. (UOP LLC, 2007). [Online]. Available: https://www.uop.com/wp-content/uploads/2012/12/UOP-aromatics-paraxylene-capture-paper1.pdf

[77] D. Kim, M. Y. Jeon, B. L. Stottrup, and M. Tsapatsis, "para-xylene ultra-selective zeolite mfi membranes fabricated from nanosheet monolayers at the air–water interface," Angewandte Chemie International Edition, vol. 57, no. 2, pp. 480–485, 2018.

[78] M. Schleiffelder and C. Staudt-Bickel, "Crosslinkable copolyimides for the membrane-based separation of p-/o-xylene mixtures," Reactive and Functional Polymers, vol. 49, no. 3, pp. 205 – 213, 2001.

[79] R. Lively, "Carbon molecular sieve membranes aim to cut energy use in hydrocarbon separations," Membrane Technology, vol. 2017, no. 1, pp. 9 – 10, 2017.

[80] M. Snyder and M. Tsapatsis, "Hierarchical nanomanufacturing: From shaped zeolite nanoparticles to high-performance separation membranes," Angewandte Chemie International Edition, vol. 46, no. 40, pp. 7560–7573, 2007.

[81] B. Shi, P. Marchetti, D. Peshev, S. Zhang, and A. G. Livingston, "Will ultra-high permeance membranes lead to ultra-efficient processes? challenges for molecular separations in liquid systems," Journal of Membrane Science, vol. 525, pp. 35 – 47, 2017.

[82] R. Agrawal and D. M. Herron, "Optimal thermodynamic feed conditions for distillation of ideal binary mixtures," AIChE Journal, vol. 43, no. 11, pp. 2984–2996, 1997.

[83] W. J. Koros and R. P. Lively, "Water and beyond: Expanding the spectrum of large-scale energy efficient separation processes," AIChE Journal, vol. 58, no. 9, pp. 2624–2633, 2012.

[84] U. Nallasivam, V. H. Shah, A. A. Shenvi, J. Huff, M. Tawarmalani, and R. Agrawal, "Global optimization of multicomponent distillation configurations: 2. enumeration based global minimization algorithm," AIChE Journal, vol. 62, no. 6, pp. 2071–2086, 2016.

[85] J. A. Caballero and I. E. Grossmann, "Structural considerations and modeling in the synthesis of heat-integrated-thermally coupled distillation sequences," Industrial & Engineering Chemistry Research, vol. 45, no. 25, pp. 8454–8474, 2006.

[86] Z. Jiang, G. Madenoor Ramapriya, M. Tawarmalani, and R. Agrawal, "Minimum energy of multicomponent distillation systems using minimum additional heat and mass integration sections," AIChE Journal, vol. 64, no. 9, pp. 3410–3418, 2018.

[87] R. T. Gooty, R. Agrawal, and M. Tawarmalani, "An minlp formulation for the optimization of multicomponent distillation configurations," Computers & Chemical Engineering, vol. 125, pp. 13 – 30, 2019.

[88] A. A. Shenvi, D. M. Herron, and R. Agrawal, "Energy efficiency limitations of the conventional heat integrated distillation column (hidic) configuration for binary distillation," Industrial & Engineering Chemistry Research, vol. 50, no. 1, pp. 119–130, 2011.

[89] (2010) Boiler efficiency guide. (CleaverBrook, 2010). [Online]. Available: http://cleaverbrooks.com/uploadedfiles/internet_content/reference_center/insights/boiler%20efficiency%20guide.pdf

[90] T. J. Kotas, The exergy method of thermal plant analysis. Exergon Publishing Company UK Ltd, 2012.

[91] G. Soave, "Equilibrium constants from a modified redlich-kwong equation of state," Chemical Engineering Science, vol. 27, no. 6, pp. 1197 – 1203, 1972.

[92] D.-Y. Peng and D. B. Robinson, "A new two-constant equation of state," Industrial & Engineering Chemistry Fundamentals, vol. 15, no. 1, pp. 59–64, 1976.

[93] D. S. H. Wong and S. I. Sandler, "A theoretically correct mixing rule for cubic equations of state," AIChE Journal, vol. 38, no. 5, pp. 671–680, 1992.

[94] W. Rodrigues, S. Mattedi, and J. C. N. Abreu, "Experimental vapor-liquid equilibria data for binary mixtures of xylene isomers," Brazilian Journal of Chemical Engineering, vol. 22, pp. 453 – 462, 09 2005.

[95] Q. N. Ho, K. S. Yoo, B. G. Lee, and J. S. Lim, "Measurement of vapor–liquid equilibria for the binary mixture of propylene (r-1270)+propane (r-290)," Fluid Phase Equilibria, vol. 245, no. 1, pp. 63 – 70, 2006.

[96] Structured Packings for Distillation, Absorption and Reactive Distillation. (Sulzer Chemtech). [Online]. Available: https://www.sulzer.com/-/media/files/products/separation-technology/liquid_liquid_extraction/brochures/structured_packings.ashx

[97] A. Underwood, "Fractional distillation of multi-component mixtures," Chem. Eng. Prog., vol. 44, pp. 603–614, 1948.

[98] V. S. Chakravarthy, R. Jibb, J. Royal, and M. Lockett, "Developments in falling film type (downflow) reboilers in the air separation industry," in Fifth International Conference on Enhanced, Compact and Ultra-Compact Heat Exchangers: Science, Engineering and Technology, pp. 264–272, 2005.

[99] J. Smolarek and K. J. Potempa, "Cryogenic rectification system for lower pressure operation," Patent, May, 1995, uS Patent 5,410,885.

[100] M. Gahleitner and C. Paulik, Polypropylene. Wiley-VCH Verlag GmbH & Co. KGaA, 2014, ch. Polypropylene, pp. 1–44.

[101] J. D. Seader, E. J. Henley, and D. K. Roper, Separation Process Principles, 3rd ed. Wiley & Sons, Inc., 2010.

[102] T. Mix, J. Dweck, M. Weinberg, and R. Armstrong, "Energy conservation in distillation," Chem. Eng. Progr., vol. 74, no. 4, p. 49, 1978.

[103] X. Ma, P. Kumar, N. Mittal, A. Khlyustova, P. Daoutidis, K. A. Mkhoyan, and M. Tsapatsis, "Zeolitic imidazolate framework membranes made by ligand-induced permselectivation," Science, vol. 361, no. 6406, pp. 1008–1011, 2018.

[104] B. Belaissaoui, Y. L. Moullec], H. Hagi, and E. Favre, "Energy efficiency of oxygen enriched air production technologies: Cryogeny vs membranes," Separation and Purification Technology, vol. 125, pp. 142 – 150, 2014.

[105] P. S. Gomes, M. Minceva, and A. E. Rodrigues, "Operation of an industrial smb unit for p-xylene separation accounting for adsorbent ageing problems," Separation Science and Technology, vol. 43, no. 8, pp. 1974–2002, 2008.

[106] W. J. Cannella, Xylenes and Ethylbenzene. John Wiley & Sons, Inc, 2007.

[107] S. Kim, S. Jeong, and E. Heo, "Effects of the shale boom on ethylene and propylene prices," Energy Sources, Part B: Economics, Planning, and Policy, vol. 14, no. 3, pp. 49–66, 2019.

[108] A. M. Aitani, "Chapter 6 - propylene production," in Encyclopedia of Chemical Processing. Taylor and Francis, 2007, pp. 2461–2466.

[109] Z. Olujić, L. Sun, A. [de Rijke], and P. Jansens, "Conceptual design of an internally heat integrated propylene-propane splitter," Energy, vol. 31, no. 15, pp. 3083 – 3096, 2006, eCOS 2004 - 17th International Conference on Efficiency, Costs, Optimization, Simulation, and Environmental Impact of Energy on Process Systems.

[110] Y. Pan, T. Li, G. Lestari, and Z. Lai, "Effective separation of propylene/propane binary mixtures by zif-8 membranes," Journal of Membrane Science, vol. 390-391, pp. 93 – 98, 2012.

[111] X. Ma, S. Williams, X. Wei, J. Kniep, and Y. Lin, "Propylene/propane mixture separation characteristics and stability of carbon molecular sieve membranes," Industrial & Engineering Chemistry Research, vol. 54, no. 40, pp. 9824–9831, 2015.

[112] J. Liu, Y. Xiao, and T.-S. Chung, "Flexible thermally treated 3d pim-cd molecular sieve membranes exceeding the upper bound line for propylene/propane separation," Journal of Materials Chemistry A, vol. 5, no. 9, pp. 4583–4595, 2017.

[113] I. S. Chae, S. W. Kang, J. Y. Park, Y.-G. Lee, J. H. Lee, J. Won, and Y. S. Kang, "Surface energy-level tuning of silver nanoparticles for facilitated olefin transport," Angewandte Chemie International Edition, vol. 50, no. 13, pp. 2982–2985, 2011.

[114] D. S. Hubbell and P. W. Rutten, "Crystallization process for purification of paraxylene," Sep. 22 1998, uS Patent 5,811,629.

[115] R. Agrawal and D. M. Herron, "Efficient use of an intermediate reboiler or condenser in a binary distillation," AIChE Journal, vol. 44, no. 6, pp. 1303–1315, 1998.

[116] ——, "Intermediate reboiler and condenser arrangement for binary distillation columns," AIChE Journal, vol. 44, no. 6, pp. 1316–1324, 1998.

[117] N. Felbab, B. Patel, M. M. El-Halwagi, D. Hildebrandt, and D. Glasser, "Vapor recompression for efficient distillation. 1. a new synthesis perspective on standard configurations," AIChE Journal, vol. 59, no. 8, pp. 2977–2992, 2013.

APPENDICES

A. MATHEMATICAL PROOFS

Proof of Property P3-1

Physically, the local permeate composition (y) is always greater than the local retentate composition (x). Otherwise, the permeate flow would become more enriched in the least permeable component, which is physically infeasible. Mathematically, this can be shown from (1.5). First, we rearrange (1.5) in the following form:

$$y - x = \frac{k(S-1)^2(1-y)y}{S(1-y)+y}. \tag{A.1}$$

We can infer $y \geq x$ if the RHS of the above equation is positive. Except for k, it is evident that all factors in the above equation are positive. To investigate the sign of k, we rearrange (1.6) in the form shown below:

$$k = \frac{S(1-e^{-C_A u}) - (1-e^{-C_B u})}{(S-1)^2} \tag{A.2}$$

For a gaseous mixture, both C_A and C_B are equal to 1. This simplifies the above equation to $k = \frac{(S-1)(1-e^{-u})}{(S-1)^2} \geq 0$, since $u > 0$. In the case of a liquid mixture, both C_A and C_B are very close to each other, because the molar volume of liquids have a similar magnitude. Since the term $(1 - e^{-C_A u})$ in (A.2) is multiplied by S, which is usually much greater than 1, the numerator is positive. Consequently, k is also positive. This implies that $y - x \geq 0$, or $y \geq x$.

We now prove that y increases monotonically with x. We begin with (A.1), and rearrange it as follows:

$$\frac{y-x}{y} = \frac{k(S-1)^2(1-y)}{S(1-y)+y} \tag{A.3}$$

Differentiating the above equation w.r.t y yields

$$\frac{d}{dy}\left(\frac{y-x}{y}\right) = -\frac{k(S-1)^2}{\left[S(1-y)+y\right]^2}, \tag{A.4}$$

$$\implies -\frac{1}{y^2}\left(y\frac{dx}{dy} - x\right) = -\frac{k(S-1)^2}{\left[S(1-y)+y\right]^2}, \tag{A.5}$$

$$\implies \frac{dx}{dy} = \frac{1}{y}\left\{x + \frac{ky^2(S-1)^2}{\left[S(1-y)+y\right]^2}\right\}. \tag{A.6}$$

Since all the terms on the right hand side are non-negative, $\frac{dx}{dy} \geq 0$, and $\frac{dy}{dx} = \left(\frac{dx}{dy}\right)^{-1} \geq 0$. This implies that y increases monotonically with x.

Proof of Property P3-2

From (A.4), observe that $\frac{d}{dy}\left(\frac{y-x}{y}\right) \leq 0$. Therefore, $\left(\frac{y-x}{y}\right)$ decreases monotonically with y.

B. CLARIFYING NOTES

1.- Clarification over the definition of thermal separation processes

In this work, we refer to a process as a thermal separation method if the main driving force for separation is heat transfer. Nevertheless, the net energy input to the process could be in any form. For example, we would refer to distillation as a thermal separation process since the driving force is heat transfer at the reboiler, regardless of whether external energy is supplied as heat (heat supplied distillation) or electrical work (e.g. heat pump distillation).

2.- Definition of purity and recovery

The term purity employed throughout this work refers to the molar fraction of the most volatile (or most permeable) component in the product stream of interest, which for the separation examples that we analyzed, corresponds to the distillate (or net permeate) stream.

On the other hand, the term recovery is defined as the ratio between the molar flow of the most volatile (or most permeable) component that is recovered in the distillate (or net permeate) to the molar flow of the same component in the feed.

C. HEAT SUPPLIED DISTILLATION VS HEAT PUMP DISTILLATION

Usually, the energy needed to operate a distillation column is supplied in the form of heat at the reboiler, which is used to boil up part of the bottom liquid and provide the necessary vapor reflux. In addition, to make feasible the separation, some heat needs to be removed from the system. This step is accomplished by the partial or total condensation of the vapor that leaves the top of the column. When distillation is operated above ambient conditions, it is common to reject this heat to the environment mainly due to practical reasons as it is usually easy and economical. Nevertheless, when the amount of heat released at the condenser is high and it is at significantly high temperature, it is desirable to recover and re-utilize this heat to enhance the overall energy efficiency.

There are several ways in which the condenser heat can be reused. For instance, it can be employed to provide energy to another process unit within the same plant or can be used to extract electrical work from it. Another way to reuse the heat removed from the condenser that is very effective in some cases is to transfer it to the reboiler with the aid of a heat pump. Several configurations of heat pump distillation have been proposed, but probably one of the most efficient and common schemes is the vapor recompression cycle (Fig. C.1). In this arrangement, the vapor that leaves the column is compressed to increase its temperature before it is condensed against the bottom liquid, which needs to be vaporized. We recall that when operating a distillation column with a heat pump, all the input energy can be supplied in the form of electricity, without requiring any external source of heat. This approach allows a considerable improvement of the overall energy efficiency for many cases, particularly, when the temperature difference across the column is small, and when the heat that

would have been rejected at the condenser is at relatively high temperature and is not utilized downstream. Nevertheless, in the opposite scenario heat supplied distillation is usually more energetically favored.

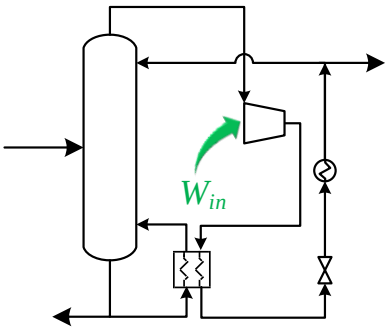

Fig. C.1. Heat pump distillation

Figure C.2 qualitatively depicts the region where heat supplied distillation or heat pump distillation are more energy efficient (see Appendix D for the calculation details). The blue curve shows the vapor flow (V, per unit of feed flow) that leaves the top of the distillation column as a function of relative volatility (α) for an equimolar liquid feed. The relative volatility is taken as a proxy of the temperature difference along the column (ΔT_{col}). The molar vapor flow in the column can be expressed as the ratio of the reboiler heat duty (Q_{reb}) and the molar enthalpy of vaporization ($\Delta H_{m,vap}$). Thus, the vapor flow can be treated as a proxy for the reboiler heat duty. We observe that as α decreases (as well as ΔT_{col}) the vapor flow increases, and so does the reboiler heat duty. Thus, when α is close to 1, heat supplied distillation is unattractive as the amount of thermal energy needed at the reboiler is high. This scenario can be encountered for instance in the separation of mixtures composed by isomers (e.g. p-xylene/o-xylene, as shown in Fig. C.2).

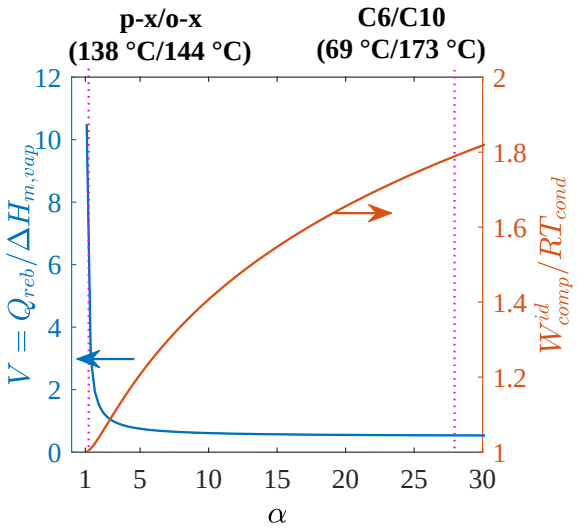

Fig. C.2. Vapor flow and compression work in distillation vs relative volatility. Blue curve: vapor flow leaving the distillation column. Orange curve: ideal compressor work for heat pump distillation divided by RT_{cond}. R is the ideal gas constant, and T_{cond} is the condenser temperature. The calculations were made for an equimolar feed at saturated liquid conditions. The temperatures shown in parenthesis correspond to the normal boiling points (1 bar) of p-xylene, o-xylene, hexane and decane respectively.

Simulataneously, the orange curve included in Fig. C.2, which relates to the amount of work needed for heat pump distillation shows a trend to decrease as $\alpha \to 1$. This behavior is reasonable since as ΔT_{col} becomes lower, a smaller compression ratio is needed to sufficiently increase the vapor temperature so as to perform heat integration with the bottoms liquid. Based on these observations, we expect that, when α is small, heat pump distillation would have a higher energy efficiency compared to conventional heat supplied distillation (provided the condenser heat is not further utilized). On the other hand, when α is high, such as in the separation of hexane/decane (also marked in Fig. C.2), the vapor flow is much lesser, and the reboiler heat duty correspondingly reduces. In contrast, the magnitude of W^{id}_{comp}/RT_{cond} increases because the pressure ratio for the compression of vapor is much higher. Therefore, when α is high, it is more efficient to operate distillation with heat rather than with work. This is because of the inefficiency of generating work from a heat source.

The effect of the column temperature difference over the feasibility of operating distillation with heat or work can be seen alternatively in Fig. C.3. This graph shows the approximate ratio between the compressor work (W_{comp}) for heat pump distillation and the equivalent work for heat driven distillation ($W_{eq,reb}$) as a function of the condenser and reboiler temperature ratio. The equivalent work for heat driven distillation is defined as the amount of electrical work that could have been extracted in a power plant from the steam used to supply the heat needed at the distillation reboiler. Refer to Section 2.5.1 of Chapter 2 to see how W_{eq} is calculated.

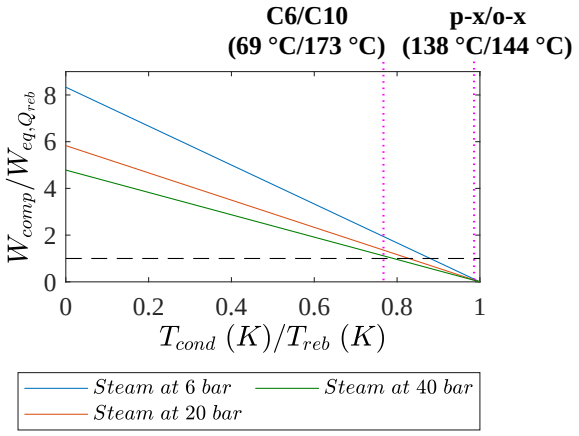

Fig. C.3. Ratio of the work needed for heat pump distillation (W_{comp}) and the equivalent work for heat supplied distillation ($W_{eq,Q_{reb}}$) as a function of T_{cond}/T_{reb}. We consider the use of co-generated steam for heat supplied distillation. The compressor work used for this plot was calculated under the assumption that it is 2 times higher than the ideal work that would be required for a reversible heat pump. The rest of the assumptions and details behind the calculations of this plot are given in Appendix E.

We can observe clearly that there exist a region where the work consumed for heat pump distillation is lower than the equivalent work needed by heat supplied distillation.

The graph presented in Fig. C.3 can be used as a quick screening method to estimate for a given separation if it is more energy efficient to operate distillation driven by heat or work input. Felbab et al. [117] developed an alternative graphical method to identify which operation mode for distillation is more efficient. It requires the knowledge of at least the temperatures of the condenser and the reboiler. However, such method was derived assuming a reversible distillation column, which introduces a strong degree of simplification.

Regardless of whether using the plot of Fig. C.3 or Felbab's method, the reader should be aware that they provide a first level of approximation. To perform a more accurate comparison it is better to perform rigorous simulation of the distillation schemes to calculate the compressor work as well as the reboiler heat duty. Then, the energy performance of heat and work supplied distillation can be compared following the framework described in Chapter 2.

D. VAPOR FLOW AND COMPRESSION WORK FOR DISTILLATION

The vapor flow (V) shown in Figure C.2 was calculated with equation (D.1). This expression, which is applicable to a saturated liquid feed (binary), is derived from the McCabe-Thiele method under the assumptions of complete separation and that the column operates at its minimum reflux ratio.

$$V = \frac{(1 - x_f) + \alpha x_f}{\alpha - 1} \tag{D.1}$$

The term x_f refers to the composition of the most volatile component in the feed, and α represents the volatility of the most volatile component relative to that of the least volatile component.

The second curve (W^{id}_{comp}/RT_{cond}) shown in Figure C.2 was derived using the following procedure. First, we assumed that the heat pump coupled to the distillation column operates reversibly. Under this scenario, the ratio between the ideal compressor work (W^{id}_{comp}) and the reboiler heat (Q_{reb}) depends only on the temperature of the reboiler (T_{reb}) and that of the condenser (T_{cond}). This relation is shown below in equation (D.2):

$$\frac{W^{id}_{comp}}{Q_{reb}} = T_{cond}\left(\frac{1}{T_{cond}} - \frac{1}{T_{reb}}\right). \tag{D.2}$$

The term Q_{reb} was then replaced by the product of the vapor flow (V, equation (D.1)) and the molar enthalpy of vaporization ($\Delta H_{m,vap}$) to obtain:

$$\frac{W^{id}_{comp}}{T_{cond}} = V\Delta H_{m,vap}\left(\frac{1}{T_{cond}} - \frac{1}{T_{reb}}\right). \tag{D.3}$$

Finally, the term $\left(\frac{1}{T_{cond}} - \frac{1}{T_{reb}}\right)$ was eliminated using the Clausius-Clapeyron equation according to the approach of Agrawal & Herron [82]. The resulting expression is shown below:

$$\frac{W_{comp}^{id}}{RT_{cond}} = \frac{(1 - x_f + \alpha x_f)\ln\alpha}{\alpha - 1}. \tag{D.4}$$

E. CALCULATIONS OF ($W_{COMP}/W_{EQ,Q_{REB}}$)

The lines of $W_{comp}/W_{eq,Q_{reb}}$ shown in Fig. C.3 were obtained by dividing the following equations (Eq. (E.2) and (E.1)).

$$W_{eq,Q_{reb}} = Q_{reb}\eta \tag{E.1}$$

$$W_{comp} = 2W_{comp}^{id} \tag{E.2}$$

To convert the reboiler heat (Q_{reb}) into an equivalent work ($W_{eq,Q_{reb}}$), we employed the efficiency factors (η) given in Table 2.4, as we considered that the heat comes from a co-generation power plant.

The compressor work (W_{comp}) that would be consumed by heat pump distillation in a real operation was assumed to be two times the compressor work that would be required if distillation operates with an ideal heat pump (W_{comp}^{id}). The factor of two is intended to capture the inefficiencies that occur in a real heat pump (e.g. compressor inefficiencies, pressure losses, etc.). The ideal compressor work was calculated using Eq. (D.2).

The final expression for $W_{comp}/W_{eq,Q_{reb}}$ is obtained after combining Eqs. (D.2), (E.2) and (E.1).

$$\frac{W_{comp}}{W_{eq,Q_{reb}}} = 2\left(1 - \frac{T_{cond}}{T_{reb}}\right)\left(\frac{1}{\eta}\right) \tag{E.3}$$